

CARBON - BASED COMPOSITE MATERIALS FOR ELECTROCHEMICAL SENSORS AND BIOSENSORS

Teză destinată obținerii
titlului științific de doctor inginer
la
Universitatea "Politehnica" din Timișoara
în domeniul INGINERIE CHIMICĂ
de către

Ing. Elida Cristina Ilinoiu

Conducător științific: Prof. dr.ing. Rodica Pode
Referenți științifici: Prof. M.D. PhD Pier Andrea Serra
Prof. dr.ing. Ciprian Radovan
Prof.dr.ing. Nicolae Vasilcsin

Ziua susținerii tezei: 18.01.2013

Seriile Teze de doctorat ale UPT sunt:

- | | |
|---|--|
| 1. Automatică | 9. Inginerie Mecanică |
| 2. Chimie | 10. Știința Calculatoarelor |
| 3. Energetică | 11. Știința și Ingineria Materialelor |
| 4. Ingineria Chimică | 12. Ingineria sistemelor |
| 5. Inginerie Civilă | 13. Inginerie energetică |
| 6. Inginerie Electrică | 14. Calculatoare și tehnologia informației |
| 7. Inginerie Electronică și Telecomunicații | 15. Ingineria materialelor |
| 8. Inginerie Industrială | 16. Inginerie și Management |

Universitatea *Politehnica* Timișoara a inițiat seriile de mai sus în scopul diseminării expertizei, cunoștințelor și rezultatelor cercetărilor întreprinse în cadrul școlii doctorale a universității. Seriile conțin, potrivit H.B.Ex.S Nr. 14 / 14.07.2006, tezele de doctorat susținute în universitate începând cu 1 octombrie 2006.

Copyright © Editura Politehnica – Timișoara, 2013

Această publicație este supusă prevederilor legii dreptului de autor. Multiplicarea acestei publicații, în mod integral sau în parte, traducerea, tipărirea, reutilizarea ilustrațiilor, expunerea, radiodifuzarea, reproducerea pe microfilme sau în orice altă formă este permisă numai cu respectarea prevederilor Legii române a dreptului de autor în vigoare și permisiunea pentru utilizare obținută în scris din partea Universității *Politehnica* Timișoara. Toate încălcările acestor drepturi vor fi penalizate potrivit Legii române a drepturilor de autor.

România, 300159 Timișoara, Bd. Republicii 9,
tel. 0256 403823, fax. 0256 403221
e-mail: editura@edipol.upt.ro

FOREWARD

One of the joys of completion and satisfaction is to look over the entire journey of 3 years, entitled PhD, and remember all the friends and colleagues who have helped and supported me along this road.

I would like to express my gratitude to my thesis coordinator, Professor Rodica Pode, who has given me the opportunity to follow the science path 5 years ago, for which I was so enthusiastic about.

The deepest knowhow and experience encountered in this thesis comes from Associate Professor Florica Manea, who was not only my supervisor but also the person who shaped and guided the direction of this 3 years project. Thank you deeply, Florica!

I know that it wasn't an easy task for Professor Pier Andreea Serra to manage my presence in his laboratory for 8 months, so, for the simplest reason that he opened my mind to electronics, microsensors and neuroscience, Thank You! The entire neuroscience department from Sassari University will always have a place in my heart. They have given me in 8 months another perspective of what patience and teamwork means.

A special attention goes to my examiners Professor Pier Andrea SERRA, Professor RADOVAN, Professor Nicolae VASZILCSIN because giving advices and guidance is not always easy to accept.

The thesis, as a sustained project, would not have been possible without the financial support of the strategic grants, POSDRU 2009 project ID 50783, POSDRU/89/1.5/S/63700, co-financed by the European Social Found-Investing in People.

Laboratory activities would not have been the same without the presence and constructive discussions with Aniela Pop and Laura Cocheci.

I have to thank to my colleagues, Colar Liliana, Anamaria Baciuc and Sorina Motoc, who were part of my 3 years sorrows and joyful moments, but also part of my eagerness from university studies. I lived with you 8 beautiful years which will be hard to forget. I wish you all the best!

During this "painful" journey I bumped into great friends who made my PhD period a continuously get-together. Strange ideas, life philosophies brought us together. A special thanks goes to Mihaela Vida, who listened, consoled me and practically adopted me from day -20 of the PhD. You were my surrogate family!

Nevertheless, to my mum, I can not thank you enough for your constant optimism, jokes and life vision.

Timișoara, 2013

Elida Cristina Ilinoiu

Ilinoiu, Elida Cristina

Carbon - based composite materials for electrochemical sensors and biosensors

Teze de doctorat ale UPT, Seria 4, Nr. 68, Editura Politehnica, 2013, 150 pagini, 79 figuri, 90 tabele.

ISSN: 1842-8223

ISBN: 978-606-554-608-0

Cuvinte cheie: rețea de senzori de tip compozit pe bază de grafit-zeolit natural/sintetic prinși în matrice de epoxi, macroelectrozi compoziți pe bază de grafit, detectia in-vitro/in-vivo, dopamina, acid ascorbic

Rezumat,

Domeniul senzorilor și biosenzorilor electrochimici privind aplicațiile clinice in-vivo reprezintă un domeniu de mare interes, dezvoltându-se în special pentru aplicații non-invazive de monitorizare a unor substanțe biologice active cu rol covarsitor în sănătatea umană.

Obiectivul principal al tezei de doctorat îl constituie dezvoltarea unui nou design pentru senzori de tip compozit pe baza de grafit-zeolit natural/sintetic prinși în matrice de epoxi potriviți pentru detectia in-vitro/in-vivo a dopaminei și a oxigenului molecular, pornind de la următoarele ipoteze:

a. înlocuirea microsenzorului de Pt datorită pretului ridicat al acestuia și efectului de colmatare, cu materiale pe baza de grafit, care este economic și biocompatibil;

b. utilizarea unui material compozit permite o regenerare foarte rapidă a suprafeței prin simpla șlefuire și mai ales, o compozite specifică poate prezenta caracteristici de rețea de microelectrozi, care permite obținerea unor semnale analitice îmbunătățite

Pentru atingerea obiectivului general, doctoranda și-a propus următoarele obiective specifice:

1. Optimizarea metodei de obținere a materialului compozit pe baza de grafit și modificat cu zeolit natural/sintetic în vederea obținerii microsenzorului caracterizat de cele mai bune proprietăți electrochimice. Pe baza cercetărilor întreprinse în această etapă au rezultat trei tipuri de senzori: grafit-epoxi (considerat ca și martor), grafit-zeolit natural-epoxi, grafit-zeolit sintetic-epoxi, cu o anumită compoziție selectată pe baza comportării electrochimice a acestora.

2. Testarea microelectrozilor pentru detectia in-vitro a dopaminei.

Noutatea acestui studiu de cercetare reiese chiar din obținerea materialelor de electrod compozit pe baza de grafit și modificat cu zeolit care constituie microsenzorii, continuându-se și în caracterizarea și testarea acestora pentru aplicații in-vivo, demonstrându-se de fapt utilitatea practică prin implantarea acestora.

Table of Contents

CHAPTER 1	17
Carbon based composite electrodes.....	17
1.1 Generalities.....	17
1.2 Conductive fillers used in carbon-based composite sensing devices.....	19
1.2.1 Graphite.....	19
1.2.2 Carbon nanotubes.....	20
1.3 Epoxy as binding material.....	21
1.4 Graphite-epoxy composite electrodes.....	22
1.4.1 Preparation of GEC composites.....	23
1.5 Conclusions.....	23
1.6 References.....	24
CHAPTER 2	27
Chemically modified electrodes.....	27
2.1 Generalities.....	27
2.2 Zeolite modified electrodes.....	28
2.2.1 Zeolite structure.....	28
2.2.2 Types of zeolites.....	29
2.2.3 Preparation methods.....	30
2.2.4 Applications of zeolites in electroanalysis.....	30
2.3 Coating electrodes with polymeric films.....	33
2.3.1 Implication of Nafion® in coating electrodes with polymeric films.....	33
2.4 Conclusions.....	35
2.5 References.....	36
CHAPTER 3	39
Introduction in microsensors applied in electroanalysis.....	39
3.1 Generalities.....	39
3.2 Configurations of microelectrodes.....	39
3.3 Properties of microelectrodes.....	40
3.3.1 Single microelectrodes.....	40
3.3.2 Composite microelectrodes.....	41
3.4 Consequences of the microelectrodes properties.....	43
3.5 Applications of microelectrodes.....	43
3.6 Conclusions.....	45
3.7 References.....	46
CHAPTER 4	48
Electrochemical techniques used in sensors applications.....	48
4.1 Cyclic voltammetry.....	48
4.1.1 Reversible Systems.....	49
4.1.2 Irreversible and Quasi-reversible systems.....	51
4.2 Constant Potential Amperometry.....	51
4.3 Pulse voltammetry.....	52
4.3.1 Differential pulse voltametry.....	52
4.3.2 Square wave voltammetry.....	53
4.4 References.....	54
CHAPTER 5	55
Scope and thesis objectives.....	55

CHAPTER 6.....	57
Preparation and characterization of modified/unmodified composite microelectrodes/macroelectrodes.....	57
6.1 Introduction.....	57
6.2 Design and graphite composite electrodes construction.....	58
6.2.1 Experimental section.....	58
6.2.1.1 Materials and reagents.....	58
6.2.1.2 Apparatus and experimental measurements.....	59
6.2.1.3 Synthetic zeolite synthesis.....	59
6.2.1.4 Microelectrode design and graphite-composite microelectrodes construction.....	59
6.2.2 Results and discussions.....	61
6.2.2.1 Optimization of the graphite-composite material construction.....	61
6.2.2.1.1 Optimization of the mixing methods and the three - epoxy component ratios.....	61
6.2.2.1.2 Optimization of the graphite-epoxy weight ratio.....	62
6.2.2.2 Zeolite adsorption studies.....	64
6.2.2.3 Construction of modified composite sensing materials.....	67
6.2.2.3.1 Optimization of the graphite-zeolite-epoxy weight ratio for microelectrodes.....	67
6.2.2.3.2 Construction of synthetic/natural zeolite-graphite-epoxy macrosensors.....	67
6.2.2.3.3 Nafion® coated microelectrodes.....	68
6.2.2.3.4 Carbon nanotubes film coated microelectrodes.....	68
6.3 Characterization of microelectrodes / macroelectrodes.....	68
6.3.1 Electrochemical surface characterization of unmodified graphite-epoxy composite microelectrodes.....	68
6.3.2 Electrochemical surface characterization of film modified graphite-epoxy composite microelectrodes.....	76
6.3.3 Electrochemical surface characterization of film modified graphite-epoxy composite microelectrodes.....	78
6.4 Conclusions.....	79
6.5 References.....	80
CHAPTER 7.....	84
Applications of modified/unmodified graphite-epoxy composite macrosensors...	84
7.1 Experimental.....	84
7.1.1 Chemicals and reagents.....	84
7.1.2 Apparatus and experimental measurements.....	84
7.2 Results and discussions.....	84
7.2.1 Cyclic voltammetry of ascorbic acid/dopamine at composite macroelctrodes.....	84
7.2.2 Pulsed voltammetric techniques.....	88
7.2.2.1 Differential-pulsed voltammetry.....	88
7.2.2.2 Square-wave voltammetry.....	91
7.2.3 Cronoamperometric detection experiments.....	93
7.3 Conclusions.....	95
7.4 References.....	96
CHAPTER 8.....	97
Applications of modified/unmodified graphite-epoxy composite microsensors...	97
8.1 Preliminary studies regarding ascorbic acid and dopamine detection.....	97
8.1.1 Ascorbic acid.....	97

8.1.2 Experimental.....	97
8.1.2.1 Chemicals and materials.....	97
8.1.2.2 Apparatus and experimental measurements.....	98
8.1.3 Results and discussions.....	98
8.1.3.1 Cyclic voltammetry of ascorbic acid.....	98
8.1.3.2 Cyclic voltammetry of a mixture of ascorbic acid and dopamine...	103
8.1.4 Conclusions.....	105
8.2 Microsensors optimization for dopamine detection.....	106
8.2.1 Dopamine.....	106
8.2.2 Experimental.....	107
8.2.2.1 Chemicals and materials.....	107
8.2.2.2 Apparatus and experimental measurements.....	107
8.2.3 Results and discussions.....	107
8.2.3.1 Cyclic voltammetry of dopamine.....	107
8.2.3.1.1 Cyclic voltammetry of dopamine at microelectrodes without Nafion® membrane.....	107
8.2.3.1.2 Cyclic voltammetry of dopamine at microelectrodes with Nafion® membrane.....	111
8.2.3.1.3 Cyclic voltammetry of dopamine at microelectrodes with CNT film membrane.....	115
8.2.3.2 Effect of the scan rate in cyclic voltammetric measurements.....	117
8.2.3.3 Constant potential amperometry experiments.....	119
8.2.4 Conclusions.....	124
8.3 Interference studies.....	124
8.3.1 Introduction.....	124
8.3.2 Experimental.....	125
8.3.3 Results and discussions.....	125
8.3.4 Conclusions.....	129
8.4 Real-time monitoring of brain tissue oxygen.....	130
8.4.1 Introduction.....	130
8.4.2 Experimental.....	130
8.4.2.1 Regents and solutions.....	130
8.4.2.2 Working electrode (WE) preparation.....	130
8.4.2.3 Apparatus and measurements.....	131
8.4.2.3.1 Experiments in vitro.....	131
8.4.2.3.2 Experiments in vivo.....	132
8.4.3 Results and discussions.....	135
8.4.3.1 Micro-sensors response to oxygen.....	135
8.4.3.2 Baseline levels of striatal O ₂	138
8.4.3.3 Effect on striatal O ₂ current changes after pharmacological treatments.....	139
8.4.4 Conclusions.....	140
8.4.5 References.....	140
CHAPTER 9.....	144
Final conclusions and further perspectives.....	144

Abbreviations

AA	ascorbic acid
ANA	analcime
BDD	baron doped electrode
CA	cronoamperometry
CC	carbon composite
CF	carbon fiber
CHA	chabazite
CME	chemically modified electrode
CNS	central nervous system
CNT	carbon nanotube
CNF	carbon nanofiber
CPA	constant potential amperometry
CPE	carbon paste electrode
CV	cyclic voltammetry
DA	dopamine
DPV	differential pulse voltammetry
DOPAC	3,4-Dihydroxyphenylacetic acid
ERI	erionite
FCV	fast cyclic voltammetry
GC	glassy carbon
GEC	graphite epoxy composite
HEU	clinoptilolite
HPLC	high pressure liquid cromatography
IF/IC	faradic current/charging current
IR	ohmic drop
MA	modulation amplitude
MOR	modernite
MWCNT	multi wall carbon nanotube
Nf	nafion
PBS	hosphate buffer solution
PHI	phillipsite
SCE	calomel electrode
SP	step potential
SPE	screen printed electrode
SWCNT	single wall carbon nanotube
SQW	square wave voltammetry
THF	tetrahydrofuran
UA	uric acid
ZME	zeolite modified electrodes
ZN-GEC	natural zeolite-graphite epoxy composite
ZS-GEC	syntheticzeolite-graphite epoxy composite

ABSTRACT

Chapter 1 presents briefly the advantages of carbon based composites for and the motivation for being chosen as materials for electrochemical sensors.

Chapter 2 offers an introduction to chemically modified electrodes and especially the use of the zeolite materials as catalytic materials in the composite matrix, for the only purpose of obtaining better performances of the sensors, focusing on the advantage towards positively charged molecules. The main fields of applications of the zeolite modified electrodes are also underlined. A brief introduction of the polymeric films coated electrodes is intended with the mentioning of the advantage of using Nafion coated sensing devices.

Chapter 3 underlines the growing interest of the electrochemical sensors miniaturization and their impacts on many practical applications, with particularly fascinating studies for in-vivo monitoring of neurochemical events due to microsensors specific and attractive construction characteristics.

Chapter 4 deals with the use of voltammetric and amperometric techniques used in analytical chemistry.

Chapter 5 introduces the scope and objectives that have been the guide of this project.

Chapter 6 presents the construction of the composite macrosensor as well as its electrochemical surface characterization. The details of the design, construction and optimization of different matrixes of zeolite-graphite-epoxy composite microsensors as well as methodologies of their modification with polymer membranes or with carbon nanotube membrane are also presented within this chapter. The electrochemical surface characterizations is also present in this chapter emphasizing their macroelectrode array behavior.

Chapter 7 underlines the preliminary results obtained with the applications of the zeolite-graphite-epoxy composite macrosensors in the detection of ascorbic acid and dopamine.

Chapter 8 focuses on the integration of modified/unmodified microsensors matrixes in applications including *in vitro* voltammetric and amperometric detection of ascorbic acid and dopamine, interference studies and *in-vivo* applications for oxygen detection.

Chapter 9 summarizes the overall conclusions related to this work giving also future perspectives in this applications.

LIST OF TABLES

Table 1.1	Properties of CNTs
Table 6.1	Electrochemical parameters resulted when varying the mixing method and resin:hardener:accelerator ratios
Table 6.2	Adsorption degree of dopamine and ascorbic acid after 15 minutes adsorption time onto natural/ synthetic zeolite
Table 6.3	Electrochemical parameters for graphite : zeolite : epoxy composite construction; 2 mM K ₄ Fe(CN) ₆ / K ₃ Fe(CN) ₆ in 1M KNO ₃ supporting electrolyte; scan rate 100 mV s ⁻¹ ; potential range from -0.4 V to +0.8 V;
Table 6.4	Apparent diffusion coefficients and electroactive surface areas of μ -GEC, μ -NZ-GEC and μ -SZ-GEC microelectrodes
Table 6.5	The electrochemical parameters of the redox system (ferri/ferrocyanide) determined from the anodic branches of CVs for μ -GEC, μ -NZ-GEC and μ -SZ-GEC microelectrodes
Table 6.6	The electrochemical parameters of the redox system (ferri/ferrocyanide) determined from the cathodic branches of CVs for μ -GEC, μ -NZ-GEC and μ -SZ-GEC microelectrodes
Table 6.7	Apparent diffusion coefficients and electroactive surface areas of CNT film-ZS-GEC and μ -SZ-GEC microelectrodes
Table 6.8	Apparent diffusion coefficients and electroactive surface areas of M-GEC, M-NZ-GEC, M-SZ-GEC macroelectrodes
Table 7.2	Analytical parameters for DPV and SWV techniques for DA (concentration range between 10-50 μ M) and AA (concentration range between 100-500 μ M) simultaneous detection experiments
Table 7.3	Analytical parameters for CV technique for DA (concentration range between 10-50 μ M) and AA (concentration range between 100-500 μ M) simultaneous detection experiments
Table 8.1	Analytical parameters for CV technique for dopamine detection at microelectrodes without any protective membrane
Table 8.2	Analytical parameters for CV technique for dopamine detection (peak no.1) at microelectrodes with Nafion membrane
Table 8.3	Calibration plot parameters for all peaks at sensors covered with Nafion film
Table 8.4	Calibration plot parameters for all peaks at CNT-Film- μ -ZS-GEC microsensors
Table 8.5	Effect on the scan rate in cyclic voltammetric measurements
Table 8.6	Analytical parameters for CPA technique for dopamine detection at microelectrodes with/without Nafion film
Table 8.7	Analytical parameters for CPA technique for dopamine detection at CNT-film-ZS-GEC microelectrode
Table 8.8	Sensitivity values for main interferents occurred by cyclic voltammetry
Table 8.9	Effects of some electroactive molecules (AA, DOPAC, UA) present in the striatal extracellular fluid on the amperometric response of graphite based microsensors
Table 8.9	CV's data for O ₂ detection at μ -GEC, μ -NZ-GEC, μ -SZ-GEC
Table 8.10	Determination of dissolved O ₂ concentration according to MPTP administration

LIST OF FIGURES

- Figure 1.1** Graphite structure.
- Figure 1.2** Schematic illustration of a) SWNTs b) MWNTs and c) carbon nanofiber structure
- Figure 1.3** Reaction between epoxy resin and amine based curing agent (hardener)
- Figure 1.4** Schematic diagram showing the stages in epoxy composites preparation
- Figure 2.1** Schematic representation for various kinds of CMEs preparation routs
- Figure 2.2** Different methods for ZMEs construction
- Figure 2.3** The chemical formula of Nafion
- Figure 3.1** Types of microelectrode geometries (a) disc; (b) ring; (c) band; (d) sphere; (e) hemisphere; (f) square array; (g) hexagonal array; (h) interdigitated microband.
- Figure 3.2** Diffusion layer overlapping at closely spaced microelectrodes in a composite structured microelectrode
- Figure 4.1** Potential-time excitation signal in a cyclic voltammogram experiment
- Figure 4.2** The expected response of a reversible redox couple during a single potential cycle
- Figure 4.3** Typical constant-potential amperogram. Inset is the excitation waveform
- Figure 4.4 A** Differential pulse voltametry-Plot of voltammogram
- Figure 4.4 B** Differential pulse voltametry-Anodic scanning of the potential.
- Figure 4.5** Excitation waveform points for a square wave voltammogram.
- Figure 6.1** Sensor design.
- Figure 6.2** Mixing methods of the three-epoxy components with graphite particles.
- Figure 6.3** CVs recorded at graphite-epoxy microelectrode in a 1M KNO₃ supporting electrolyte and 2mM Fe(CN)₆^{3-/4-} at a scan rate of 100 mV s⁻¹ ; Potential Range: -0.2 V to +0.6 V, Speed: 20kHz; Sample Period: 1ms , QuadStat Filter 10kHz.
- Figure 6.4** The effect of the graphite content upon peak-to-peak separation (ΔE) at graphite- epoxy (M₁ mixing method and 100: 95:5 resin:hardener:accelerator ratio) micro-sensors in 1M KNO₃ supporting electrolyte with 2 mM K₄Fe(CN)₆/ K₃Fe(CN)₆; scan rate 100 mV s⁻¹; potential range from -0.4 V to +0.8 V; Ag/AgCl reference electrode and Pt auxiliary electrode.
- Figure 6.5** CVs recorded in 50 mL PBS of 31.25 μ M concentration of dopamine before and after adding natural zeolite and synthetic zeolite in the supporting electrolyte solution, using a Diamond Baron Doped working electrode; Pt reference electrode and Ag/AgCl auxiliary electrode; scan rate 50 mV s⁻¹.
- Figure 6.6** CVs recorded in 50 mL PBS of 31.25 μ M concentration of ascorbic acid before and after adding natural zeolite and synthetic zeolite in the supporting electrolyte solution, using a Diamond Baron Doped working electrode;Pt reference electrode and Ag/AgCl auxiliary electrode; scan rate 50 mV s⁻¹.

- Figure 6.7** Optimization of the graphite-zeolite-epoxy weight ratio.
- Figure 6.8** (A) Cyclic voltammograms recorded at μ -GEC, composite with 2 mM potassium ferricyanide/ferrocyanide at different scan rates : 25, 50, 100, 200, 333, 400, 454 mV s^{-1} in 20 mL of 1M KNO_3 supporting electrolyte; potential range from -0.4 to +0.8 V; (B) Calibration plots of the oxidative and reductive peak currents vs. square root of scan rate without charging current subtraction.
- Figure 6.9** (A) Cyclic voltammograms recorded at μ -ZN-GEC composite with 2 mM potassium ferricyanide/ferrocyanide at different scan rates : 25, 50, 100, 200, 333, 400, 454 mV s^{-1} in 20 mL of 1M KNO_3 supporting electrolyte; potential range from -0.4 to +0.8 V; (B) Calibration plots of the oxidative and reductive peak currents vs. square root of scan rate without charging current subtraction.
- Figure 6.10** (A) Cyclic voltammograms recorded at μ -SZ-GEC composite with 2 mM potassium ferricyanide/ferrocyanide at different scan rates : 25, 50, 100, 200, 333, 400, 454 mV s^{-1} in 20 mL of 1M KNO_3 supporting electrolyte; potential range from -0.4 to +0.8 V; (B) Calibration plots of the oxidative and reductive peak currents vs. square root of scan rate without charging current subtraction.
- Figure 6.11** Plot of ΔE vs. scan rate parameters recorded at GEC, NZ-GEC, SZ-GEC, microelectrodes in 20 mL of 1M KNO_3 supporting electrolyte with 2 mM potassium ferricyanide/ferrocyanide at different scan rates : 25, 50, 100, 200, 333, 400, 454 mV s^{-1} ; potential range from -0.4 to +0.8 V; Ag/AgCl reference electrode and Pt auxiliary electrode.
- Figure 6.12** Plots of $\log(v)$ vs. $\log(i)$ parameters recorded at GEC, NZ-GEC, SZ-GEC, microelectrodes in 20 mL of 1M KNO_3 supporting electrolyte with 2 mM potassium ferricyanide/ferrocyanide at different scan rates : 25, 50, 100, 200, 333, 400, 454 mV s^{-1} ; potential range from -0.4 to +0.8 V; Ag/AgCl reference electrode and Pt auxiliary electrode.
- Figure 6.13** (A) Cyclic voltammograms recorded at CNT film μ -ZS-GEC composite with 2 mM potassium ferricyanide/ferrocyanide at different scan rates : 25, 50, 100, 200, 333, 400, 454 mV s^{-1} in 20 mL of 1M KNO_3 supporting electrolyte; potential range from -0.6 to +0.8 V; (B) Calibration plots of the oxidative and reductive peak currents vs. square root of scan rate without charging current subtraction.
- Figure 7.1** Cyclic voltammograms (CV) recorded at (A) M-GEC, (B) M-ZN-GEC and (C) M-ZS-GEC, in 50 mL of 50 mM PBS supporting electrolyte with increasing concentrations of AA : 100 μM , 200 μM , 300 μM , 400 μM , 500 μM , followed by the addition of consecutive concentrations of DA: 10 μM , 20 μM , 30 μM , 40 μM , 50 μM ; Pt reference electrode and Ag/AgCl auxiliary electrode; potential range from -0.8 V to +1.0 V; scan rate 50 mV s^{-1} .
- Figure 7.2** Calibration plots of the current densities vs. (A) AA and (B) DA concentrations at M-GEC, M-ZN-GEC and M-ZS-GEC, calculated without background current subtraction;
- Figure 7.3** Differential-pulsed voltammograms (DPV) recorded at (A) M-GEC, (B) M-ZN-GEC and (C) M-SZ-GEC, in 50 mL of 50 mM PBS supporting electrolyte with increasing concentrations of AA:100 μM ,

- 200 μM , 300 μM , 400 μM , 500 μM , followed by the addition of consecutive concentrations of DA: 10 μM , 20 μM , 30 μM , 40 μM , 50 μM ; Pt reference electrode and Ag/AgCl auxiliary electrode; potential range from 0.0 V to +1.0 V; step potential 0.05 V; modulation amplitude 0.1 V;
- Figure 7.5** Square-wave voltammograms (SWV) recorded at (A) M-GEC, (B) M-ZN-GEC and (C) M-SZ-GEC, in 50 mL of 50 mM PBS supporting electrolyte with increasing concentrations of AA : 100 μM , 200 μM , 300 μM , 400 μM , 500 μM , followed by the addition of consecutive concentrations of DA: 10 μM , 20 μM , 30 μM , 40 μM , 50 μM ; Pt reference electrode and Ag/AgCl auxiliary electrode; potential range from 0.0 V to +1.0 V; step potential 0.05 V; modulation amplitude 0.1 V; Frequency 50Hz
- Figure 7.6** CPA recorded at (A) M-GEC, (B) M-ZN-GEC and (C) M-ZS-GEC in 50 mL of 50 mM PBS supporting electrolyte with adding 500 μM AA followed by increasing concentrations of Dopamine : 10 μM , 20 μM , 30 μM , 40 μM , 50 μM , Pt reference electrode and Ag/AgCl auxiliary electrode; Potential value +0.100 V; inset: calibration plots for current densities vs. DA concentration calculated without background current subtraction.
- Figure 8.1** Cyclic voltammograms recorded at (A) μ -GEC in 20 mL of 50 mM PBS supporting electrolyte with increasing concentrations of AA : 125 μM , 250 μM , 500 μM , 750 μM , 1 mM, 1,25 mM, 1.5 mM; Pt reference electrode and Ag/AgCl auxiliary electrode; potential range from -1.0 V to +1.2 V; scan rate 250 mV s^{-1} . (B) Calibration plot of the anodic currents densities recorded at $E=+0.365$ V vs. AA concentration, calculated without background current subtraction.
- Figure 8.2** Cyclic voltammograms recorded at (A) μ -ZN-GEC in 20 mL of 50 mM PBS supporting electrolyte with increasing concentrations of AA : 125 μM , 250 μM , 500 μM , 750 μM , 1 mM, 1,25 mM, 1.5 mM; Pt reference electrode and Ag/AgCl auxiliary electrode; potential range from -1.0 V to +1.2 V; scan rate 250 mV s^{-1} . (B) Calibration plot of the anodic current densities recorded at $E=+0.303$ V vs. AA concentration, calculated without background current subtraction.
- Figure 8.3** (A) Cyclic voltammograms recorded at (A) μ -SZ-GEC in 20 mL of 50 mM PBS supporting electrolyte with increasing concentrations of AA : 125 μM , 250 μM , 500 μM , 750 μM , 1 mM, 1,25 mM, 1.5 mM; Pt reference electrode and Ag/AgCl auxiliary electrode; potential range from -1.0 V to +1.2 V; scan rate 250 mV s^{-1} . (B) Calibration plot of the anodic current densities recorded at $E=+0.521$ V vs. AA concentration, calculated without background current subtraction.
- Figure 8.4** (A) Cyclic voltammograms recorded at (A) CNT-Film- μ -SZ-GEC in 20 mL of 50 mM PBS supporting electrolyte with increasing concentrations of AA : 125 μM , 250 μM , 500 μM , 750 μM , 1 mM, 1,25 mM, 1.5 mM; Pt reference electrode and Ag/AgCl auxiliary electrode; potential range from -1.0 V to +1.2 V; scan rate 250 mV s^{-1} . (B) Calibration plot of the anodic current densities recorded at $E=+0.521$ V vs. AA concentration, calculated without background current subtraction.
- Figure 8.5** A-Cyclic voltammograms recorded at μ -SZ-GEC, in 20 mL of 50 mM PBS supporting electrolyte with increasing concentrations of AA

- followed by increasing concentrations of DA: 125 μM , 250 μM , 500 μM , 750 μM , 1 mM, 1.25 mM, 1.5 mM; B- Calibration plots of the current densities vs. DA concentration at a potential value of $E = +0.385\text{ V}$ and AA concentration at a potential value of $E = +0.521\text{ V}$; calculated without background current subtraction; Pt reference electrode and Ag/AgCl auxiliary electrode; potential range from -1.0 to +1.2 V; scan rate 250 mV s^{-1} ;
- Figure 8.6** A - Cyclic voltammograms recorded at $\mu\text{-SZ-GEC}$, in 20 mL of 50 mM PBS supporting electrolyte with increasing concentrations of DA followed by increasing concentrations of AA: 125 μM , 250 μM , 500 μM , 750 μM , 1 mM, 1.25 mM, 1.5 mM; B - Calibration plots of the current densities vs. DA concentration at a potential value of $E = +0.275\text{ V}$ and AA concentration at a potential value of $E = +0.521\text{ V}$; calculated without background current subtraction; Pt reference electrode and Ag/AgCl auxiliary electrode; potential range from -1.0 to +1.2 V; scan rate 250 mV s^{-1} .
- Figure 8.7** Cyclic voltammograms recorded at (A) $\mu\text{-GEC}$, (B) $\mu\text{-ZN-GEC}$, (C) $\mu\text{-SZ-GEC}$, in 20 mL of 50 mM PBS supporting electrolyte with increasing concentrations of DA : 125 μM , 250 μM , 500 μM , 750 μM , 1 mM, 1.25 mM, 1.5 mM; Pt reference electrode and Ag/AgCl auxiliary electrode; potential range from -1.0 V to +1.2 V; scan rate 250 mV s^{-1} ; and (a) Calibration plot of the anodic current densities recorded at $E=+0.281\text{ V}$ vs. DA concentration, calculated without background current subtraction (b) Calibration plot of the anodic current densities recorded at $E=+0.281\text{ V}$ vs. DA concentration, calculated without background current subtraction and (c) Calibration plot of the anodic current densities recorded at $E=+0.161\text{ V}$ vs. DA concentration, calculated without background current subtraction.
- Figure 8.8** Cyclic voltammograms recorded at (A) $\mu\text{-GEC}$, (B) $\mu\text{-ZN-GEC}$, (C) $\mu\text{-SZ-GEC}$ with Nafion membrane, in 20 mL of 50 mM PBS supporting electrolyte with increasing concentrations of DA : 125 μM , 250 μM , 500 μM , 750 μM , 1 mM, 1.25 mM, 1.5 mM; Pt reference electrode and Ag/AgCl auxiliary electrode; potential range from -1.0 V to +1.2 V; scan rate 250 mV s^{-1} .
- Figure 8.9** Calibration plots of the anodic/cathodic current densities recorded at (A) $\mu\text{-GEC}$, (B) $\mu\text{-ZN-GEC}$, (C) $\mu\text{-ZS-GEC}$ microsensors covered with Nafion membrane vs. DA concentration, calculated without background current subtraction.
- Figure 8.10** (A) Cyclic voltammograms recorded at CNT-film- $\mu\text{-SZ-GEC}$, in 20 mL of 50 mM PBS supporting electrolyte with increasing concentrations of DA : 125 μM , 250 μM , 500 μM , 750 μM , 1 mM, 1.25 mM, 1.5 mM; Pt reference electrode and Ag/AgCl auxiliary electrode; potential range from -1.0 V to +1.0 V; scan rate 250 mV s^{-1} ; (B) Calibration plots of the anodic/cathodic current densities vs. dopamine concentrations, calculated without background current subtraction.
- Figure 8.11** CVs for 500 μM DA in 50 mM PBS supporting electrolyte at different scan rates at $\mu\text{-SZ-GEC}$: 0.110 Vs^{-1} ; 0.2 Vs^{-1} ; 0.25 Vs^{-1} ; 0.3 Vs^{-1} ; 0.4 Vs^{-1} ; 0.45 Vs^{-1} ; Inset: Plot of the anodic current (I_a) vs. square root of the scan rate (V s^{-1})^{1/2} at the same experimental conditions;

- Pt reference electrode and Ag/AgCl auxiliary electrode; potential range from -1.0 V to +1.2 V;
- Figure 8.12** CVs for 500 μM DA in 20 mL of 50 mM PBS supporting electrolyte at different scan rates at $\mu\text{-GEC}$: 0.110 Vs^{-1} ; 0.2 Vs^{-1} ; 0.25 Vs^{-1} ; 0.3 Vs^{-1} ; 0.4 Vs^{-1} ; 0.45 Vs^{-1} ; Inset: Plot of the anodic current (I_a) vs. square root of the scan rate (V s^{-1})^{1/2} at the same experimental conditions; Pt reference electrode and Ag/AgCl auxiliary electrode; potential range from -1.0 V to +1.2 V;
- Figure 8.13** CVs for 500 μM DA in 20 mL of 50 mM PBS supporting electrolyte at different scan rates at $\mu\text{-NZ-GEC}$: 0.110 Vs^{-1} ; 0.2 Vs^{-1} ; 0.25 Vs^{-1} ; 0.3 Vs^{-1} ; 0.4 Vs^{-1} ; 0.45 Vs^{-1} ; Inset: Plot of the anodic current (I_a) vs. square root of the scan rate (V s^{-1})^{1/2} at the same experimental conditions; Pt reference electrode and Ag/AgCl auxiliary electrode; potential range from -1.0 V to +1.2 V;
- Figure 8.14** CVs for 500 μM DA in 20 mL of 50 mM PBS supporting electrolyte at different scan rates at CNT-film- $\mu\text{-SZ-GEC}$: 0.110 Vs^{-1} ; 0.2 Vs^{-1} ; 0.25 Vs^{-1} ; 0.3 Vs^{-1} ; 0.4 Vs^{-1} ; 0.45 Vs^{-1} ;
- Figure 8.15** (A) CPA recoded at $\mu\text{-SZ-GEC}$ microelectrode without Nafion film in 20 mL of 50 mM PBS supporting electrolyte with increasing concentrations of Dopamine : 25 nM, 50 nM, 100 nM, 250 nM, 500 nM, 750 nM, 1 μM ; Pt reference electrode and Ag/AgCl auxiliary electrode; Potential value +0.150 V; (B) Calibration plots of the anodic/cathodic current densities vs. dopamine concentrations, calculated without background current subtraction
- Figure 8.16** (A) CPA recoded at $\mu\text{-SZ-GEC}$ microelectrode with Nafion membrane in 20 mL of 50 mM PBS supporting electrolyte with increasing concentrations of Dopamine : 25 nM, 50 nM, 100 nM, 250 nM, 500 nM, 750 nM, 1 μM ; Pt reference electrode and Ag/AgCl auxiliary electrode; Potential value 0.430 V; (B) Calibration plots of the anodic/cathodic current densities vs. dopamine concentrations, calculated without background current subtraction.
- Figure 8.17** (A) CPA recoded at CNT-Film- $\mu\text{-SZ-GEC}$ microelectrode membrane in 20 mL of 50 mM PBS supporting electrolyte with increasing concentrations of Dopamine : 25 nM, 50 nM, 100 nM, 250 nM, 500 nM, 750 nM, 1 μM ; Pt reference electrode and Ag/AgCl auxiliary electrode; Potential value 0.250 V; (B) Calibration plots of the anodic/cathodic current densities vs. dopamine concentrations, calculated without background current subtraction.
- Figure 8.18** (A) CPA recoded at CNT-Film- $\mu\text{-SZ-GEC}$ microelectrode membrane in 20 mL of 50 mM PBS supporting electrolyte with increasing concentrations of Dopamine : 25 nM, 50 nM, 100 nM, 250 nM, 500 nM, 750 nM, 1 μM ; Pt reference electrode and Ag/AgCl auxiliary electrode; Potential value 0.150 V; (B) Calibration plots of the anodic/cathodic current densities vs. dopamine concentrations, calculated without background current subtraction.
- Figure 8.19** CVs recorded at (A) $\mu\text{-GEC}$, (B) $\mu\text{-ZN-GEC}$, (C) $\mu\text{-SZ-GEC}$ without Nafion membrane, in 20 mL of 50 mM PBS supporting electrolyte with increasing concentrations of DOPAC : 125 μM , 250 μM , 500 μM , 750 μM , 1 mM, 1.25 mM, 1.5 mM; Pt reference electrode and Ag/AgCl auxiliary electrode; potential range from -1.0 V to +1.2 V; scan rate 250 mV s^{-1} .

- Figure 8.20** CVs recorded at (A) μ -GEC, (B) μ -ZN-GEC, (C) μ -SZ-GEC without/with Nafion membrane, in 20 mL of 50 mM PBS supporting electrolyte in the presence of 1 mM AA; Pt reference electrode and Ag/AgCl auxiliary electrode; potential range from -1.0 V to +1.2 V; scan rate 250 mV s⁻¹.
- Figure 8.21** Comparatively presentation of the set-up for in vitro/ in vivo experimental procedure.
- Figure 8.22** System for acquisition, transmission and elaboration of electrochemical signals.
- Figure 8.23 A** A: holes drilled for WE, ref/aux and screws implantation.
- Figure 8.23 B** B: sensors implantation.
- Figure 8.23 C** C: fixing the 'basement' to the skull.
- Figure 8.23 D** D: suturing the skin.
- Figure 8.24** Cyclic voltammograms recorded at (A) μ -GEC, (B) μ -NZ-GEC and (C) μ -SZ-GEC, microelectrode covered with 4% cellulose nitrate solution (1 dip and left overnight) in 10 mL of 50 mM PBS supporting electrolyte and 100% O₂ for O₂ response; scan rate 250mVs⁻¹ ; potential range -1.0V to +0.4V; Ag/AgCl reference electrode and Pt auxiliary electrode.
- Figure 8.25** In vitro pre-calibration of oxygen micro-sensor using CPA performed at -350 mV vs. Ag/AgCl reference electrode with low concentrations of O₂; the oxygen sensor response was tested by exposing them to known volumes (200 μ L, +204 μ L, +208 μ L, +212 μ L, +216 μ L) of saturated O₂ solution (1.25mM) to a 10 mL saturated nitrogen PBS. *Inset*: In vitro pre/post calibration plots of the current I vs. dissolved O₂ concentration at NZ-GEC response characteristic for O₂ reduction.
- Figure 8.26** Effect of pharmacological treatments on striatal dissolved oxygen. (A) exemple for day 7.
- Figure 8.27** Current increase in day 1, 2, 3 and 7 of implantation when MPTP neurotoxin was administrated at a dossage of 18, 13, 8 and respectively 15 mg/kg after baseline stabilization; applied potential is -350mV.

CHAPTER 1

Carbon based composite electrodes

1.1 Generalities

The objective of setting the reasons for choosing and applying carbon electrodes for analytical applications makes the topic of the following discussion. As with any electrode material or electroanalytical technique, the choice depends on the application. There is no "ideal" electrode for all situations.

Why carbon materials in the forms of graphite, glassy carbon, carbon fibers, carbon nanotubes, etc., have been important players in solid electrode development are explained by the main advantages:

(i) They are available in a variety of forms and are generally inexpensive, especially when they are compared with other materials such as gold or platinum ;

(ii) The slow kinetics and high chemical inertia of carbon materials lead to a wide useful potential range, particularly in the positive direction. This characteristic is an important advantage over platinum and mercury, which exhibit significant or overwhelming background oxidation currents [1.1];

(iii) Carbon has a rich surface chemistry, which can be exploited to influence reactivity. In particular, a wide variety of chemical derivatizations is possible on graphite and glassy carbon surfaces [1.2];

(iv) Controlled variation of electron transfer kinetics and adsorption on carbon surface faces can be used to enhance analytical utility.

Overall, the mentioned advantages, combined with the fact that carbon materials present low electrical resistances and a highly pure crystal structure, yields low residual currents and consequently a favorable signal-to-noise-ratio. A key feature in any electrochemical sensor is a good detection limit that is associated with a high signal-to-noise ratio. The residual current and the noise in a macrosensor made of a pure conducting phase depends on the sensing area, meaning that a contraction of the sensing area produces a reduction in noise, reason why makes them suitable for various sensing and detection applications [1.3].

As defined by Tallman and Petersan [1.4], a composite sensing material is "a material consisting of at least one conducting phase commingled with at least one insulator phase". The two materials possess significantly different physical or chemical properties which remain separate and distinct at the macroscopic or microscopic scale within the finished structure.

The conductive materials involve the use of different carbon-based matrixes, such as: glassy carbon, graphite, fullerene, graphene, carbon fibers and nanotubes. The main purpose of the conducting phase in the composite is to supply the electrical conductivity needed for the conduction of the electrical signal. The second material, consisting in an agglutinating agent (insulator material), such as: epoxy resins, silicone, polyurethane, methacrylate resin, Teflon, etc. The main purpose of agglutinating agents is mechanical consistence assuring the durability and resistance to the electrolytic working medium.

The first classification that comes first is related to the nature of the conducting material (type of carbon used, which will be in detail discussed in the next section). Carbon-based materials are used frequently as conductive phase in composites used for electrochemical sensors. Conductive particles may be graphite (the most widespread

type), glassy carbon (GC). Other carbonaceous materials aside from carbon are used on rare occasions, such as charcoal, soot [1.5], carbon microspheres and foam [1.6], carbon nanotubes [1.7-1.8], and powdered diamonds [1.9].

Another classification is given by the arrangement of conducting particles in the polymer matrix. A composite formed from carbon fibers and an adhesive polymer matrix is an example where the carbon has an orderly distribution [1.10]. This ordered material is difficult to achieve. If the carbon is distributed randomly, the composite is easier to prepare. In this particular case, the conducting particles have the probability of occupying any given space in the matrix.

Moreover, composites can be classified according to their rigidity as rigid composites or soft composites (known also as pastes or inks). Paste electrodes contain a liquid binder, which is usually an electric insulator, such as paraffin oil, silicone oil, bromonaphtalene, and esters such as organosphospates and phthalates. If the matrix is a solid, it is usually a polymer, which is either simply dissolved in a corresponding solvent or consists of monomers which will undergo polymerization during the curing process. It can be generally be stated that the mechanical stability of solid electrodes is superior to paste electrodes. Nevertheless, paste electrodes are enormously important for the quick and simple testing of new designs, for developing and optimizing new analytical methods, and for performing certain analyses in the laboratory and occasionally also in the field.

In this field of composite electrodes, Adam [1.11] was the one who pioneered in 1950s the work by using carbon paste as electrochemical transducers. Also, several examples of composites electrodes can be found in the literature [1.12-1.18], that have been proposed for amperometric and voltammetric determinations in the quantifications of different analytes. Several reviews on carbon paste electrodes (CPEs) are present in literature [1.19], with their some undesirable features like low chemical and physical surface stability. At the beginning of the 1990s, amperometric sensors based on rigid composites started to appear as new composites with advantageous physical, mechanical, economical and electrochemical features.

Considering **carbon composites** (CC) in general, their properties present improvements over conventional solid carbon electrodes. These are due to some interesting advantages:

1. The mouldability of these composites permits the construction of sensors in different configurations and sizes such as planar, cylindrical, tubular or microsize electrodes. When the polymer is hardened the material can be machined, cut and polished without affecting its properties. The smoothing/polishing offer the advantage to provide fresh, active material ready to be used in a new assay (an interesting issue for biosensor devices), each new surface yields reproducible results because all individual compounds are homogeneously dispersed or compressed in the bulk of the composite.

2. The support for the conducting filler given by the polymer matrix, provides mechanical and chemical stability to the composite.

3. Low background currents since the electrode capacitance is strongly influenced by the exposed carbon.

4. Depending on the conductive load, composites can behave as microelectrode arrays which are known to provide efficient mass transport of the electroactive species due to the radial diffusion on the spaced carbon particles. Also, ensembles of microelectrodes are desirable. These ensembles/arrays can be seen as a macroelectrode formed by a great number of carbon fiber or graphite particles microelectrodes. These microelectrodes are separated by the insulator and connected

and the signal they produce is the sum of the individual currents generated by each microelectrode. This is why, the end product, is a sensor with a signal as strong as that of a macroelectrode but showing the signal-to-noise ratio of a microelectrode [art8-electrozi compositi]. The improved mass transport favors the sensitive electroanalysis of a variety of reagents, including electrocatalysts, enzymes and chemical recognition agents [1.20].

5. They can be easily miniaturized and show good compatibility, property that enabled early applications to in vivo electroanalysis of neurotransmitters [1.21-1.22].

Both particles themselves and the binder can be modified with redox catalysts or selective receptors, modified composite electrodes have found widespread biomedical applications ranging from the in vivo detection of nitric oxide [1.23] to bulk modified enzyme based biosensors [1.24-1.25], especially in amperometric biosensing devices [1.26].

The electrical properties of the composite depend on the nature of each of the components, their relative quantities and their distribution. The electrical resistance is determined by the connectivity of the conducting particle inside the polymeric matrix. This means that the relative quantity has to be studied to determine the optimal composition.

Polymer type has a significant effect on the amount of filler required for percolation. Polymer surface tension, crystallinity, polarity and molecular weight are the major factors affecting the percolation threshold [1.27-1.28]. Percolation threshold tends to increase with increasing polymer surface tension. The higher the polymer surface tension the lower the filler-polymer interfacial tension. At low filler-polymer interfacial tension, the polymer matrix can easily wet the filler particles and therefore distribute them well. Well distributed conductive fillers increase the percolation threshold. On the other hand, at high filler-polymer interfacial tension, filler particles tend to agglomerate and form a conductive network within the polymer matrix. Similarly, percolation threshold increases with increasing polymer polarity because of the better interaction between the filler and polymer will better distribute the filler. Better conductivity and lower percolation threshold could be achieved in a semi-crystalline polymer versus an amorphous polymer. Filler particles will be ejected from the crystalline region during crystallization and concentrate in the amorphous region.

1.2 Conductive fillers used in carbon-based composite sensing devices

1.2.1 Graphite

In order to understand the basic structure and properties of graphite, it is necessary to review its structure. Graphite is a dark gray, soft and porous material with adsorption capacity and is naturally abundant and highly conductive fillers (with an electrical conductivity of 10^4 S cm^{-1} at ambient temperature) for conducting polymer composites [1.29] and electrical resistivity is $50 \mu\Omega\cdot\text{m}$ [1.30] and its density is $1.95\text{-}2.3 \text{ g cm}^{-3}$. In graphite, the carbon atoms are only bonded in two dimensions, each carbon atom is sp^2 hybridized. The carbon atoms are arranged hexagonally in a planar condensed ring (see Figure 1.1). Also, the layers are stacked parallel to each other, with the atoms within the rings bonded covalently, whereas the layers are loosely bonded together by Van der Waal's forces. The

anisotropic nature of graphite is the result of the two types of bonding acting in different crystallographic directions. The ability of graphite to form a solid film lubricant may be attributed to these two contrasting chemical bonds. The weak Van der Waal's forces govern the bonding between the individual layers and also there are no bonds between the layers, the layers can easily slip off one to another, making it an ideal lubricant, and resulting in a reduced coefficient of friction.

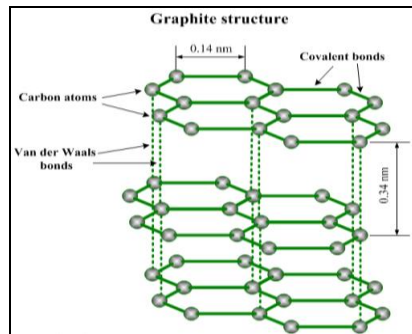


Figure 1.1 Graphite structure

On the other hand, given the good electro-catalytic properties, the graphite has been used as an electrode material in the construction of disposable amperometric biosensors for the detection of various analytes such as ethanol, phenol and glucose an many others [1.31-1.33].

1.2.2 Carbon nanofibers and carbon nanotubes

Carbon nanotubes

Carbon nanotubes (CNTs) are hexagonal networks of sp^2 carbon atoms, that can be considered as graphite layers rolled-up into a cylinder [1.34]. Depending on the arrangement of their grapheme cylinders, there are two types of nanotubes: single-walled nanotubes (SWNTs) (they present one single layer of grapheme cylinder) and multi-walled nanotubes (MWNTs) (approximately 50 layers) as shown in Figure 1.2.

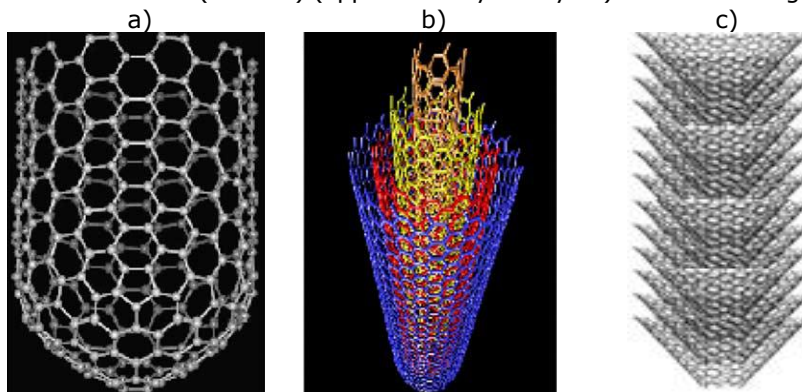


Figure 1.2 Schematic illustration of a) SWNTs (figure from [1.35]), b) MWNTs (figure from [1.36]) and c) carbon nanofiber structure [1.37];

Carbon nanotubes present extraordinary properties that make them the strongest and most flexible molecular material known due to the unique C-C covalent bonding. They present the 100 time tensile strength of steel, thermal conductivity better than all but purest diamond, and electrical conductivity similar to copper with the ability to carry much higher currents. Some properties are stated in Table 1.1.

Table 1.1: Properties of CNTs

Electrical	CNTs can be very conductive hence they are metallic; they can carry the highest current density of any known material, measured around 10^9 A/cm ² [1.38].
Mechanical	It associates high flexibility and high strength with high stiffness; the nanotube as a whole is very flexible because of the great length (1 to 50 μ m for those grown by CVD) [1.39].
Chemical	High specific surface and σ - π rehybridization facilitate molecular adsorption, doping and charge transfer
Thermal and thermoelectric	Are the stiffest known fibers with a measured Young's as high as 1-1.4 TPa [1.40] and a Tensile Strength of 50 GPa [1.41]. Thermal conductivity is also very high, typically about 1750-5800 W/mK [1.42].

For the use in sensing applications, CNT are associated with certain limitations like method of synthesis or purification. Generally, three techniques are used for producing CNTs: carbon arc discharge [1.43], laser ablation technique [1.44] and chemical vapor deposition. From all these preparation methods, nanotubes come with a number of impurities and they can be purified most of the times by oxidation [1.45-1.46], nitric acid boiling solutions [1.47] or sonication, but all purification methods can change the structural surface of CNTs by changing their final electrical and mechanical properties. Another limitation is that before their use in analytical assays, CNT must be first transformed in a soluble product, suitable for processing into thin films or for other applications of great importance.

One of the most emerging applications as sensors, it that CNT have been reported to promote a direct electron transfer between an immobilized enzyme and electrode, due to the low overpotentials of electron transfer reactions take place, fact that increased interest in researcher to couple CNT-based sensors with enzymes [1.48].

On the other hand, due to enzyme leakage limitations and its life cycle, sensing materials that promote the non-enzymatic detection of biological molecules are also of high interest [1.51].

1.3 Epoxy as binding material

The polymer is chosen according to the sensor application. For example, if a biological modification is part of the construction procedure, a polymer that calls for high curing temperatures should not be used. The same is true if the polymer contains additives which are harmful to the biological material. When a chemical modification is necessary (addition of redox mediators, catalysts, etc.) the modifying substance should not interfere with the curing of the polymer. Finally, consideration

should be given to the environment in which the sensor is going to be applied, such as a living organism, an aqueous or organic solution, a biofluid, etc. a few examples are epoxy, silicone, polyurethane, polystyrene, methacrylate or Teflon composites.

Epoxy resins have been the most important class of thermosetting resins in industry with applications as coating, composite matrix, potting compounds, encapsulants, structural adhesives and many others. The versatility of applications are attributed to their excellent chemical properties, their good adhesion to other materials, and their excellent insulating characteristics. Furthermore, they are easily to prepare, inexpensive and widely available [1.49]. The addition of powdered fillers, metallic or carbonaceous, may increase their electrical and thermal conductivity while keeping their ease of machining and their malleability.

Epoxy resin is defined as a molecule containing more than one epoxide group. The curing process is a chemical reaction in which the epoxide groups in epoxy resin react with a curing agent (hardener) to form a highly cross linked, three-dimensional network (see Figure 1.3). In order to convert epoxy resins into a hard, infusible, and rigid material, it is necessary to cure the resin with hardener. Epoxy resins cure quickly and easily at practically any temperature from 5-150°C depending on the choice of curing agent.

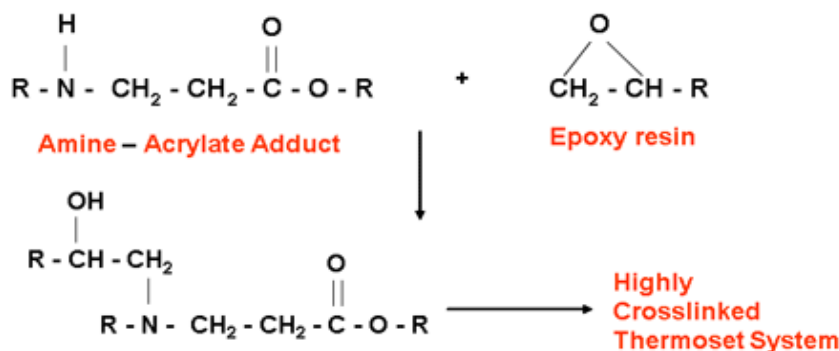


Figure 1.3 Reaction between epoxy resin and amine based curing agent (hardener)

The stoichiometry of the epoxy-hardener system also affects the properties of the cured material. Employing different types and amounts of hardener which, tend to control cross-link density vary the structure. The amine and phenolic resin based curing agents, are widely used for curing of epoxy resins.

Amines are the most commonly used curing agents for epoxy cure. Primary and secondary amines are highly reactive with epoxy. The use of some specific hardeners require the addition of an accelerator in order for the resin-hardener system to actually harden. Tertiary amines are generally used as catalysts, commonly known as accelerators for cure reactions. Use of excessive amount of catalyst achieves faster curing, but usually at the expense of working life, and thermal stability. The catalytic activity of the catalysts affects the physical properties of the final cured polymer.

1.4 Graphite-epoxy composite electrodes

Graphite and epoxy resins are employed to construct rigid composites that can be used in aqueous or nonaqueous media. In [1.50], was showed a comparison

study of the behavior of different rigid composites matrixes for the construction of amperometric tyrosinase biosensors, widely used for the detection of phenolic compounds. They presented the advantage of graphite-epoxy composites (GEC) over carbon paste composite in their tolerance to organic solvents, due to a better reproducibility of the amperometric measurements both with and without regeneration of the electrode surface by polishing.

1.4.1 Preparation of GEC composites

The epoxy composites filled with graphite are prepared, most of the times by solution intercalation method, where graphite is added to the mixtures of epoxy resin and curing agent. The materials are mechanically homogenized, in order for the epoxy resin to intercalate inside the conductive fillers, especially into the graphite layers and pores, as presented in figure 1.4. After mixing, the composite is submitted to the curing process that usually requires high temperatures.

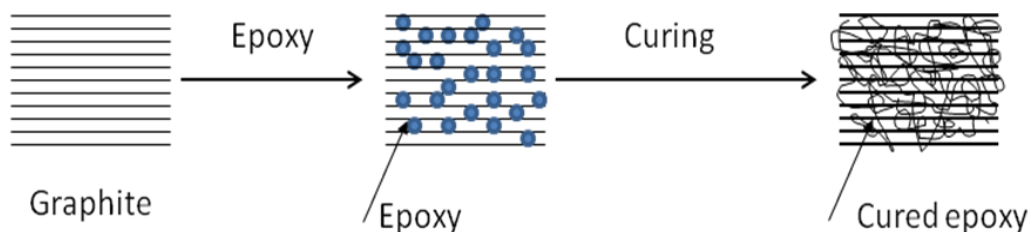


Figure 1.4 Schematic diagram showing the stages in epoxy composites preparation

1.5 Conclusions

The preferences of using carbon based materials when manufacturing electrochemical sensing devices is given by the advantages regarding their price and availability, large potential windows in experimental procedures, their rich surface chemistry, controlled kinetics and the adsorption possibility on their surfaces. As an overall advantage, it can be mentioned their low electrical resistance conducting to a favorable signal-to-noise ratio associated with improved detection limits.

Although, when considering carbon based composites, they are superior to conventional carbon electrodes due to the fact that carbon composites permits the construction of sensors in different configurations, being easily miniaturized, and allows polishing of the active surface offering in this way a new surface available for a new assay. They present low electrode capacitance and good compatibility with the biological environment. Graphite-epoxy based composite electrodes presented an advantage over carbon paste composites in their tolerance to organic solvents due to a better reproducibility in amperometric measurements.

The key feature in designing composite based electrodes is mainly due to their capability to behave as microelectrode arrays. Reason for which, the end product will have a strong signal of a macroelectrode but showing the signal-to-noise of a microelectrode improving the overall electroanalytical sensitivity.

1.6 References

- [1.1] M. Ates and A. Sarac, "Conducting polymer coated carbon surfaces and biosensor applications," *Progress in organic coatings*, vol. 66, pp. 337-358, 2009.
- [1.2] K. Kurt, S. Ivan, B. Marijo, V. Karel and W. Alain, "Electrochemical sensors and biosensors based on heterogeneous carbon materials," *Springer*, vol. 140, pp. 861-889, 2009.
- [1.3] W. J, *Analytical electrochemistry*, New York: Wiley-VCH, 2001.
- [1.4] C. Calixto and R. Mendes, "Development of graphite-polymer composites as electrode materials," *Material research*, vol. 10, pp. 109-114, 2007.
- [1.5] R. Adams, *Electrochemistry at solid electrodes*, New York: Dekker, 1969.
- [1.6] N. Edson and Z. Aldo, "Carbon paste electrodes made from novel carbonaceous materials: Preparation and electrochemical characterization," *Electrochimica acta*, vol. 54, no. 2, p. 582-589, 2008.
- [1.7] M. Rubianes and G. Rivas, "Carbon nanotubes paste electrode," *Electrochemical communications*, vol. 5, no. 8, p. 689-694., 2003.
- [1.8] R. Deo and P. Lawrence, "Detection of Homocysteine at Carbon Nanotube Paste Electrodes.," *Talanta*, 2004.
- [1.9] R. Stefan and S. Bairu, "Monocrystalline diamond paste-based electrodes and their applications for the determination of Fe(II) in vitamins," *Analytical Chemistry*, vol. 75, no. 20, pp. 5394-5398, 2003.
- [1.10] C. Lowry, H. Jhonatan and W. Mark, "Flow rate independent amperometric cell," *Analytical chemistry*, vol. 54, no. 14, p. 2532-2535, 1982.
- [1.11] R. Adams, "Carbon paste electrodes," *Analytical chemistry*, vol. 30, pp. 1576-1586, 1958.
- [1.12] L. Moreno, A. Merkoci and S. Alegret, "Graphite-epoxy composites as an alternative material to design mercury free working electrodes for stripping voltammetry," *Electrochimica acta*, vol. 48, no. 18, pp. 2599-2605, 2003.
- [1.13] A. Domenech and J. Alarcon, "Determination of hydrogen peroxide using glassy carbon and graphite polyester composite electrodes modified by vanadium doped zirconias," *Analytica chimica acta*, vol. 452, no. 1, pp. 11-22, 2002.
- [1.14] A. Domenech-Carbo, M. Domenech-Carbo, L. Osete-Cortina, J. Gimeno-Adelantado, F. Bosh-Reig and R. Mateo-Castro, "Electrochemical identification of metal ions in archeological ceramic glazes by stripping voltammetry at graphite polyester composite electrodes," *Talanta*, vol. 56, no. 1, pp. 161-174, 2002.
- [1.15] F. Albertus, A. Llerena, J. Alpizar, V. Cerda, M. Luque, A. Rios and M. Valcarcel, "A PVC graphite composite electrode for electroanalytical use. Preparation and some applications," *Analitica chimica acta*, vol. 355, no. 1, pp. 23-32, 1997.
- [1.16] J. Park, J. Ko, O. Park and D. Kim, "Capacitance properties of graphite polypyrrole composite electrode prepared by chemical polymerization of pyrrole on graphite fiber," *Journal power source*, vol. 105, no. 1, pp. 20-25, 2002.

- [1.17] H. Lee, J. Kim, J. Park, Y. Joe and T. Lee, "Performance of polypyrrole impregnated composite electrode for unitized regenerative fuel cell," *Journal of Power Sources*, vol. 131, pp. 188-193, 2004.
- [1.18] L. Navarro, J. Trijueque, F. Vicente and H. Scholl, "Voltammetric determination of optimal conductive load proportion in graphite epoxy composite electrodes," *Journal of electroanalytical chemistry*, vol. 379, pp. 159-163, 1994.
- [1.19] V. Stara and M. Kopanika, "Chemically modified carbon paste and carbon composite electrodes," *Electroanalysis*, vol. 1, pp. 13-16, 1989.
- [1.20] W. S and H. J, "Chemically modified carbon-based electrodes and their applications as electrochemical sensors for analysis of biologically important compounds. A review," *Analyst*, vol. 117, pp. 1215-1229, 1992.
- [1.21] P. Kissinger, J. Hart and R. Adams, "Voltammetry in brain tissue a new neurophysiological measurement," *Brain research*, vol. 55, p. 209-213, 1973.
- [1.22] R. O'Neill, R. Grunwald, M. Fillenz and W. Albery, "Linear sweep voltammetry with carbon paste electrodes in the rat striatum," *Neuroscience*, vol. 7, pp. 1945-1954, 1982.
- [1.23] E. Leung, "A novel nitric oxide in vivo sensor," *Chemical communications*, vol. 1, pp. 23-24, 1996.
- [1.24] W. Joseph, F. Lu, D. Lopez and H. Tobias, "Highly Selective and Sensitive Amperometric Biosensing of Glucose at Ruthenium-Dispersed Carbon Paste Enzyme Electrodes," *Analytical letters*, vol. 26, no. 9, p. 23, 1993.
- [1.25] F. Cespedes, E. Martinez and S. Alegret, "Amperometric glucose biosensor based on an electrocatalytically bulk-modified epoxy-graphite biocomposite," *Analytica chimica acta*, vol. 284, no. 1, p. 21-26, 1993.
- [1.26] T. Dodevska, E. Horozova and N. Dimceva, "Electrocatalytic reduction of hydrogen peroxide on modified graphite electrodes: application on the development of glucose biosensors," *Analytical and bioanalytical chemistry*, vol. 386, pp. 1413-1418, 2006.
- [1.27] J. Huang, "Carbon black filled conducting polymers and polymer blends," *Advances in polymer technology*, vol. 21, no. 4, pp. 299-313, 2002.
- [1.28] K. Miyasaka, K. Watanabe, E. Jojima, H. Aida, M. Sumita and K. Ishikawa, "Electrical conductivity of carbon polymer composites as a function of carbon content," *Journal of material science*, vol. 17, no. 6, pp. 1610-1616, 1982.
- [1.29] X. Du, M. Xiao and Y. Meng, "Synthesis and characterization of polyaniline graphite conducting nanocomposites," *Journal of polymer science part B: Polymer physics*, vol. 42, pp. 1972-1978, 2004.
- [1.30] R. Sengupta, M. Bhattacharya and S. Bondyopadhyay, "A review on the mechanical and electrical properties of graphite and modified graphite reinforced polymer composites," *Progress in polymer science*, In press.
- [1.31] A. Kirgoz, D. Odaci, S. Timur, A. Merkok, S. Alegret, T. Besun and A. Telefoncu, "A biosensor based on graphite epoxy composite electrode for aspartame and ethanol detection," *Analytica chimica acta*, vol. 570, pp. 165-169, 2006.
- [1.32] X. Llopis, A. Merkoci and S. Alegret, "Integration of a glucose biosensor based on an epoxy graphite TTF TCNQ GOD biocomposite into a FIA system,"

- Sensors and actuators B:Chemical*, vol. 107, no. 2, pp. 742-748, 2005.
- [1.33] P. Mailley, E. Cummings, S. Mailley, B. Eggins, E. McAdams and S. Cosnier, "Composite carbon paste biosensor for phenolic derivates based on in situ electrogenerated polypyrrole binder," *Analytical chemistry*, vol. 75, pp. 5422-5428, 2003.
- [1.34] M. Dresselhaus, G. Dresselhaus and P. Eklund, *Science of fullerenes and carbon nanotubes*, New York: Academic press, 1996.
- [1.35] W. Yihong, "Carbon nanowalls," [Online]. Available: <http://www.ece.nus.edu.sg/showcase/Wiyihong.htm>.
- [1.36] A. Rocherfort, "Nano-CERCA," [Online]. Available: http://www.cs.infn.it/de_martino_1.ppt.
- [1.37] C. Wei and D. Srivastava, "Nanomechanics of carbon nanofibers: structural and elastic properties," *Applied physical letters*, vol. 85, no. 12, pp. 2208-2228, 2004.
- [1.38] B. Wei, R. Vajtai and P. Ajayan, "Reliability and current carrying capacity of carbon nanotubes," *Applied physical letters*, vol. 79, pp. 1172-1174, 2001.
- [1.39] "Department of electronic materials engineering, The Australian National University, Canberra," [Online]. Available: <http://www.anutech.com.au/TD/InfoSheets/Nanotubesbrochure.pdf>.
- [1.40] M. Yu, B. Files and S. Arepalli, "Tensile Loading of Ropes of SingleWall Carbon Nanotubes and their Mechanical Properties," *Physical review letters*, vol. 84, no. 24, pp. 5552-5555, 2000.
- [1.41] "Carbon nanotechnologies," [Online]. Available: <http://www.cnanotech.com>.
- [1.42] J. Hone, M. Whitney, C. Piskoti and A. Zettl, "Thermal conductivity of single walled carbon nanotubes," *Physical review B*, vol. 59, no. 4, 1999.
- [1.43] S. Iijima, P. Ajayan and T. Ichihashi, "Growth Model for Carbon Nanotubes," *Physical review letters*, vol. 69, 1992.
- [1.44] A. Thess, R. Lee and H. Nikolaev, "Crystalline Ropes of Metallic Carbon Nanotubes," *Science*, vol. 273, 1996.
- [1.45] S. Gajewski, H. Meneck and K. Tanigaki, "Purification of single walled carbon nanotubes by thermal gas phase oxidation," *Diamond and related materials*, vol. 12, pp. 816-820, 2003.
- [1.46] H. Hiura and T. Ebbesen, "Opening and purification of carbon nanotubes in high yields," *advanced materials*, vol. 7, p. 275-276, 1995.
- [1.47] D. Erik, E. Thomas, K. Ajit and T. Michael, "Purification of Single-Shell Nanotubes," *Advanced materials*, vol. 10, pp. 611-613, 1998.
- [1.48] S. Wang, Q. Zhang, R. Wang and S. Yoon, "A novel multi-walled carbon nanotube-based biosensor for glucose detection," *Biochemical and biophysical research communications*, vol. 311, p. 572-576, 2003.
- [1.49] D. Marcel, *Epoxy resins*, New York: Chemistry and technology, 1988.
- [1.50] B. Serra and A. Pinggaron, "Composite multienzyme amperometric biosensors for an improved detection of phenolic compounds," *Electroanalysis*, vol. 15, no. 22, pp. 1737-1744, 2003.
- [1.51] A. Pop, F. Manea, C. Orha, S. Motoc, **E. Ilinoiu**, N. Vaszilcin and J. Schooman, "Copper decorated carbon nanotube based composite electrodes for non-enzymatic detection of glucose," *Nanoscale research letters*, in press.

CHAPTER 2

Chemically modified electrodes

Because among the working sensing device that make the subject of this thesis enter in the category of chemically modified electrodes, a brief introduction in what they consist in is necessary.

2.1 Generalities

In order to broaden the applicability of electrode materials, they can be chemically modified. The reasons for improvements include increased selectivity, sensitivity, chemical and electrochemical stability, as well as a larger potential window and improved resistance to fouling. The need for improved electrodes performances has achieved a rapidly growth in many areas of science.

The definition of a **chemically modified electrode (CME)** is: a conducting or semiconducting material that has been coated with a monomolecular, multi-molecular, ionic, or polymeric film (termed adlayer) which alter the electrochemical, optical and other properties of the interface [2.1-2.2]. The conductive and semiconductive substrates are derived from conventional electrode materials while the adlayers are widely diverse in either origins and properties.

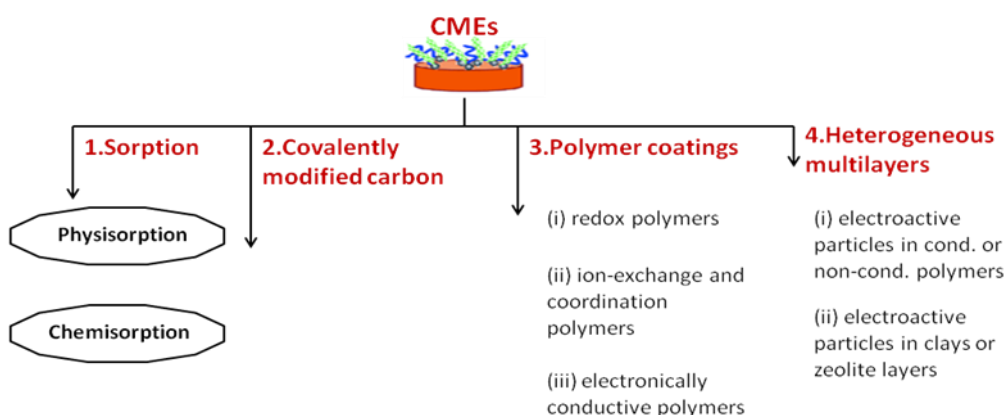


Figure 2.1 Schematic representation for various kinds of CMEs preparation routs

The substrate is the platform electrode that supports the adlayer. Commercially available or custom fabricated substrates can be used. While any conventional electrode material can serve as a substarte, some materials are more convenient to modify. Of the conductive materials, Au, Ag, and Pt are the most commonly modified [2.3]. These surfaces benefit from the ease with which reproducible and clean surfaces can be produced and maintained in the laboratory environment. Carbon electrodes [2.4-2.5], are also commonly employed for similar reasons.

Modified electrodes can be classified (see figure 2.1) by the film-substrate attachment method (e.g., physisorption, chemisorptions, and covalent attachment) and film composition (e.g., clays, zeolites, sol-gels, polymers, NDA, etc). The choice of modification method and film identity stays in demand and its end-application. Multiple combinations of attachments methodologies and film compositions may be realized.

The graphite-epoxy composites microelectrodes, that make the subject of this thesis, were modified with zeolite materials, Nafion polymer films, and carbon nanofiber/nanotube films. Only these categories of modified sensing devices will be further discussed.

2.2 Zeolite modified electrodes

Zeolite modified electrodes (ZMEs) become popular in the mid '80s. They form a subcategory of the so-called "chemically modified electrodes" (CMEs), in which the modifying agent is an inorganic material.

Within the last decade, numerous studies have been devoted to understanding the physico-chemical properties of zeolites. Some of the principal advantages of zeolites are their low cost of extraction, their availability in great volumes, and their excellent stability in chemical and thermal processes. The aluminosilicates zeolites, when incorporated into an electrochemical interphase, offer a number of chemical, physical and structural characteristics of high interest in the design of electroanalytical systems: shape, size and charge selectivities, physical and chemical stability, high ion-exchange capacity and hydrophilic character [2.6-2.9].

Firstly, zeolites combine the advantages of ion exchange voltammetry with their molecular sieving properties. They can therefore distinguish between the reactants small enough to diffuse freely within the zeolite framework, and those excluded from the structure, and thus, not directly involved in the mass transport reactions.

Secondly, new electroanalytical devices (sensors) can be developed. By combining the attractive properties of zeolite-like molecular sieves (size selectivity, ion exchange capacity, high thermal and chemical stability) with the high sensitivity of modern electrochemical techniques, improvements should be observed as compared to the other sensors based on chemically modified electrodes.

The **third** reason for investigating ZMEs is related to their possible use in electroanalysis. Zeolites attract interest for this application because they offer a selectivity based on the size (and shape) of the reactants, together with a tridimensional lattice made of interconnected cages of molecular dimension coming in a variety of support sites for various catalysts.

2.2.1 Zeolite structure

In terms of structure, zeolites are hydrated crystalline aluminosilicate minerals, natural or synthetic, with the general formulation $(C^{n+})_x[(AlO_2)_{n-x}(SiO_2)_y] \cdot m(H_2O)$ which are widely used adsorbents, ion exchangers, or catalysts. Literature is overflowing with information on this subject and reviews or books dealing with zeolite sciences (occurrences, synthesis, characterization, modification, and uses in various fields of application) [2.10-2.14].

The zeolite structure is based on a three-dimensional network of Al- or Si-centered tetrahedral which are linked to each other via doubly bridging oxygen atoms. This continuous three-dimensional pattern forms a system of cages and channels of defined dimensions with minimum and maximum diameters, conferring to the zeolites unique molecular sieving properties applied to both shape and size molecular discrimination. Adsorption of guest molecules may occur both on the external and internal surfaces of a zeolite crystal. Intercrystalline adsorption occurs by diffusion of the guest molecule into the channels and cavities of the zeolite only when the kinetic diameter of the guest molecule is smaller than the diameter of the cavity [2.15].

Substitution of Si^{4+} by Al^{3+} defines the excess negative charge of the framework requiring the introduction of charge-compensating cations (C^{n+}) into the structure. These extra-framework cations are not covalently bound to the zeolite structure, they have considerable freedom of movement and can be readily substituted with a variety of other cations, conferring ion exchange properties to these aluminosilicates.

The ion-exchange behavior of zeolite depends on a series of factors including the framework structure, ion size and shape, charge density of the anionic framework, ionic charge and concentration of the external electrolyte solution [2.16-2.17]. In the same time, the size, number and position of the exchanged cations contribute significantly to the catalyst activity [2.15].

2.2.2 Types of zeolites

Since the original discovery of zeolitic minerals in a volcanogenic rock, zeolitic tuffs have been found in many areas of the world. Up to date, approximately 170 conventional types of zeolites have been prepared in synthetic form and about 63 are present as natural compounds [2.18-2.19]. Only 6 of the natural zeolites commonly occur in large beds: analcime (ANA), chabazite (CHA), clinoptilolite (HEU), erionite (ERI), modernite (MOR), and phillipsite (PHI) [2.20].

Among the natural zeolites, clinoptilolite is the most abundant and widely used in the world. Many zeolites can be synthesized with SiO_2 higher or lower than in nature for the same framework type. Higher SiO_2 generally gives greater hydrothermal stability, stronger-acid catalytic activity, and greater hydrophobicity as adsorbents. Conversely, lower SiO_2 gives greater cation exchange capacity and high adsorbance for polar molecules. Controlling these synthesis process optimizes a zeolite for different applications.

Although, zeolites did not find any significant commercial use until synthetic zeolites were discovered and developed (large, mineable deposits of natural zeolites were not discovered until the late 1950s). Several research applications especially as support for catalysts, in heterogeneous photocatalysis for water treatments have been reported [2.49-2.51]. With Barrer's 1948 synthesis of small-pore modernite at high temperatures and pressures started the area of synthetic zeolites [2.21].

From 1949 through the early 1950s, the commercially significant zeolites A, X and Y were discovered by Milton and Breck at the Tonawanda, New York, laboratories of the Linde Air Products Division. Many of the new synthetic zeolites had larger pore size than most of the known natural zeolites, allowing applications involving larger molecules. In addition, many had larger pore volume, giving higher capacity.

In 1953, Linde Type A zeolite became the first synthetic zeolite to be commercialized as an adsorbant to remove oxygen impurity from argon [2.22].

Zeolite A, is a kind of molecular sieve that has a crystal cubic lattice structure. Zeolite A is usually produced in sodium form. Zeolite A is one of the most important molecular sieves because of its high adsorption capacity.

Different Si and Al sources are used for the synthesis of zeolite A. Clinoptilolite can be considered both Si and Al source but depending on the Si/Al ratio of clinoptilolite, only one source can be considered from clinoptilolite [2.23].

2.2.3 Preparation methods

Due to the electronically insulating character of zeolites, their implication in electrochemistry requires close contact to an electronically conducting material, various strategies being applied to prepare ZMEs from zeolite particles and conventional electrode materials. Conditions for a desired electrode material (e.g. low resistance and low capacitance, high mechanical stability, long-term durability, reproducible signals) are not easily achieved when zeolites are used as an electrode modifier. This is because its insulating character will lower the electrode conductivity, and individual solid crystals of micrometer dimensions and rigid structure will result in heterogeneous composition. Figure 2.2 shows that most ZMEs are prepared according to two main methods: (a) zeolite-polymer films coated on solid electrode surfaces and (b) bulky zeolite-carbon or zeolite-carbon-binder composites. The most widely used method to prepare ZMEs is the incorporation of the zeolite particle into the bulk of a so-called carbon paste. Carbon paste was invented a long time ago and consists of a homogeneous mixture of carbon powder and pasting liquid [2.24] giving good electrochemical characteristics to the final sensing device [2.25].

The use of mixtures of zeolite and graphite has been proposed since the 1980s. These mixtures are used in various forms, either as already mentioned carbon paste electrodes, where the carbon powder and the zeolite are mixed with a pasting wax [2.26] or liquid [2.27] or by pressing a mixture onto a metal grid [2.28] or disc [2.29], providing electrodes with good properties.

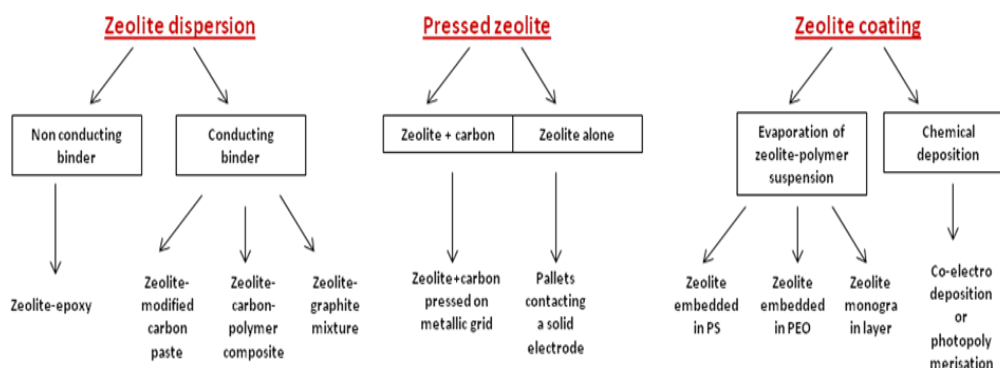


Figure 2.2 Different methods for ZMEs construction

2.2.4 Applications of zeolites in electroanalysis

The applications of ZMEs can be classified into five main categories, including molecular recognition, charge and mass transport characterization,

electrocatalysis, batteries, and electroanalysis. The analytical applications of ZMEs can also be classified into:

1. Direct amperometric detection;
2. Voltammetric detection after accumulation at open circuit;
3. Indirect amperometric detection of nonelectroactive species;
4. Amperometric biosensors;
5. Potentiometry using zeolite membranes;

Direct amperometric detection

The direct detection of electroactive species is achieved either by exchanging charge transfer mediators within the zeolite or by using the microporous solid as a support for the electrode itself.

Voltammetric detection after accumulation at open circuit

The voltammetric detection after accumulation recalls for the ion exchange capacity of the zeolite, which can be coupled to their size and charge selectivities, as well with subsequent electrochemical detection of the accumulated species. This has been applied for the determination of metal cations and some organic species.

The voltammetric analysis of mercury (II) at trace levels has been optimized in [2.30] in comparison with atomic absorption spectrometric experiments at a carbon paste electrode modified with a natural zeolite.

The accumulation of Ag^+ species by ion exchange at zeolite A in preconcentration/voltammetric measurements was investigated in [2.31] with good affinity results, where the accumulation by ion exchange was found to improve the voltammetric detection without any electrochemical preconcentration step.

Walcarius [2.32] investigated the relationship between the voltammetric response of ZMEs to Cu(II) and its ion exchange with Na(I). The conclusion explained why zeolites with large pores were preferentially used for the trace analysis of this specie.

Organic cations, e.g. methylviologen or dopamine were found to be easily accommodated by zeolites X or Y and further detected by voltammetry at ZMEs [2.33], [2.1]. By using a zeolite modified carbon paste electrode was found that with appropriate accumulation times, the quantitative determination of methylviologen was achieved in a wide concentration range, allowing further the establishment of the ion exchange isotherm associated to the methylviologen/sodium exchange in zeolite Y [2.1]. The selective detection of dopamine in the presence of ascorbic acid was achieved by Wang and Walcarius in [2.33] by using a carbon paste electrode modified by zeolite Y. A catalytic effect was observed for the oxidation of dopamine, while the presence of zeolite into the paste inhibited the response of ascorbic acid. Moreover, the positively charged dopamine was concentrated by zeolite while rejecting the ascorbic acid. The zeolite acted as a permselective substrate for the positively charged organic species, with no need of an additional membrane coated on the electrode surface.

Indirect amperometric detection of nonelectroactive species

Zeolites present the property to discriminate species on the basis of their size relative to the pore aperture of the aluminosilicate. If zeolites are efficient supports for the preconcentration of many small cations, they cannot normally

accommodate cations larger than their pore size. This peculiarity was exploited when using doped ZMEs for the indirect amperometric detection of species that cannot usually be detected by this way, this approach being considered one of the most elegant electroanalytical application.

This principle was used for the analysis of alkali metal cations in organic and hydroorganic media by using silver-exchanged zeolites X and Y modified electrodes [2.34]. The amperometric signals were monitored by the amount of Ag^+ that is released from the zeolite by ion exchange with the cationic analyte.

The methylviologen exchanged zeolite modified carbon paste electrode was used by Walcarius [2.35] for the amperometric detection of nonreducible cations in aqueous media. The electrode response was found to be dependent on both charge and size of the analyte: higher the positive charge of ions higher were the currents, while for the same charge the sensitivity was found to decrease when increasing the size of the hydrated cation.

The indirect detection process is mainly controlled by the kinetics of the ion-exchange reaction and thus by the diffusion of the cationic analytes within the zeolite framework, rather than by the affinity of the zeolite for one cation or another.

Amperometric biosensors

A biosensor consists of three components: a biological detection system, a transducer and an output system. An amperometric biosensor is an analytical device containing an immobilized biologically sensitive material in contact or integrated in an electrochemical transducer that ultimately converts a biological signal to a measurable electrical signal. One key factor in biosensor construction is the development of immobilization technologies for stabilizing biomolecules and tethering them to surfaces. An important possibility in this construction is the addition of an associated charge-transfer mediator that would increase the detection selectivity by lowering overpotentials. This should be mobile enough to act as a cofactor between the biomolecule and the electrode surface and at the same time sufficiently immobilized to ensure long-term stability.

The first example of zeolite-modified enzyme electrode is rather recent, since 1995 when Kotte [2.36] prepared a screen-printed thick-film sensor made of a polyurethane hydrogel immobilizing an enzyme (tyrosinase), coated on a mediator-modified carbon electrode containing zeolite particles. The role of the zeolite was clearly defined as being a host for the positively charged mediator (methylphenazonium) which was fixed on the Y-type zeolite by ion-exchange. Good sensitivities were found for the detection of eight phenolic compounds, but long term stability was not achieved. This introduces another use of zeolites in the biosensing field, by exploiting their ability to concentrate positively mediators by ion exchange. The mediation process often proceeds well, but long term stability of the biosensor suffers from leaching of the cationic mediator into the external solution as a consequence of back ion exchange with the supporting electrolyte cations [2.7], [2.37]. Another issue raised here is that although cationic mediators can be exchanged in zeolites and serve as efficient electron shuttle between the enzyme and the electrode surface, but due to the insulating character of the zeolite, a mediator is able to undergo the electron transfer reaction only after being exchanged by the cation of the supporting electrolyte. As a consequence, the reservoir of the mediator species in zeolites grows smaller as the number of experiments increases, due to their progressive leaching out to the solution.

Incorporation of zeolite particles into enzyme-based carbon paste bioelectrodes results in improved sensitivity and extended linear range. These were attributed to higher active enzyme loadings due to the formation of a porous paste network that exposes the enzyme contained in the interior of the paste to the substrate solution, thanks to the hydrophilic character of the zeolite [2.38-2.39]. This effect was further confirmed by using modified zeolite Y as a matrix to incorporate horseradish peroxidase and methylene green onto a glassy carbon electrode to fabricate a biosensor for hydrogen peroxide [2.38]. The high selectivity is the result of the combined use of methylene green as electron-transfer mediator, which minimizes interference from other electroactive species, and the selectivity of the zeolite Y membrane coating, which reduces interference from anionic species.

2.3 Coating electrodes with polymeric films

Polymer modification has been used with success for reducing adsorption phenomena of the non-electroactive interferences on the electrode surface during voltammetric scans.

In 1978, Miller's group and Bard's group showed that chemically modified electrodes could be prepared by coating electrode surfaces with polymer films [2.39-2.40]. This has since proven to be the most versatile approach for preparing chemically modified electrodes.

There are many reasons for the popularity of polymer films as electrode modifying agents. First, it is easy to prepare multilayer films using the polymer route, even if, the quantity of polymer deposited (i.e., the thickness of the film) can be reliable and reproducibly varied.

All these polymers can be divided in three main groups: (i) redox polymers, (ii) ion-exchange and coordination polymers, and (iii) electronically conductive polymers.

Redox polymers are polymers that contain electroactive functionalities either within the main polymer chain or inside groups pendant to this chain. One example is given by the poly(vinylferrocene).

Ion-exchange and coordination polymers are not electroactive themselves, but can incorporate electroactive guest molecules or counterions, where the most used one is du Pont's perfluorosulfonate ionomer, Nafion® [2.41].

The third class of polymers used to prepare chemically modified electrodes are the electronically conductive polymers [2.42], where the polymer chains in this family of materials are themselves electroactive.

A number of different methods can be used to prepare polymer film-coated electrodes. The simplest is to dip the surface to be coated into a solution of the polymer, remove the electrode from the solution, and allow the solvent to evaporate. While this method is simple, it is difficult to control the amount of material that ends up on the electrode surface. Polymer films can also be electropolymerized directly onto the electrode surface.

2.3.1 Implication of Nafion® in coating electrodes with polymeric films

Nafion® film-coated electrodes have an interesting early history. Such electrodes are prepared by applying a solution of the polymer to the electrode surface. However, prior to 1982, only du Pont knew how to dissolve the polymer,

and they gave solutions of this polymer to only U.S. laboratories. These laboratories showed that this polymer was an extremely interesting and versatile material for preparing chemically modified electrodes. Unfortunately, no other laboratory could get its hands on the polymer solution. This situation changed dramatically when Martin's group developed a procedure for dissolving the film form of Nafion®. Since then, Nafion® film-coated electrodes have become the most extensively investigated chemically modified electrodes.

Nafion® is one of the mostly conductive membranes, in spite of its well known limitations like high cost, low performance under low humidity and at high temperatures [2.43-2.44]. Above all, its preparation involves environmentally non-friendly fluorine based technology.

Nafion® is *highly conductive* due to its structural property. The material, Nafion®, consists of three regions (see figure 2.3): (i) a polytetrafluoroethylene-like backbone, (ii) side chains of $-O---CF_2---CF---O---CF_2---CF_2---$ which connect the molecule at backbone to the third region, and (iii) ion clusters consisting of sulfonic acid ions. A key property of sulphonic acid is that it is highly hydrophilic. So, when the membrane becomes hydrated, the hydrogen ions in the third region become mobile by bonding to the water molecules and moving between successive sulfonic acid groups.

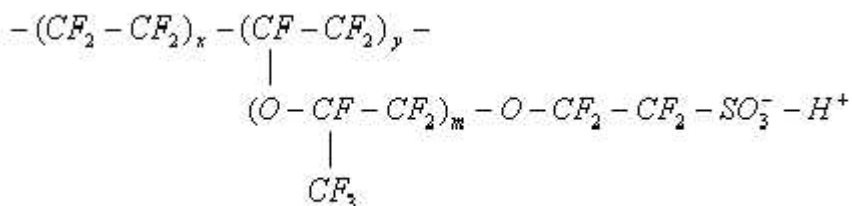


Figure 2.3 The chemical formula of Nafion®

The *high electronegativity* (i.e. electron affinity) of the fluorine atom, bonded to the same carbon atom as the SO_3H group, makes the sulfonic acid a superacid. Nafion® has the maximum electronegative environment possible, hence competing Nafion® with its conductivity may not be a good starting point.

In Nafion®, the *proton transport* is due to the classical ion-exchange mechanism [2.45]. Fully hydrated membrane contains a water phase similar to bulk water. The phase separation is caused due to the extreme hydrophobicity of the perfluorinated polymer with the extreme hydrophilicity of the terminal sulfonic acid group of the Nafion® [2.46]. In the presence of water the hydrophilic part is hydrated and helps in further phase separation. The hydrophobic part provides good mechanical stability even in the presence of water while the hydrated hydrophilic domains provides the high proton conductivity, separation that is not possible in other systems [2.47].

Starting with the pioneering investigations by Ralph Adams, electrochemists have become interested in the electrochemical detection of a class of amino-based neurotransmitters in living organisms. One of the most typical example representing the class of neurotransmitters is the molecule dopamine. Electrochemists showed that this molecule can be detected in the brains of living rats by surgically implanting electrodes into the rats' brain [2.48].

There is, however, a major problem with this analysis. The cerebral fluid analyzed also contains relatively high concentrations of ascorbate. Ascorbate is oxidized closely at the same potential as dopamine. Hence, ascorbate interferes with the determination of dopamine in the in vivo electrochemical analysis. The solution of this problem, coating the surface of the electrode to be implanted with a thin Nafion[®] film, came out of a collaborative research effort between Martin's group and Adam's group. To note that at physiological pH values, dopamine is a cation and ascorbate is an anion. Because Nafion[®] is a cation-exchange polymer, it transports dopamine but rejects ascorbate. Hence, the Nafion[®]-coated electrode provides the selectivity required for in vivo analysis of dopamine and other cationic neurotransmitters. The use of Nafion[®]-coated electrodes has become standard procedure for such investigations.

2.4 Conclusions

Starting from the idea that there is no "ideal" electrode, but only the ones that fit experimental expectations, electrode materials also have been submitted to chemical modifications to achieve better performances. In this direction, introducing aluminosilicates zeolites in electrochemical interphases, offer a number of chemically, physically and structural characteristics of high interest in the design of electroanalytical systems: shape, size and charge selectivity, physical and chemical stability, high ion-exchange capacity and hydrophilic character.

Although all desired properties for an electrode material are not easily achieved when zeolites are used as electrode modifiers due to their insulating character, but based on an optimal composition ratio of the zeolite modified carbon based composite, they find useful applications in various fields including direct amperometric detection, voltametric detection after accumulation in an open circuit, indirect amperometric detection of nonelectroactive species and amperometric biosensors.

Of main interest is considered the catalytic effect of zeolites towards the oxidation of positive charged molecules, acting as a permselective substrate for positively charged organic species, with no need for other additional membrane coated on the electrode surfaces.

The exploitation of zeolite's selectivity towards negative charged species is also applied in biosensor constructions in order to reduce interferences and as a matrix for enzyme immobilization.

The problem of zeolite carbon based composite biosensors arises when the final application is in-vivo implantation. Although there is no report, up to date, about this type of sensing devices used for in vivo application, we consider as typical example for all implanted devices the main interference of ascorbic acid, which requires that at the implantation moment electrodes to be coated with protective membranes for a minimum interference.

In the class of coated electrodes with polymeric films, Nafion provides the best protection especially for the class of amino-based neurotransmitters in living organisms, being considered now days a standard procedure for such investigations.

2.5 References

- [2.1] W. Kutner, J. Wang, M. L'her and R. Buck, "Analytical aspects of chemically modified electrodes: classification, critical evaluation and recommendations," *Pure applied chemistry*, vol. 70, pp. 1301-131, 1998.
- [2.2] R. Durst, "Chemically modified electrodes: Recommended terminology and definitions," *Pure and applied chemistry*, vol. 69, pp. 1317-1324, 1997.
- [2.3] A. Bard and I. Rubinstein, "Electrochemistry of organized monolayers of thiols and related molecules on electrodes," *Electroanalytical chemistry: A series of advances*, vol. 19, pp. 109-335, 1996.
- [2.4] L. McCreery and K. Kline, Carbon electrodes, New York: Marcel Dekker, 1996.
- [2.5] L. McCreery, Carbon electrodes: Structural effects on electron transfer kinetics, New York: Marcel Dekker Inc., 1984.
- [2.6] A. Walcarius, "Zeolite-modified electrodes in electroanalytical chemistry," *Electrochimica analytica acta*, vol. 384, p. 1-16, 1999.
- [2.7] D. Rolison, T. Nowak, A. Welsh and C. Murray, "Analytical implications of zeolites in overlayers at electrodes," *Talanta*, vol. 38, p. 27-35, 1991.
- [2.8] J. Lipkowski and P. Ross, The electrochemistry of novel materials, New York: VCH publishers Inc., 1994.
- [2.9] A. Walcarius, "Zeolite modified electrodes: analytical applications and prospects," *Electroanalysis*, vol. 8, pp. 971-985, 1996.
- [2.10] R. Barrer, Zeolites and clay minerals as sorbents and molecular sieves, London: Academic Press, 1978.
- [2.11] R. Townsend, "Properties and applications of zeolites," *Chemical society*, vol. 33, 1980.
- [2.12] A. Dyer, An introduction to zeolite molecular sieves, Chichester: Wiley, 1988.
- [2.13] R. Szostak, Handbook of molecular sieves, New York: Van Nostrand Reinhold, 1992.
- [2.14] H. Chon, S. Woo and E. Park, "Recent advances and new horizons in zeolite science and technology," *Study off surface science and catalysis*, vol. 102, 1996.
- [2.15] K. Ahmed, M. Sahar and S. Hanafy, "Exchanged zeolites with transition metals of the first period as photocatalysts for hexadecane degradation," *Journal of molecular catalysis A: Chemical*, vol. 288, pp. 52-57, 2008.
- [2.16] D. Bish and D. Ming, "Applications of natural zeolites in water and wastewater treatment,," *Natural zeolites: Occurrence, properties, applications*, vol. 45, pp. 519-550, 2001.
- [2.17] D. Kallo, "Applications of natural zeolites in water and wastewater treatment," *Natural zeolites: Occurrence, Properties, Applications*, pp. 519-550, 2001.
- [2.18] M. Gerardo, N. Eng-Poh, L. Louwanda and M. Svetlana, "What more in nanosized molecular sieves".
- [2.19] S. John, "Synthetic zeolites and other microporous oxide molecular sieves," *National academy of science*, vol. 96, p. 3471-3478, 1999.
- [2.20] R. Sheppard, "Zeolites in sedimentary deposits in the United States: A review," *Advances in Chemical series*, vol. 101, pp. 279-310, 1971.

- [2.21] R. Barrer, "Syntheses and reactions of mordenite," *Journal of the chemical society*, pp. 2158-2163, 1948.
- [2.22] Milton, "Molecular Sieves," *Soc. Of Chem. Ind. London*, p. 199-203, 1968.
- [2.23] K. Hossein, M. Hamid, K. Masoud and F. Farshid, "Synthesis of submicron zeolite LTA particles from natural clinoptilolite and industrial grade chemicals using one stage procedure," *Powder Technology*, vol. 196, p. 22-25, 2009.
- [2.24] R. Adams, *Electrochemistry at solid electrodes*, New York: Dekker, 1969.
- [2.25] D. Rolison, "Zeolites-modified electrodes and electrode-modified zeolites," *Chemical review*, vol. 90, p. 867, 1990.
- [2.26] M. Xu, W. Horsthemke and M. Schel, "Comparison of zeolite-modified electrodes with a graphite electrode: Postulated enhancement of electroactivity through stabilization of intermediates," *Electrochimica acta*, vol. 38, p. 919-925, 1993.
- [2.27] A. Walcarius, P. Mariaulle and L. Lamberts, "Use of a zeolite modified electrode for the study of the methylviologen - sodium ion exchange in zeolite Y," *Journal of electroanalytical chemistry*, vol. 463, pp. 100-108, 1999.
- [2.28] E. Briot, F. Bedioui and K. Balkus, "Electrochemistry of zeolite-encapsulated complexes: new observations," *Journal of electroanalytical chemistry*, vol. 454, p. 83-89, 1998.
- [2.29] M. Lemos, P. Sousa and F. Lemos, "Reactions Kinetics and the Development of Catalytic Processes," *Studies in surface science and and catalysis*, vol. 122, pp. 443-446, 1999.
- [2.30] P. Hernandez, E. Alda and L. Hernandez, "Determination of mercury(II) using a modified electrode with zeolite," *Journal of analytical chemistry*, vol. 327, pp. 676-678, 1987.
- [2.31] J. Wang and T. Martinez, "Accumulation and voltammetric measurement of silver at zeolite-containing carbon-paste electrodes," *Analytica chimica acta*, vol. 207, p. 95-102, 1988.
- [2.32] A. Walcarius and T. Barbaise, "Factors affecting the analytical applications of zeolite modified electrodes: preconcentration of electroactive species," *Analytica chimica acta*, vol. 340, pp. 61-76, 1997.
- [2.33] A. Walcarius and J. Wang, "Zeolite modified carbon paste electrode for selective monitoring of dopamine," *Journal of electroanalytical chemistry*, vol. 407, pp. 183-187, 1996.
- [2.34] M. Baker and C. Senaratne, "Effects of supporting electrolyte and zeolite co-cations on the electrochemical response of zeolite-modified electrodes," *Analytical chemistry*, vol. 64, pp. 3187-3192, 1992.
- [2.35] A. Walcarius, L. Lamberts and E. Derouane, "Cation determination in aqueous solution using the methyl viologen doped zeolite modified carbon paste electrode," *Electroanalysis*, vol. 7, pp. 120-128, 1995.
- [2.36] H. Kotte, B. Grundig, K. Vorlop, B. Strehlitz and U. Stottmeister, "Methylphenazonium-Modified Enzyme Sensor Based on Polymer Thick Films for Subnanomolar Detection of Phenols," *Analytical chemistry*, vol. 67, pp. 65-70, 1995.

- [2.37] B. Liu, F. Yan, J. Kong and J. Deng, "A reagentless amperometric biosensor based on the coimmobilization of horseradish peroxidase and methylene green in a modified zeolite matrix," *Analytica chimica acta*, vol. 386, p. 31–39, 1999.
- [2.38] A. Walcariu and J. Wang, "Zeolite containing oxidase-based carbon paste biosensors," *Journal of electroanalytical chemistry*, vol. 7, pp. 237–242, 1996.
- [2.39] B. Liu, R. Hu, H. Liu and J. Deng, "Studies on the Fabrication of a TCNQ - Mediating Glucose Biosensor Based on Immobilizing Enzyme in β Zeolite Matrix," *Acta chimica sinica*, vol. 56, pp. 682–687, 1998.
- [2.40] L. Miller and M. Van de Mark, "A poly-p-nitrostyrene electrode surface. Potential dependent conductivity and electrocatalytic properties," *Journal of american society of chemistry*, vol. 100, p. 3223–3225, 1978.
- [2.41] A. Merz and J. Bard, "A stable surface modified platinum electrode prepared by coating with electroactive polymer," *Journal of american society of chemistry*, vol. 100, p. 3222–3223, 1978.
- [2.42] M. Szentirmay and C. Martin, "Ion-Exchange Selectivity for Nafion films on electrode surfaces," *Journal of electrochemical society*, vol. 56, p. 1898, 1984.
- [2.43] C. Martin and S. Van Dyke, *Molecular design of electrode surfaces*, New York: John Wiley, 1992.
- [2.44] J. Sumner, S. Creager, J. Ma and D. Desmarteau, "Proton Conductivity in Nafion® 117 and in a Novel Bis[(perfluoroalkyl)sulfonyl]imide Ionomer Membrane," *Journal of electrochemical society*, vol. 145, pp. 107–110, 1998.
- [2.45] J. St-Pierre and D. Wilkinson, "Fuel cells: A new, efficient and cleaner power source," *AIChE Journal*, vol. 7, p. 1482–1486, 2001.
- [2.46] D. Siuzdak and K. Mauritz, "Perfluorosulfonate ionomer/mixed inorganic oxide nanocomposite via polymer in situ gel chemistry," *Chemical materials*, vol. 7, pp. 192–200, 1995.
- [2.47] K. Kruer, "On the development of proton conducting polymer membranes for hydrogen and methanol fuel cells," *Journal of Membrane Science*, vol. 185, p. 29–39, 2001.
- [2.48] V. Baglio, A. Arico, V. Antonucci, I. Nicotera, C. Oliviero, L. Coppola and P. Antonucci, "An NMR spectroscopic study of water and methanol transport properties in DMFC composite membranes: Influence on the electrochemical behaviour," *Journal of power sources*, vol. 163, p. 52–55, 2006.
- [2.49] L. Colar, **E. Ilioiu**, F. Manea, R. Pode and C. Lazau, "Photocatalytic activity of a silver doped TiO₂ modified zeolites in the degradation of reactive yellow 125 azo dye," *Environmental engineering and management journal*, vol. 11, pp. 61–68, 2012.
- [2.50] **E. Ilioiu**, R. Pode, F. Manea, L. Colar, A. Jakab, C. Orha, C. Ratiu and C. Lazau, "Photocatalytic activity of a nitrogen doped TiO₂ modified zeolite in the degradation of Reactive Yellow 125 azo dye," *Journal of Taiwan Institute of Chemical Engineers*, p. DOI:10.1016/j.jtice.2012.09.006, 2012.
- [2.51] L. Colar, **E. Ilioiu**, S. Motoc, F. Manea, R. Pode and G. Burtica, "Photo-degradation of phtachlorophenol in the aqueous solution," *Chemical Bulletin of Politehnica Timisoara*, vol. 55, pp. 55–58, 2010.

CHAPTER 3

Introduction in microsensors applied in electroanalysis

3.1 Generalities

Chemical sensors are increasingly used in numerous applications, such as analysis setups, chemical processes, food industry, environmental control (water, air, industrial wastes, combustion monitoring, etc.), and biomedical applications (analysis and monitoring). Other new fields of applications could arise in the near future. Electrochemical sensors are particularly attractive because the chemical quantities which are measured are directly transduced in electrical signals. In this field, digital electronic development is a tool which is well suited for sophisticated devices. The basic idea in miniaturization techniques is to adapt microelectronic technology to the fabrication of electrochemical sensors.

The term "microsensor" is used to define sensors with at least one dimension not greater than 25 μm , miniaturization being an important direction in the field of analytical chemistry and biochemistry. Their small size, make them extremely useful to analyze small analyte concentrations and can be applicable in small spaces.

Microsensors were pioneered in 1940s, by the work of Lydersen [3.1], who attained a fast current stabilization at a 25 μm radius Pt disc. Later, in the 1970s, miniaturized electrodes were used for in-vivo measurements [3.2-3.3]. Their beneficial properties have been recognized during 1980s, when the microelectronics technology made it possible to measure reliably very low currents and to construct reproducible very small electrodes. Of course, there are still problems that require much attention in their design and applications.

3.2 Configurations of microelectrodes

Electrodes of different materials have been miniaturized in many geometrical shapes, see figure 3.1. In addition, because the electrodes themselves are smaller than their associated diffusion layers, arrays of closely spaced microelectrodes have also been of considerable practical and theoretical interest.

Special attention should be given to proper sealing (between the active surface and the insulating sheath) to assure good performances and to minimize stray capacitance. The choice of the electrode geometry depends on the objectives of the experiment.

Diffusion is the most commonly encountered mode of mass transport in microelectrode experiments, and each electrode geometry leads to a different solution to the relevant diffusion equations. Hence, each geometry has a unique current-voltage relationship.

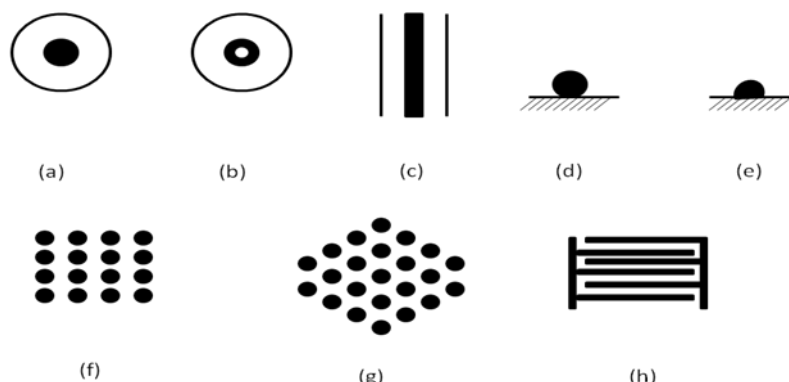


Figure 3.1 Types of microelectrode geometries (a) disc; (b) ring; (c) band; (d) sphere; (e) hemisphere; (f) square array; (g) hexagonal array; (h) interdigitated microband.

Cylindrical electrodes. The practical advantage of a cylinder electrode is that while it has a micrometer sized radius and thus exhibits the beneficial features of a microelectrode, its length gives rise to easily measured currents so that high-sensitivity potentiostats are not required.

Disk electrodes. For disk electrodes, the quality of the seal is very important.

Band electrodes. They exhibit the properties of microelectrodes by virtue of their narrow width, yet pass large currents due to their length.

Ring electrodes. They have been of interest because they can be constructed with very small surface areas.

3.3 Properties of microelectrodes

When the dimensions of a working electrode became progressively smaller, the behavior of the electrode begins to depart from that of a large electrode which can be approximated by an electrode of infinite dimension. These differences are caused by changing conditions of the mass transport from the bulk of solution toward the electrode and have several practical implications.

3.3.1 Single microelectrodes

The most important factor determining the behavior of an electrode is the mass transport in solution in the vicinity of the electrode. When considering an uncomplicated charge-transfer reaction, the voltammetric current signal is proportional to the flux of the electroactive substance toward the solution-electrode interface described by Fick's first law.

A reaction occurring at the surface of the electrode produces a concentration gradient in solution in the vicinity of the electrode, which in turn give rise to a diffusional flux described by the Fick's second law, which states that the time-dependent changes in the concentration of the substance amount caused by the flux, as presented in eq.3.1 [3.4]:

$$\frac{\partial C}{\partial t} = D\nabla^2 C \quad (3.1)$$

where C is the concentration of diffusing species, t is time, D is the diffusion coefficient, and ∇ is the so-called Laplacian diffusion operator.

The diffusion operator takes on a different form for each diffusion geometry, so that Fick's second law has a unique solution for each electrode geometry. The total diffusion-controlled current is composed of the planar flux and radial flux diffusion components:

$$i_{total} = i_{planar} + i_{radial} \quad (3.2)$$

For disk, spherical, and hemispherical geometries, the general expression for the radial component in eq.2 is given by eq.3:

$$i_{radial} = arnFDC \quad (3.3)$$

where r is the electrode radius and a is a function of the electrode geometry. For disk, spheres, and hemispheres the a value are equal to 4, 4π , and 2π , respectively. Such radial diffusion leads to a larger flux at the perimeter of the electrode than at the center, and hence to a nonuniform current density.

The extent to which the planar or radial component dominates depends on the relative dimensions of the electrode and the diffusion layer, as expressed by the dimensionless parameter Dt/r_0^2 where t is the electrolysis time and r_0 is the smallest dimension of the electrode [3.5]. For large (>1) values of Dt/r_0^2 (i.e., diffusion layer thickness that exceeds the size of the electrode), the current approaches steady state, and sigmoidal voltammograms are observed. In contrast, planar diffusion dominates at $<1/r_0^2$, and a peak-shaped behavior is observed. Hence, depending on the time scale of the experiment (i.e., scan rate), the same electrode may exhibit peak-shaped or sigmoidal voltammograms.

3.3.2 Composite microelectrodes

If the theory of single microelectrodes is well established, with even precise analytical expressions, in contrast, the theory of composite microelectrodes is still not well developed due to their complexity.

Although, composite microelectrodes couple the advantages of single microelectrode systems with significantly higher currents due to larger surface areas [3.6]. They can generally be divided into array microelectrodes and ensemble electrodes, depending whether the surface of the composite microelectrodes consists of uniform (array) or random (ensemble) dispersions of a conductor region within a continuous insulating matrix. Typically, the surface of an assembly is inlaid with plenty of dispersed conducting carbon micro disks, embedded in epoxy resin.

Unlike single microelectrodes, for microelectrode arrays, the geometry of microelectrodes, i.e., the ratio of interelectrode distance or spacing to the electrode dimension (e.g., electrode diameter for disc microelectrodes), have to be considered, in order to get a collective current response while maintaining the excellent features if single microelectrodes.

When considering the diffusional flux toward a microelectrode array, three principal cases can be distinguished [3.7-3.8]:

- The gaps between the individual electrodes are wide compared to the diffusion layer thickness. Thus, the diffusion layers of the individual electrodes do not overlap. This separation of diffusion layers occurs for $\delta < d/2$, where the total width is $d = d_e + d_g$, where δ being the diffusion layer thickness, d_e being the electrode width equivalent to $2r$, and d_g being the gap width. The microelectrodes do not affect one another and the overall current measured is the sum of the currents passing through the individual microelectrodes.
- If $\delta > d/2$, then the diffusion layers of the individual microelectrodes, A and B, partially overlap (Figure 3.2). The angle ψ represents the degree of overlap. The overall current is then smaller than the sum of the currents passing through the microelectrodes when they operate independently.
- For the value $\psi = \pi/2$, (i.e., when $\delta \gg d/2$) the diffusion layers totally overlap so that the array behaves as a continuous microelectrode having the surface area equal to that of the whole array. Under these conditions, the signal is proportional to the surface area of the whole array, while the noise is proportional only to the area of the microelectrodes. Thus, the signal-to-noise is greatly improved.

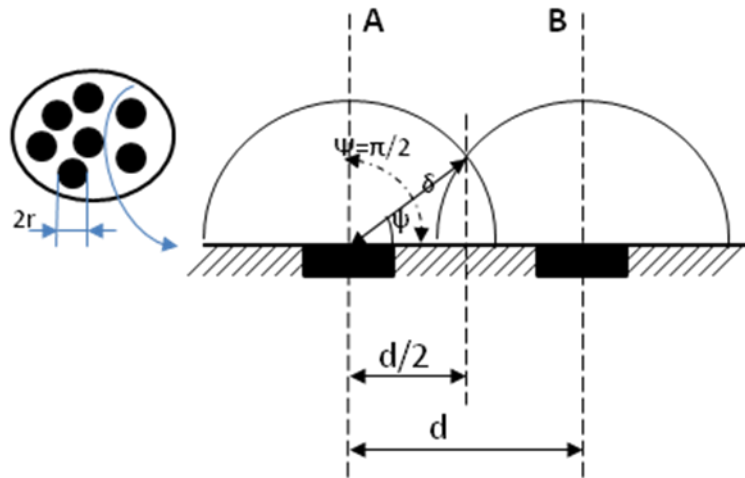


Figure 3.2 Diffusion layer overlapping at closely spaced microelectrodes in a composite structured microelectrode

Ideally, an array of microelectrodes should yield a current amplification by a factor of m relative to a single microelectrode. In practice, several requirements should be met in order to attain this signal amplification. One of them is related to the packaging density of microelectrodes. It has been assessed that loosely packed arrays where the inter-electrode distance $d \gg 2r$ (r being the radius of a single microelectrode) yield the expected current signal (m times amplified) whereas closely packed arrays, where $d \approx 2r$, behave as a macroelectrode having a current that is proportional to the total geometric area of the microelectrodes in the array [3.9].

3.4 Consequences of the microelectrodes properties

The principal consequences of the properties of microelectrodes are as follows:

- A **steady-state or quasi-steady-state currents** for the faradic process is attained very rapidly resulting in a small RC time constant and high-speed experiments can be performed as the applied potential can be scanned very rapidly [3.10].
- The **faradic-to-charging current ratio, I_F/I_C is improved**, as the charging current decreases in proportion to decreasing area of the electrode, while the steady-state faradic current is proportional to its characteristic dimension. Therefore, the I_F/I_C ratio increases and the sensitivity of measurement is enhanced, facilitating assays in very small sample volumes [3.11].
- The **ohmic drop of potential, IR, is decreased** as the measured currents by microelectrodes are extremely small, allowing stripping analysis also to be performed in high resistive media or even without the need for a supporting electrolyte, minimizing the chemical contamination [3.12].
- The rate of mass transport to and from the electrode (and hence the current density) increases as the electrode size decreases. The high mass transport occurred by radial diffusion of microelectrodes makes the natural convection less problematic and thus stirring becomes unnecessary during the preconcentration step [3.13].
- As a consequence of the increase in the mass transport rates and the reduced charging currents, microelectrodes exhibit **excellent signal-to-noise ratio** characteristics in comparison to their larger counterparts, when an individual microelectrode performs under steady-state conditions or when the diffusion layers totally overlap in an array of microelectrodes.

3.5 Applications of microelectrodes

The applications of microelectrodes and microelectrode array are based on their typical characteristics listed above. They can be divided into the following fields:

Electrochemical reaction mechanisms and kinetics.

The study of reaction mechanisms makes primary use of the decreased resistance and capacitance at microelectrodes permitting the use of various voltammetric techniques with very fast potential scans (up to ca. 10^6 V/s), measurement in a steady state and applications of a great variety of solvents and supporting electrolytes including solvents of low relative permittivity values or samples without a supporting electrolyte added.

Elimination of supporting electrolyte helps to keep the media pure. The first papers dealing with voltammetric measurements in solvents containing no deliberately added electrolyte appeared in 1984 [3.14-3.15]. Of course, there is a solvent limit in measurements without supporting electrolyte, and this limit can be correlated with the dielectric constant of the solvent [3.16].

Fast voltammetry offers another chance in analytical chemistry. Robinson and McCreery were first to notice that reduced values of resistance and capacitance

allow substantial shortening of the time of voltammetric experiments. Much faster sweep rates and much shorter pulse times can be employed with microelectrodes compared to regular-area electrodes. A very short measurements time may be desirable for a number of reasons:

- the electric signals should intrude upon the living species as short as possible during *in vivo* experiments;
- voltammetric curves in flowing systems can be obtained as fast as possible over a wide range of potentials;
- secondary chemical reactions are eliminated that can often lead to the formation of polymers and to poisoning of the electrode surfaces; otherwise the electrode surface can be cleaned before each scan in order to get reproducible curves;

In vivo measurements of biological molecules

Microelectrodes are very well suited for monitoring important compounds in the cells of living organisms; simultaneous determination of ascorbic acid and dopamine may serve as a typical example. Numerous clinical trials and intensive research efforts indicated that continuous metabolic monitoring holds great potential to provide an early indication of various body disorders and diseases. Development of biosensors has become an area of intense scientific and technological studies driven by the need to replace existing diagnostic tools, such as glucose test strips, chromatography, mass spectroscopy, with faster and cost effective diagnostic devices.

In the class of implantable devices that are intensively researched include sensors for nerve stimulation capable of alleviating acute pain [3.17], sensors for detecting electric signals in brain [3.18] and sensors for monitoring bio-analytes in brain [3.19].

The reliability of such implantable systems is often determined by factors including biofouling [3.20] and foreign body response [3.21]. Of course, the selectivity and sensitivity of measurement can be adjusted, to a certain extent, by a suitable pretreatment of the electrode surface.

First of all, the small size of the electrode is essential. Miniaturization cause less tissue damage and therefore less inflammation and foreign body response [3.22]. Typically, tissue inflammation and foreign body response sets in within short periods of time after sensor implantation [3.23]. As a result of this, the implanted sensor becomes fouled with proteins and cells. This cellular encapsulation forms a mass transfer barrier for analyte (glucose, lactate, etc.) diffusion to the sensing element, thereby degrading the *in vivo* sensor performance and long-term stability.

Regarding sensitivity and selectivity, they both can be considered interrelated based on the fact that when improving sensitivity of a sensor usually degrade the selectivity. Membrane-based improvements in selectivity typically interfere with the sensitivity of the sensors and in most cases decrease it. The sensitivity of an implantable biosensor is dependent on: (1) physical design; (2) surface activity of the working electrode; (3) inner polymer membrane (covering the surface of the working electrode) that are used to either immobilize enzymes or eliminate interferences; (4) supplementary enzyme and its activity.

Since their discovery 40 years ago of Clark and Lyons [3.24] type biosensors, technologies have been growing in terms of device complexity and usability, growth which was accelerated thanks to the field of nanotechnology.

Environmental applications

Lately, diverse electrochemical sensors have been developed for the trace metal analysis in water, using either microlithographically fabricated or screen printed microelectrode arrays. The sensors are based on the principles of stripping voltammetry (anodic, cathodic, and adsorptive voltammetry) and stripping potentiometry. *In situ* measurements based on stripping analysis is a very promising approach for the speciation determination of heavy metals especially in natural waters [3.13].

Microelectrodes demonstrated a great potential in the field analysis of trace metals mainly because of (i) the more useful properties of microelectrodes in comparison with conventional electrodes, (ii) the possibility of fabrication of microelectrode array with well defined and reproducible geometries in silicon technology and microelectronics (e.g., photolithography, screen printing), (iii) the growing need for dynamic analytical approaches in environmental monitoring and pollution surveillance (e.g., portable instruments for rapid, continuous, and cost effective analysis) and (iv) the need of metal speciation determination for getting a better understanding of heavy metals behavior in aquatic systems. Trace analysis mainly utilizes the improved I_F/I_C ratio, leading to an improvement of the limits of determination. The wide range of solvents available extends the applicability in trace analysis. The small IR drop sometimes permits measurement on samples of small concentrations (e.g. natural waters) or without supporting electrolytes; this not only improves the reliability of determinations, but also greatly facilitates speciation.

Daniele et al [3.25] reported remote electrochemical sensors for the measurement of trace metals (Cu, Pb, Hg, Se) in natural waters, showing that there is no need of deoxygenation, electrolyte addition or forced convection when employing microelectrodes in stripping analysis.

Detection in flowing liquids

Flow detection is a very wide area involving continuous monitoring of substances in streams of liquids, continuous flow and flow injection determination and, most important, detection in high-performance liquid chromatography (HPLC) and capillary electrophoresis. In order to avoid peak broadening due to the detection, effective volume of a detection cell should not be larger than the volume of one theoretical plate characterizing the separation system. Therefore, microelectrodes are indispensable for detection in the capillary separation system. The use of rapid potential scan voltammetry permits separation in two domains (time and potential) and greatly facilitates identification of the analytes. Microelectrode arrays enhance the measuring sensitivity due to the replenishment of the diffusion layer during the solution passage over the gaps between the electrodes and improve the selectivity and reliability of the measurement because the array differentiates, to a certain degree, between reactions controlled by mass transport and those controlled by the charge transfer.

3.6 Conclusions

The study of microelectrodes is large and from far in this introduction chapter were reached all applications and all theoretical aspects. From what it is expected, a continuous development of microelectrode systems can be achieved in the future due to the growing trend in the field of analytical chemistry.

Miniaturization of working electrodes having an impact on many practical applications, with particularly fascinating the recent studies for in vivo monitoring of neurochemical events, namely due to their specific and attractive construction characteristics.

3.7 References

- [3.1] D.Lydersen, *Acta chemica scanivavia*, vol. 3, p. 259, 1949.
- [3.2] R.N.Adams, "Probing brain chemistry with electroanalytical techniques," *Analytical chemistry*, vol. 48, no. 14, pp. 1126A-1138A., 1976.
- [3.3] R. F. M. J.L.Panchon, "Normal pulse polarography with carbon fiber electrodes for in vitro and in vivo determination of catecholamines," *Analytical chemistry*, vol. 51, no. 9, 1979.
- [3.4] J. W. M. Michael Nastasi, *Ion Implantation and synthesis of materials*, Elsevier, 2010.
- [3.5] J. Heinze, "Ultramicroelectrodes in Electrochemistry," *Angewandte Chemie*, vol. 32, no. 9, p. 1268-1288, 1993.
- [3.6] Y. S. a. M.V.Mirkin, "Nanometer-Sized Electrochemical Sensors," *Analytical chemistry*, vol. 69, no. 8, 1997.
- [3.7] H. G. H.Ju, "Investigation on microelectrodes: Part XVI. Study of the shielding effect at a microband-array electrode," *Journal of electroanalytical chemistry*, vol. 341, no. 1-2, pp. 35-46, 1992.
- [3.8] S. D. V. P.Tomcik, *Chemical listy*, vol. 92, 1998.
- [3.9] W. a. N. F. d. Rooij, "Performance of amperometric sensors based on multiple microelectrode arrays," *Sensors and actuators B*, vol. 44, p. 538-541, 1997.
- [3.10] B. C.M.A, "Electroanalytical techniques for the future:the challenges of miniaturization and of real-time measurements," *Electroanalytical*, vol. 11, pp. 1030-1016, 1999.
- [3.11] A. W. K. S. Wang J., "Adsorptive stripping analysis of trace nikel at iradium-based ultramicroelectrode arrays," *Electroanalytica*, vol. 12, pp. 44-47, 1999.
- [3.12] W. D. a. e. A.G., "Anodic stripping voltammetry at mercury films deposited on ultrasmall carbon-ring electrodes," *Analytical chemistry*, vol. 62, pp. 2697-2702, 1990.
- [3.13] J. a. H. Horvai, "In situ monitoring of aquatic systems-chemical analysis and speciation," *Jong Wiley & Sons*, 2000.
- [3.14] M. a. J.Robinson, "Electrochemistry in organic solvents without supporting electrolyte using platinum microelectrodes," *Journal of electroanalytical chemistry*, vol. 168, p. 299-312, 1994.
- [3.15] J. a. M. M.A.Bond, "Voltammetric measurements using microelectrodes in highly dilute solutions: Theoretical considerations," *Journal of electroanalytical chemistry*, vol. 172, p. 11-25, 1984.
- [3.16] Z. S. J. O. M. Ciszowska, "Pulse voltammetric techniques at microelectrodes in pure solvents," *Analytical chemistry*, vol. 62, pp. 349-353, 1990.

- [3.17] S. T. Schneider A, "Implantable flexible electrodes for functional electrical stimulation," *Med Device Technology*, vol. 15, pp. 16-18, 2004.
- [3.18] Y. H. a. G. S. Wilson, "Rapid Changes in Local Extracellular Rat Brain Glucose Observed with an In Vivo Glucose Sensor," *Journal of Neurochemistry*, vol. 68, pp. 1745-1752, 1997.
- [3.19] R. D. O'Neill, "Microvoltammetric techniques and sensors for monitoring neurochemical dynamics in vivo. A review," *Analyst*, vol. 5, pp. 767-779, 1994.
- [3.20] R. K. J. B. S. K. B. A. M. & W. G. Gifford, "Protein interactions with subcutaneously implanted biosensors," *Biomaterials*, vol. 27, pp. 2587-2598, 2006.
- [3.21] R. M. Wisniewski N, "Methods for reducing biosensor membrane biofouling," *Colloids Surf B Biointerfaces*, vol. 18, pp. 197-219, 2000.
- [3.22] T. I. B. A. M. G. C. S. P. K. T. B.-R. E. H. H. E. J. Peter Holding Kvist, "Biocompatibility of an Enzyme-Based, Electrochemical Glucose Sensor for Short-Term Implantation in the Subcutis," *Diabetes Technology & Therapeutics*, pp. 546-559, 2006.
- [3.23] Y. Onuki, "A Review of the Biocompatibility of Implantable Devices: Current Challenges to Overcome Foreign Body Response," *Journal of diabetes science and technology*, vol. 2, pp. 1003-1015, 2008.
- [3.24] C. L.C.Clark Jr, "Electrode systems for monitoring in cardiovascular surgery," *Annals of the New York Academy of Sciences*, vol. 102, pp. 29-45, 1962.
- [3.25] B. M. a. B. C. Daniele S., "In situ monitoring of electroactive species by using voltammetry at microelectrodes," *Journal of Brazilian chemical society*, vol. 13, pp. 425-432, 2002.

CHAPTER 4

Electrochemical techniques used in sensors applications

Electroanalytical chemistry involves the analysis of chemical species through the use of electroanalytical methods. Generally, the alterations in chemical species concentrations are monitored by measuring changes in current in response to an applied voltage in respect with time. According to Faraday's law, the change is directly proportional to the amount of species undergoing a loss (oxidation) or gain (reduction) of electrons. Constant potential amperometry (CPA), fast cyclic voltammetry (FCV), and differential pulse voltammetry (DPV) are the most common voltammetric techniques in detection of neurotransmitters. Each method has its pros and cons.

4.1 Cyclic voltammetry

Cyclic voltammetry is the most widely used technique for acquiring qualitative information about electrochemical reactions and is often the first experiment performed in an electroanalytical study. It provides information on the thermo-dynamics of redox processes, on the kinetics of heterogeneous electron-transfer reactions, and on coupled chemical reactions or adsorption processes. In particular, it offers a rapid location of redox potentials of the electroactive species, and convenient evaluation of the effect of media upon the redox process.

Cyclic voltammetry consists of scanning linearly the potential of a stationary working electrode using a triangular potential waveform (Figure 4.1). During the potential sweep, the potentiostat measures the current resulting from the applied potential. The resulting plot of current versus potential is termed a *cyclic voltammogram*.

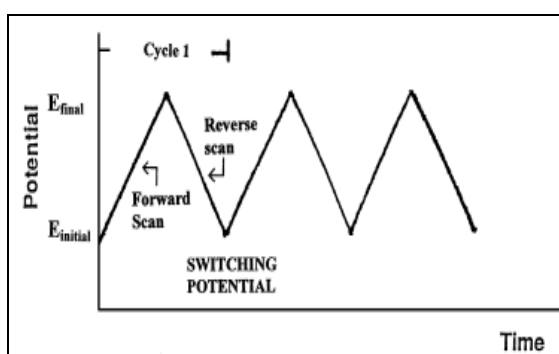


Figure 4.1 Potential-time excitation signal in a cyclic voltammogram experiment

Figure 4.2 illustrates the expected response of a reversible redox couple during a single potential cycle, and several characteristic regions are observed as

well as revealing some important parameters of a cyclic voltammogram (peak potentials and peak currents):

Starting background current (part A in Figure 4.2). The potential is not sufficient enough to cause the discharge of the analyte, the measured background current is due to several causes, like resistance of the cell, the discharge of residual oxygen, the capacitive current and the electronic noise of the electrical circuit.

Ascending part of the peak (part B in Figure 4.2). Close to the discharge potential, the curve rear up: the analyte ions discharge themselves to the electrode at velocity every time faster; the diffusion layer become every time poorer and a spontaneous flow of other analyte ions is established from bulk solution. The velocity of the motion of analyte ions toward the diffusion layer is proportional to the concentration in the bulk.

Descending part of the peak (part from C to D in Figure 4.2). The concentration of analyte into the layer of solution close to the electrode is practically equal to zero because the diffusion layer became dramatically poor in the analyte. The current decreases because the potential scanning velocity is so high that the electro active compound is not able to reach the electrode. At these values of potential, all analyte ions arriving to the electrode are reduced immediately and their concentration in the diffusion layer is very low, Current then trends to diminish (*point D in Figure 4.2*).

Peak potential and peak current height (point C, F in Figure 4.2). The higher point of the peak, E_{pa} (with value i_{pa}), correspond to the point in which the oxidation takes place. The second higher point is at E_{pc} (corresponding value, i_{pc}), where the reduction of the analyte is occurring. The potential peak is an analytical parameter that allows to make qualitative characterization of a redox couple in a solution. The peak current height is proportional to the concentration of the electro active compound in the solution and corresponds to the analytical parameter useful for quantitative analysis.

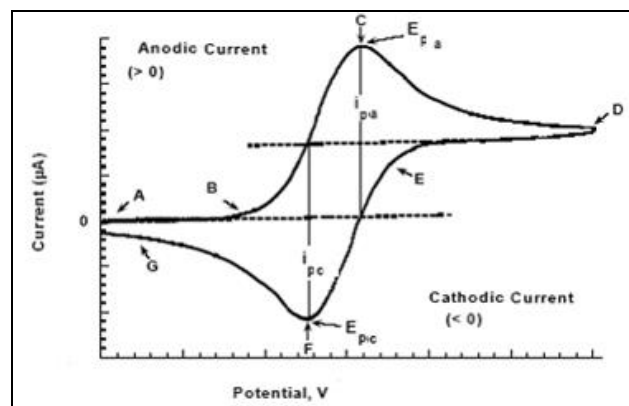


Figure 4.2 The expected response of a reversible redox couple during a single potential cycle

4.1.1 Reversible Systems

To distinguish between a reversible (diffusion controlled) and irreversible (charge-transfer controlled) kinetics of electrode process potential scan-rate is used as diagnostic tool: the rate of reagent transport is proportional to square root of

scan-rate. Analysis of ΔE_p vs. $v^{1/2}$ gives information on reversibility and applicability of further calculations.

An electrochemical process occurs at the interference of two different phases, the electrode and the electroactive species in solution. For the electron transfer to occur, the molecules in solution have to approach the electrode. In a cyclic voltammetry experiment, the solution is kept unstirred, situation when mass transport can occur only by diffusion due to the concentration gradients created around the electrode surface. The current intensity (representing the signal of the diffusional properties of the system) will depend on the surface area of the working electrode and the concentration of the electro-active species. The expression of the peak current in a reversible system (25°C) is given by the Randles-Sevcik equation (4.1) [4.1]:

$$I_p = 2.69 \times 10^5 AD^{1/2} n^{3/2} v^{1/2} C \quad (4.1)$$

where: A represents the area of the electrode (cm^2), n is the number of electrons participating in the reaction, D is the diffusion coefficient of the molecule in solution ($\text{cm}^2 \text{s}^{-1}$), C is the concentration of the probe molecule in the solution (mol cm^{-3}), and v is the scan rate (V s^{-1}).

Some other indicators for a reversible electron transfer are:

1. The ratio of the reverse-to-forward peak currents, $i_{pr}/i_{pf} = 1.0$ (as observed in Figure 2, where $i_{pr}=i_{pc}$ and $i_{pf}=i_{pa}$) for a simple reversible couple . When the redox system is perturbed by a following chemical reaction, the cyclic voltammogram will exhibit a smaller reverse peak(because the reaction product is chemically removed from the surface). Then, the peak ratio, i_{pr}/i_{pf} will be smaller than unity.
2. The cathodic and anodic potentials, E_{pa} and E_{pc} , are independent of the scan rate and concentration
3. The formal potential, $E^{0'}$, for a reversible couple is centered between E_{pa} and E_{pc} :

$$E^{0'} = \frac{E_{pa} + E_{pc}}{2} \quad (4.2)$$

4. The separation can be used to determine the number of electrons transferred, and as a criterion for a Nerstian behavior. A fast one-electron process exhibits a ΔE_p of about 59mV:

$$\Delta E_p = E_{pa} - E_{pc} = \frac{0.059}{n} \quad (4.3)$$

However, the measured value for a reversible process is generally higher due to uncompensated solution resistance and non-linear diffusion. Larger values for ΔE_p , which increase with increasing scan rate, are characteristic of slow electron transfer kinetics.

Another useful parameter obtained from Randles-Sevcik equation is the "true" area of the electrode. In many cases the geometric area of an electrode is not the same as the electrochemically active area. Geometric area calculations assume a smooth surface, but any surface roughness actually increases the available area of the electrode.

4.1.2 Irreversible and Quasi-reversible systems

For irreversible processes (those with sluggish electron exchange), the individual peaks are reduced in size and are widely separated. Totally irreversible systems are characterized by a shift of the peak potential with the scan rate [4.2]:

$$E_p = E^0 - \frac{RT}{\alpha n_a F} \left[0.78 - \ln \frac{k^0}{D^{\frac{1}{2}}} + \ln \left(\frac{\alpha n_a F v}{RT} \right)^{1/2} \right] \quad (4.4)$$

where a is the transfer coefficient and n_a is the number of electrons involved in the charge-transfer step. Thus, E_p occurs at potentials higher than E^0 , with the over-potential related to k^0 and a . Independent of the value k^0 , such peak displacement can be compensated by an appropriate change of the scan rate. The peak potential and the half-peak potential (at 25°C) will differ by $48/an$ mV. Hence, the voltammogram becomes more down-out as an decreases.

The peak current given by [4.3]:

$$i_p = (2.99 \times 10^5) n (\alpha n_a)^{1/2} A C D^{1/2} v^{1/2} \quad (4.5)$$

is still proportional to the bulk concentration, but will be lower in height (depending upon the value of a). Assuming a value of 0.5, the ratio of the reversible-to-irreversible process is about 80% of the peak for a reversible one).

For quasi-reversible systems (with $10^{-1} > k^0 > 10^{-5}$ cm s⁻¹) the current is controlled by both charge transfer and mass transport. The shape of the cyclic voltammogram is a function of $\frac{k^0}{\sqrt{\pi a D}}$ (where $a = nFv/RT$). As $\frac{k^0}{\sqrt{\pi a D}}$ increases, the

process approaches the reversible case. For small values of $\frac{k^0}{\sqrt{\pi a D}}$ (i.e., at very fast v) the system exhibits an irreversible behavior. Overall, the voltammograms of a quasi-reversible system are more drawn-out and exhibit a larger separation in peak potential compared to those of a reversible system.

4.2 Constant Potential Amperometry

Constant-potential amperometry (CPA) is a simple electrochemical technique in which a potential sufficient to oxidize or reduce the molecule of interest is applied to the electrode. The electrode responds extremely quickly to changes in analyte concentration, and high sampling rates can be used; therefore, constant-potential amperometry offers the best temporal resolution among the available techniques. However it suffers from poor selectivity, constant-potential amperometry should not be used where chemical selectivity is needed to provide confidence in the identity of the analyte. Although, its fast sampling rate, makes it ideal to study the kinetics of the electrode process [4.4]. Figure 4.3 shows a typical potential excitation waveform and the resulting current response.

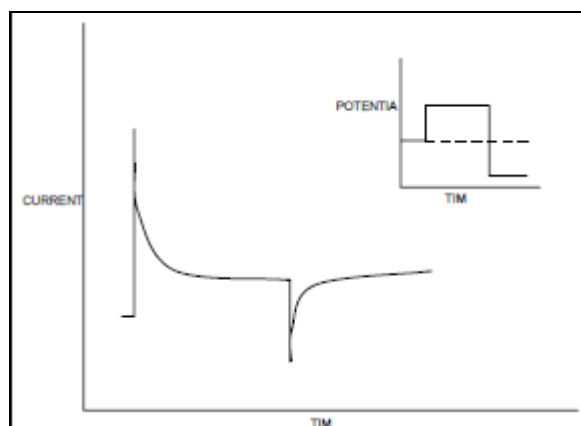


Figure 4.3 Typical constant-potential amperogram. Inset is the excitation waveform.

4.3 Pulse voltammetry

Pulse voltammetric techniques, pioneered by Barker and Jerkin [4.5], lower the detection limit of voltammetric measurements. The ratio between the faradic and nonfaradic currents is substantially increased, fact that allows detection limits around 10^{-8}M . The various pulsed techniques are all based on a sampled current potential-step experiment. A sequence of such potential steps, each with a duration of about 50ms, is applied to the working electrode. After the potential is stepped, the charging current decays rapidly (exponentially) to a negligible value, while the faradic current decays more slowly.

4.3.1 Differential pulse voltammetry

Differential pulse voltammetry is an useful technique for measuring trace levels of organic and inorganic species. In a differential-pulse voltammetry, fixed magnitude pulses-superimposed on a linear potential ramp-are applied to the working electrode at a time just before the end of the drop (Figure 4.4 A). The current is sampled twice, and if the difference between the current just before and at the end of the pulse is measured, a reading less influenced by the capacitive current can be performed. In this way, this differential reading of the current generates a peak shaped voltammogram, as seeing in Figure 4.4B.

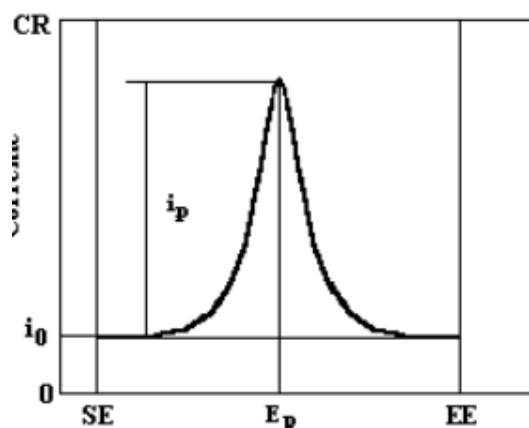


Figure 4.4(A) Differential pulse voltammetry-Plot of voltamogram

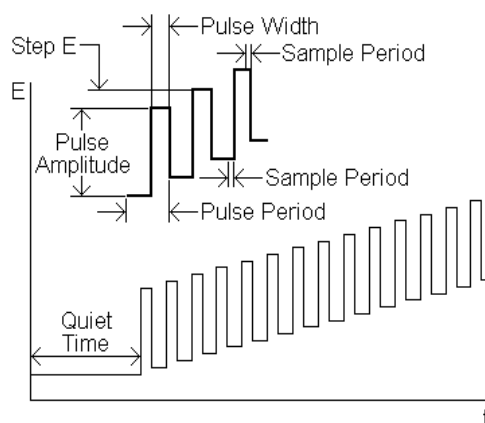


Figure 4.4(B) Differential pulse voltammetry-Anodic scanning of the potential

The peak-shaped response of a differential-pulse measurements results in improved resolution between two species with similar redox potentials. In various situations, peaks separated by 50mV may be measured. Such quantitation depends not only upon the corresponding peak potentials but also on the widths of the peak. The width of the peak (at half-height) is related to the electron stoichiometry.

The peak-shaped response, coupled with the flat background current, makes this technique for analysis of mixtures.

4.3.2 Square wave voltammetry

This technique represents a further development of the preceding one. A rapid step scanning of potential is applied to the electrode and, in plus, on each step is superimposed an high frequency square wave (20-100Hz). The current is sampled two times at the end of the two half times as presented in figure 4.5.

The sensitivity of this technique can be increased by enhancing the amplitude of the square wave of the frequency. The limits of the enhancing is strictly related to the kinetics aspects of the redox system: it has not to be slower than the velocity of the scanning of potential. The interference due to capacitive

current are lowered to minimum because the current is sampled just at the end of the half waves, when the current of the double electrical layer is the least.

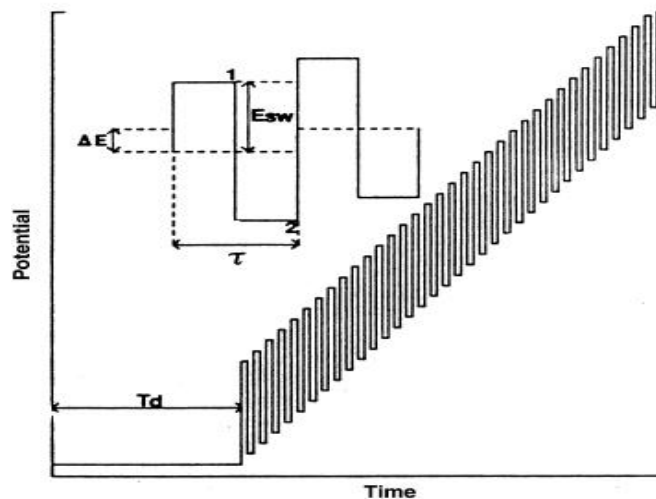


Figure 4.5 Excitation waveform points for a square wave voltammogram

One of the advantages of the square wave voltammetry is the speed. Since it removes effectively the background current from the measurement, it allows to use higher scan rates, reducing thus the analysis time, a voltammogram being recorded within few seconds, as compared to 2-3 minutes needed in an differential pulse voltammogram.

4.4 References

- [1] Pine Instrument Company, Educator's Reference Guide for Electrochemistry, Pennsylvania, 2000.
- [2] J. Wang, Analytical Electrochemistry, Willey-VCH, 2001.
- [3] C. S. H. W. J. Z. Xiao-Zi Yuan, Electrochemical Impedance Spectroscopy in PEM fuel cells, Elsevier, 2010.
- [4] P.N.Jiang, Electroanalytical chemistry research development, Nova science publishers, 2007.
- [5] S. P. Kounavers, "Voltammetric techniques," Tufts University, Chemistry Department.

CHAPTER 5

Scope and thesis objectives

The fundamental and applied research on new concepts of sensing coupled with numerous technological innovations have opened new opportunities to a wider clinical use of electrochemical sensing devices. Nevertheless, the electrochemical sensors offer numerous applications in clinical diagnosis, environmental monitoring and food analysis.

The development of highly sensitive, cost-effective, miniaturized sensors requires advanced technology coupled with fundamental knowledges in chemistry, biology, and material sciences.

In general, the sensor efficiency can be assessed in terms of response time, signal-to-noise (S/N) ratio as sensitivity, selectivity, and limits of detection (LOD). In addition, particularly for *in vivo* applications, biocompatibility, non-toxicity, and long-term biostability must be fulfilled. Taking into account the typical expectations of a good electrode that must work as sensor, e.g., appropriate level of conductivity for the chosen application, the right size to meet the needs, ease of fabrication, reliability, compatibility with the environment, signal processing issues, integration into a functional system, there is a demand both for new materials as well as technologies to fabricate microelectrodes useful for recording, stimulation, and sensing.

The metallic electrodes are often not the best choice for electrochemical sensors. In comparison, carbon electrodes exhibit a wider potential window and superior selectivity toward neurotransmitter detection.

Carbon materials in the forms of graphite, glassy carbon, carbon fibers, carbon nanotubes, etc., have been important players in solid electrode development, but considering carbon composites in general, their properties present improvements over conventional solid carbon electrodes due to some interesting advantages, i.e., the mouldability that allows the construction of sensors in different configurations and sizes, the polymer matrix providing mechanical and chemical stability of the composite, low background current, microelectrode array behavior given by the conductive and easily miniaturized with good compatibility for *in-vivo* electroanalysis of neurotransmitters.

To solve the main drawback with the carbon composites regarding the slow electron transfer kinetics the incorporation of specific catalytic material in the composite matrix should be proposed. The mixture of zeolite and graphite has been proposed since 1980s in various forms, leading to a zeolite modified electrodes class (ZMEs). Combining sensitive materials with smaller geometries of the working electrodes, important sensing devices can be obtained for the *in vivo* monitoring of compounds in the cells of living organisms. Moreover, composite microelectrodes couple the advantages of the microelectrode system with the composite assuring decreased ohmic drop of potential, establishment of a steady state signal, useful current increase, and increased signal-to noise ratio.

The specific objectives of this research are the following:

- Elaboration and manufacturing of natural/synthetic zeolite-modified/unmodified graphite-based composite microelectrodes with useful properties for the *in-vitro* electrochemical detection of selective and simultaneous detection of dopamine and ascorbic acid;

- Elaboration and manufacturing of natural/synthetic zeolite-modified/unmodified graphite-based composite macroelectrodes to compare their utility the *in-vitro* electrochemical detection of selective and simultaneous detection of dopamine and ascorbic acid;
- Electrochemical characterization of the electrode materials;
- The evaluation of the electrode materials behaviour in phosphate-buffer saline at pH 7 and in the presence of the target analyte, to establish the relationship between obtained electrode material and reaction type;
- Individual detection experiments performance, which provides specific informations, i.e., voltammetric/amperometric detection type, detection potential value, concentration ranges, electrode sensitivity, stability, reproducibility and lifetime, detection limits, calibration, to elaborate the detection protocol;
- Exploitation of the specific features of the pulsed voltammetric techniques to improve the electroanalytical performance for the selective detection of the dopamine in the presence of ascorbic acid;
- Simultaneous detection experiments performance to elaborate specific simultaneous detection protocol;
- Selective detection of dopamine in the presence of ascorbic acid b with Nafion coated graphite-composite microelectrodes
- In-vitro enhanced sensitive detection of dopamine at carbon nanotubes-film coated graphite composite microelectrodes
- In-vivo amperometric monitoring of dissolved brain oxygen at optimized zeolite-modified graphite-composite microelectrodes

Our research was directed on the study of anodic response of dopamine, a most significant neurotransmitter, which plays a prime role in the functioning of the central nervous, cardiovascular and hormonal systems. Extreme abnormalities of DA concentration levels may lead to Parkinson's disease and also in some clinical manifestations of HIV infections. Thus, there is a continuing interest in the development of simple, sensitive and reliable method for the determination of dopamine. Dopamine is a neurotransmitter and a neurohormone belonging to the catecholamine family of phenolic compounds. Dopamine is used as a drug and it acts on the nervous system to increase heart rate and blood pressure. A deficiency of dopamine in the brain is believed to cause schizophrenia and Parkinson's disease. Thus sensing of dopamine in brain tissue is vital in clinical diagnoses.

Several graphite-epoxy composite microelectrodes, *i.e.*, μ -GEC, μ -ZN-GEC, μ -ZS-GEC and CNT-film μ -ZS-GEC in comparison with the same composition of macroelectrodes, *i.e.*, M-GEC, M-ZN-GEC and M-ZS-GEC were studied to select the optimum selective and simultaneous detection scheme of dopamine in the presence of ascorbic acid. The preparation protocol was established based on the optimization of mixing method and the three-epoxy component ratios, graphite-epoxy weight ratio and also, graphite-zeolite-epoxy wight ratios in relation with the electrochemical behaviour of the classical ferri/ferro redox ssystem. The effect of the presence of the carbon nanotubes in the composite composition on the sensitivity towards dopamine detection was investigated. Also, the Nafion membrane was tested to detect selectively the dopamine in the presence of other relevant components, ascorbic acid, DOPAC-a dopamine metabolite product and uric acid, which can interfere the dopamine detection.

Another research direction envisaged in-vivo amperometric monitoring of dissolved brain oxygen, the most important oxidative substrate for biochemical reactions and for the production of brain energy.

CHAPTER 6

Preparation and characterization of modified/unmodified composite microelectrodes/macroelectrodes

6.1 Introduction

Carbon based modified electrodes offer many advantages, due to the nature of the composite material itself. In this way, modifying agents can be introduced either directly into the paste, or to the material in its final state or even during composite preparation.

Since 1960s, there are present papers dealing with carbon paste modifications by Kuwana [6.1] or "direct mixing" of the modifier introduced by Ravichandran and Baldwin [6.2].

Liquid modifiers are preferential to solid ones because they yield more homogeneously modified materials. Modifiers should be insoluble in all solutions in which the sensor will be exposed to in order to avoid the leaching of the electrode.

Modified carbon composite electrodes are used in detection of inorganic analytes, especially in food analysis. For example, tin, an element present in canned food, can be detected by using adsorptive stripping analysis by proper ligands present on carbon composite electrodes [6.3]. Nitrite and nitrite have been also been investigated in drinking water samples [6.4-6.5].

Ascorbic acid (AA) was intensively investigated at carbon paste electrodes (CPEs) [6.6-6.9], and screen printed electrodes (SPEs) [6.10-6.14]. AA gives an irreversible response at carbon electrodes in the positive voltammetric potential range. Modifiers either affect the accumulation of the analyte or decrease the overpotential.

In the field of foodstuff for detection of antioxidant substances, several studies have been carried out. Quercetin [6.15-6.16], flavonols [6.17], anthocyanidins [6.18] can be detected due to the lipophilic character of carbon paste that can support the adsorptive accumulation of the analyte.

But, the most important field of applications of sensors based on carbon composite materials is the one of biosensors. Carbon composites, in the design of biosensors are common due to the easiness in modification even when it comes to complex biological systems (enzymes, proteins, nucleic acid, tissues, whole cells).

Most application involve the use of oxidases dependent oxygen or dehydrogenases (not oxygen dependent) and the most frequent analyte is glucose, because glucose levels must be frequently monitored at patients with diabetes [6.19] aiming in vivo monitoring [6.20].

The advantages of microelectrodes over macroelectrodes have already been mentioned, but on the other hand, the main goal is to develop friendly sensors as alternatives to mercury based ones, or cheaper in comparison to Pt sensors.

The most researched electrode materials for in-vivo applications consist in carbon fibers (CF) microelectrodes. They have been used since 1979 to record neuronal action potentials, being very suitable for in vivo electrochemical detection of catecholamines or other oxidizable biological species. The greatest advantage in

using CF microbiosensors are their physiochemical properties and their biocompatible nature, which makes CF suitable for the majority of voltammetric techniques *in vivo*. They can be constructed at micro or nano scale allowing minimum damage, although sometimes larger surface areas are preferred because the molecules of interest are secreted from multiple neuronal terminals.

There is an extensive literature regarding applications of CF microelectrodes in different forms, coated with different membranes [6.21-6.23], or entrapped with appropriate enzymes [6.24-6.27].

Other chemical biosensors beside CF used in neurochemical include also carbon paste microelectrodes. In the field of neurochemistry of brain tissue there is a novel idea of measuring both neurotransmitters and neuronal electrical activity by constructing arrays of microelectrodes that will capture both neurotransmitters and electrical activity from multiple neurons.

Several types of carbon based microsensors applied in clinical field have been reported[6.28]. A graphite-epoxy microsensor was reported for the detection of O₂, glucose and ascorbic acid. O₂ reduction at carbon paste electrodes presents long term stability over 12 weeks [6.29]. Another carbon paste electrode (CPE) with different sizes (diameter = 320µm, 260 µm, 160 µm) have also been reported for *in vivo* sampling of uric acid [6.30]. As well, a carbon paste electrode of 200 µm diameter immobilized with glucose oxidase enzyme (GO_x) for the detection of glucose was found to have a limited stability to a few days [6.31].

Zeolite carbon-epoxy composites microsensors haven't been yet reported, although the Alain Walcarius work is extensive regarding zeolite modified electrodes at macro scale with good results when it comes to dopamine detection and other neurotransmitters, with the remark that for *in vivo* brain electrochemical studies would require proper miniaturization of zeolite modified electrodes.

6.2 Design and graphite composite electrodes construction

6.2.1 Experimental section

6.2.1.1 Materials and reagents

Synthetic graphite powder used in this study was provided from Sigma Aldrich, with particle dimension < 20 µm. Multi-walled carbon nanotubes (MWCNTs) provided as well from Sigma Aldrich (purity>90%, length 1.5 µm, average diameter 9.5 µm).

The three-component epoxy resin, namely epoxy resin (Araldite M), epoxy hardener (Araldite M Hardener 964) and epoxy accelerator (Araldite M Accelerator 960) were purchased from Sigma-Aldrich and used as received.

Natural zeolite with high clinoptilolite content and a mass composition consisted of: 62.20% SiO₂, 11.65% Al₂O₃, 1.30% Fe₂O₃, 3.74% CaO, 0.67% MgO, 3.30% K₂O, 0.72% Na₂O, 0.28% TiO₂, was supplied by Cemacon Company, Romania. Natural zeolite was used as Si source for synthetic zeolite. [6.32].

Phosphate saline buffer solutions (PBS) supporting electrolyte, prepared from di-hydrogenphosphate, sodium chloride and sodium hydroxide of analytical reagent grade (Sigma, Aldrich) was used as received. PBS solution was kept in the refrigerator when not used. Potassium ferrocyanide, potassium ferricyanide were purchased from Sigma. Tetrahydrofuran (THF), used as dispersing agent, was purchased as well from Sigma-Aldrich BV.

6.2.1.2 Apparatus and experimental measurements

All voltammetric experiments involving **microelectrodes** were carried out at room temperature (25°C) using an eDAQ QuadStat four-channel Potentiostat (Australia) controlled with an eChem software for cyclic voltammetry in a three-electrode electrochemical cell, carbon composite microsensor as working electrodes, Ag/AgCl reference electrode and Pt auxiliary electrode. A magnetic stirrer provided the convective transport during the voltammetric experiments.

All voltammetric experiments involving **macroelectrodes** were carried out at room temperature (25°C) using a computer controlled Autolab potentiationstat/galvanostat PGSTAT 302 (EcoChemie, The Netherlands), with a standard three-electrode configuration. The three-electrode system consisted of a baron doped carbon composite macroelectrode/ baron doped diamond as working electrode, a Pt counter electrode, and an Ag/AgCl reference electrode. For adsorption experiments using baron doped diamond (BDD) electrode, the 50 mM PBS supporting electrolyte at pH 7.4 was placed into the cell, and solutions of ascorbic acid and dopamine were employed in 1g/L zeolite suspension. The scan rate for the detection experiments was 50 mV s⁻¹.

6.2.1.3 Synthetic zeolite synthesis

Preparation of synthetic zeolite was made using sodium hydroxide solution and sodium aluminate as aluminium source in according with a previous-reported method [6.32].

A solution of natural clinoptilolite, sodium hydroxide and water with 1:5:50 mass ratios were mixed for 1h at 90°C (solution I). The aluminium solution was prepared from sodium aluminate, sodium hydroxide, sodium aluminate and water with 1:1.5:7.8 mass ratios, were mixed and heated to make a clear solution (solution II). The solutions II and I with 1:1.9 mass ratio were mixed together. Then, the mixture was heated at 90°C and stirred with a mixing rate of 1000 rpm for 2 hours. The synthetic zeolite was thermally treated at 105°C for 8 h for a good crystallinity.

The surface morphology of synthetic zeolite is similar to natural zeolite, revealed a more uniform structure with smooth edged lamellar crystals. The particles size of the natural zeolite ranged between 4-11 µm and the particles size of the synthetic zeolite A was in the range 20 to 300 nm. Si/Al ratio was 4-5 for natural zeolite and 1.0-1.14 for the synthetic zeolite.

6.2.1.4 Microelectrode design and graphite-composite microelectrodes construction

In figure 6.1 the design of the micro-sensor is presented and also shortly described in [6.33]. It was made using a Classical Multi Core Cu wire (5 cm in length, i.d.=150 µm). Its plastic insulator was removed at one edge and 2.2 cm of Cu wire was exposed and inserted in a Fused Silica Tube (i.d.=180 µm). At one end, 1 mm of Silica tube was left free in order to allow the filling with the graphite-epoxy composite, while the Cu wire guaranteed the electrical contact with the composite matrix. The geometrical area of the sensor surface with disk geometry was 2.5 10⁻⁴ cm² and the final length of the sensor used for all electrochemical detections was approximately 5 cm.

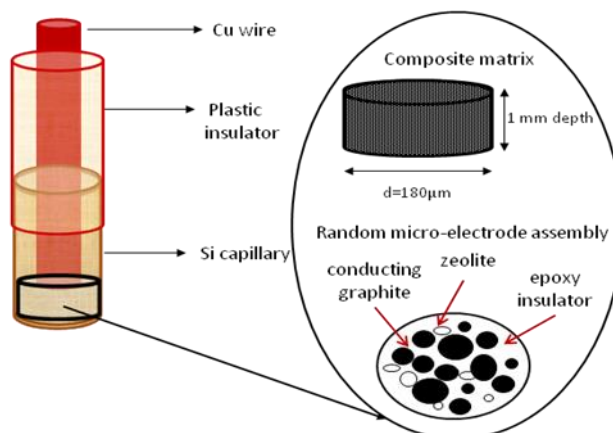


Figure 6.1 Sensor design

Carbon-epoxy based micro-composites were constructed according to the following procedure. All sensors were prepared by manually mixing the graphite particles and zeolites within the three-component epoxy resin for about 20-30 min (depending on the below-presented mixing method employed). Before curing, the material was filled inside the Si capillary (by dipping the sensor body into the composite) and the electrical contact of the composite with the copper wire was checked under microscope, as well as the exterior walls of the Si capillary in order to be clean, to not interfere later in the voltammetric experiments.

A bare graphite-epoxy composite (μ -GEC) microsensor was firstly elaborated and considered as blank sensors, after finding the proper conditions for the three-component epoxy resin polymerization (curing at 105°C for 30 min). In order to estimate the best three-component epoxy ratio (resin:hardener:accelerator) and the best mixing method in terms of the electrochemical behaviour, e.g. reversibility (peak-to-peak separation, ΔE) and sensitivity (peak current, ΔI), cyclic voltammetry of 2 mM potassium ferricyanide/ferrocyanide system was performed at a scan rate of 100 mV s⁻¹ between potential -0.4 and +0.8 V (vs. Ag/AgCl). Only two mixing methods (discussed in section 3.1) and two resin ratios (100:95:5 and 100:10:5 resin:hardener:accelerator) were evaluated as concrete criteria of appreciation. The best graphite-epoxy weight ratio, was found to be 55% wt. graphite and 45% wt. epoxy with 100:95:5 resin:hardener:accelerator weight ratio, using the same voltammetric procedure.

The third material in the composite matrix was incorporated by mechanical dispersion of a constant 20% wt. ratio natural or synthetic zeolite, while the graphite and epoxy concentrations were varied, resulting in two new μ -ZMEs: graphite 45%-natural zeolite 20%-epoxy composite 35%, wt. (μ -NZ-GEC) and graphite 45%-synthetic zeolite 20%-epoxy composite 35%, wt. (μ -SZ-GEC).

Prior to be used, the hardened composite material surface was polished using a mechanical drill and checked again under microscope for a perfect disk shape of the microelectrode electroactive surface.

6.2.2 Results and discussions

6.2.2.1 Optimization of the graphite-composite material construction

Because the sensor composite material consisted of a conducting phase (graphite particles) and an insulator phase (epoxy resin and zeolite), the resulted sensing devices can exhibit large resistances and capacitances, thereby each step in the composite matrix construction was tested and assessed in terms of reversibility (peak-to-peak separation, ΔE) and sensitivity (peak current, ΔI) using 2 mM $\text{Fe}(\text{CN})_6^{3-/4-}$ in 1 M KNO_3 supporting electrolyte at a scan rate of 100 mV s^{-1} . The oxidation of ferricyanide to ferrocyanide in aqueous solutions is known as a classical method in electrochemistry, involving one electron transfer in the redox reaction, as well as the presence of defined oxidation-reduction peaks, providing information related to the electroactive properties of the electrode material.

Higher ΔI and wider ΔE are desired in a reversible system. The higher ΔI , the greater electroactive surface area or increased rate of diffusive transport of the ferricyanide reactant to the sensing material, while larger ΔE inform about slow kinetics, restricting the experimental timescales, as well as a proof of increased ohmic drop and higher electrical resistances.

6.2.2.1.1 Optimization of the mixing methods and the three - epoxy component ratios

Four mixing methods of the three-epoxy component with graphite particles (M_1, M_2, M_3, M_4) (mixing procedures being presented in figure 6.2) and different resin:hardener:accelerator ratios (100:90:5, 100:60:5, 100:40:5, 100:20:10, 100:10:5) were employed, keeping a constant content of graphite of 55%, wt. Based on the electrochemical behavior, two mixing methods and two epoxy ratios were appreciated as optimum in order to proceed with composite matrix construction, as concluded from table 6.1. In terms of process sensitivity, method M_1 with 100:95:5 resin:hardener:accelerator ratios was found to present the higher ΔI (285 nA), but in terms of reversibility, method M_2 with 100:10:5 resin:hardener:accelerator ratios presented the smallest peak-to-peak separation, 0.413 V, although this value is characteristic for a quasi-reversible system.

All values were recorded at a scan rate of 100 mV s^{-1} where the ratio of the ferricyanide anodic peak current and cathodic peak current, $\Delta I_a/\Delta I_c$ presented values close to 1, respectively 0.95 for M_1 with 100:95:5 resin:hardener:accelerator ratio and 0.98 for M_2 with 100:10:5 resin:hardener:accelerator ratio, showing that the redox system is stable. The curing conditions in the oven were fixed for a temperature of 105°C and a time of 30 min.

For the methods M_4 and M_3 , voltammogram values could not be read. Examples of voltammetric curves for different mixing methods and different resin ratios, M_1 with 100:95:5 wt., M_2 with 100:10:5 wt., M_4 with 100:60:5 wt. and M_4 with 100:40:5 wt. are presented in figure 7.3. For methods M_4 with 100:60:5 and M_4 with 100:40:5 the voltammograms do not present a peak shaped response. A reason that can explain this type of behavior is the possible current leakage that can appear for a weak conduction pathway formed between the conducting graphite particles and the insulating epoxy resin which occurred during the mixing mechanism. We excluded by checking under the microscope the possibility that the current leakage occurs because of a poor mechanical seal between the microelectrode material and electrical contact.

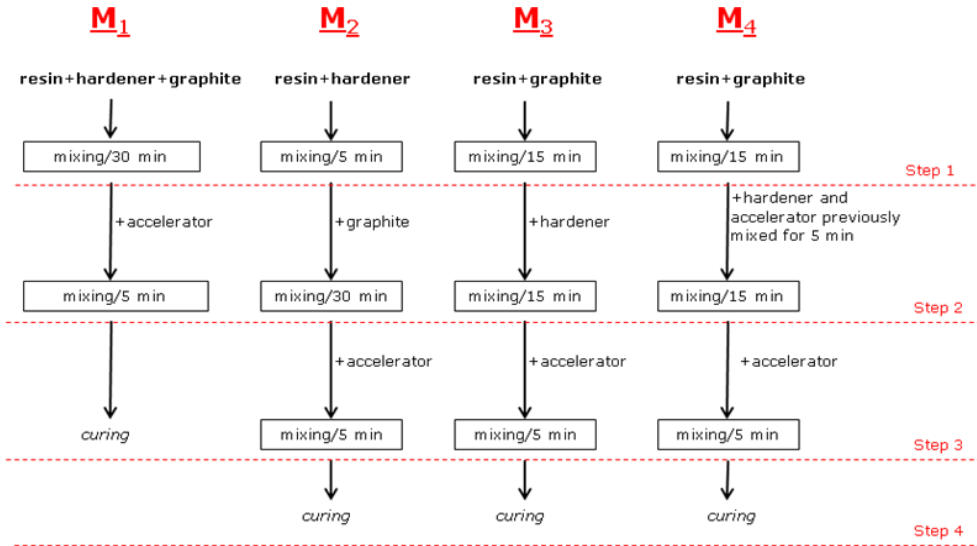


Figure 6.2 Mixing methods of the three-epoxy components with graphite particles

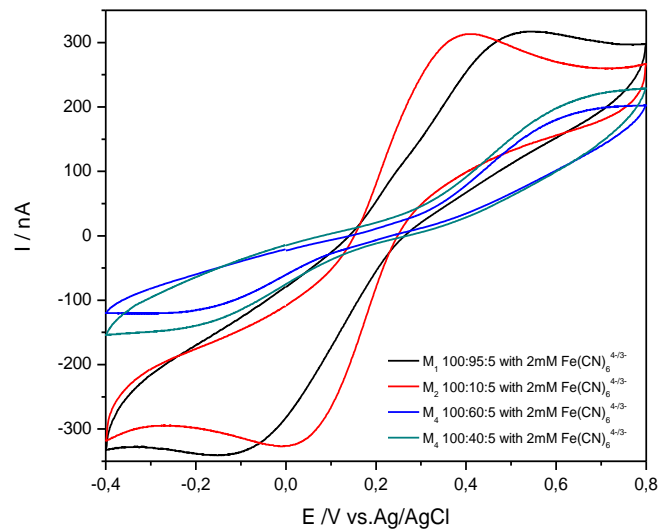


Figure 6.3 CVs recorded at graphite-epoxy microelectrode in a 1M KNO_3 supporting electrolyte and 2mM $\text{Fe}(\text{CN})_6^{3-/4-}$ at a scan rate of 100 mV s^{-1} ; Potential Range: -0.2 V to +0.6 V, Speed: 20kHz; Sample Period: 1ms, QuadStat Filter 10kHz.

6.2.2.1.2 Optimization of the graphite-epoxy weight ratio

Many factors contribute to the conductivity of the composites, such as characteristics of fillers and polymers, diameter and structure of fillers, concentration

of fillers, states of dispersion, processing methods. Conductive composites are characterized by a percolation threshold or a critical value at which the conductivity starts to increase as a function of filler content. However, the mechanical properties decrease drastically at high filler contents, typically greater than 15 wt %.

Some examples are present in literature regarding best responses in terms of graphite loadings. In [6.34] the best graphite-epoxy loading was found for 70% graphite w/w. Other research group presents an optimum graphite load of 60% w/w in the composite matrix [6.35] and a content of 62% graphite close to the second percolation threshold was found in [6.36].

Table 6.1: Electrochemical parameters resulted when varying the mixing method and resin:hardener:accelerator ratios

Method	resin:hardener:accelerator (R/H/A) ratios	Scan rate (V s ⁻¹)	ΔE (V)	ΔI_a (nA)	$\Delta I_a / \Delta I_c$
M ₁	100:95:5	100	0.695	285.31	0.95
	100:60:5		0.802	254.23	1.39
	100:40:5		0.749	192.19	1.60
	100:20:10		0.645	172.47	1.55
	100:10:5		0.697	217.43	1.61
M ₂	100:95:5		0.692	222.83	0.92
	100:60:5		0.501	281.4	0.92
	100:40:5		0.567	249.31	0.93
	100:20:10		0.515	236.76	0.90
	100:10:5		0.413	287.05	0.98
M ₃	100:95:5		0.585	266.38	0.94
	100:60:5		0.488	235.12	0.91
	100:10:5		0.454	226.59	0.95
M ₄	100:95:5		0.398	249.49	0.94
	100:60:5		-*	-	-
	100:40:5	-	-	-	
	100:20:10	-	-	-	
	100:10:5	-	-	-	
** No voltammetric behaviour was found					

The voltammetric response of the composite electrodes showed to be highly dependent on the graphite content in the total mass of composite. Varying the graphite content in the matrix, from 50% to 60%, an optimum value of 0.240 V for ΔE was obtained for 55% wt. graphite in the total mass of the composite. Variations were carried out using the two mixing methods, M₁ and M₂, and the epoxy ratios that were previously determined as optimum. This bare graphite-epoxy micro-composite, μ -GEC, (M₁ and 100:95:5 resin:hardener:accelerator ratio) was considered as blank sensing device. The effect of the graphite content upon peak-to-peak separation (ΔE) at graphite-epoxy micro-sensors when employing M₁ mixing method with 100:95:5 resin:hardener:accelerator ratio is presented in figure 6.4.

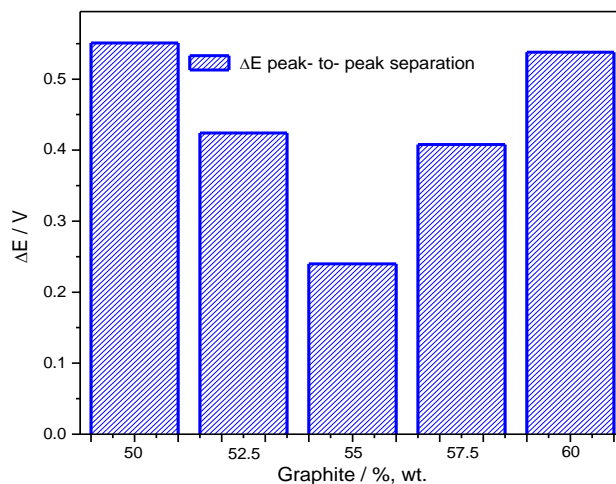


Figure 6.4 The effect of the graphite content upon peak-to-peak separation (ΔE) at graphite-epoxy (M_1 mixing method and 100: 95:5 resin:hardener:accelerator ratio) micro-sensors in 1M KNO_3 supporting electrolyte with 2 mM $K_4Fe(CN)_6$ / $K_3Fe(CN)_6$; scan rate 100 mV s^{-1} ; potential range from -0.4 V to +0.8 V; Ag/AgCl reference electrode and Pt auxiliary electrode.

6.2.2.2 Zeolite adsorption studies

Literature data states that zeolite materials exhibit high cation exchange and adsorption capacity [6.37-6.38]. The excess of the negative charge in the zeolite framework differentiates the adsorption capacity behavior between different molecules of interest, especially when process mechanism is governed by the charge neutralization.

The sensor material based on BDD electrode known for its chemical inertness and resistance to fouling properties [6.39], was chosen to investigate the interaction of dopamine and ascorbic acid with natural and synthetic zeolite particles.

Organic cations, like dopamine, were found to be easily accommodated by zeolites and further detected by voltammetry at zeolite modified electrodes [6.40], reason for which the scope of the further experiments are to clarify the behavior of zeolites towards ascorbic acid and dopamine.

A concentration of 1g/L natural and synthetic zeolite was immersed in the PBS supporting electrolyte. Under stirring conditions, concentrations of $31.25\ \mu\text{M}$ of dopamine and ascorbic acid were left to adsorb on the zeolite surface for 15 minutes, period after which the concentration of the analyte in PBS solution was determined. The scan rate employed for all adsorption experiments was 50 mV s^{-1} .

The loading percentage of dopamine and ascorbic acid onto the natural zeolite and synthetic zeolite particles was investigated by cyclic voltammetry as response of boron doped diamond (BDD) electrode in dopamine/ascorbic acid-containing PBS supporting electrolyte .

Figure 6.5 displays CVs recorded with Boron Doped Diamond electrode in $31.25\ \mu\text{M}$ of dopamine before and after natural and synthetic zeolite addition in the solution, while figure 9.6 presents the same experiment performed for ascorbic acid analyte.

The adsorption results expressed as adsorption degree (%) are gathered in Table 6.2.

Table 6.2: Adsorption degree of dopamine and ascorbic acid after 15 minutes adsorption time onto natural/ synthetic zeolite

Analyte	Zeolite	Adsorption degree [%]
DA	natural	16
	synthetic	34
AA	natural	0.75
	synthetic	1.31

The adsorption of a guest molecule may occur both on the external and internal surfaces of the zeolite crystal. Also, the ion-exchange behavior of zeolite depends on a series of factors including the framework structure, ion size and shape, charge density of the anionic framework, ionic charge and concentration of the external electrolyte solution.

Dopamine oxidation occurs at a potential value of 0.666 V at BDD electrode, and a 34% diminution of the dopamine signal was observed after 15 min of the synthetic zeolite addition into the PBS supporting electrolyte, while only 16% reduction of signal was observed for the case of natural zeolite. The signal reduction after 15 minutes adsorption time represents the adsorption degree onto zeolite.

In the PBS solution at pH of 7.4, dopamine exists as cation. It can be seen that there is a strong electrostatic attraction between positively charged dopamine and the synthetic zeolite, leading to an incorporation of dopamine in the zeolite lattice.

Although, for AA, which exists as an anion at pH of 7.4, no significant reduction in current signal is observed, according to figure 6.6.

The ion-exchange incorporation of dopamine into the zeolite lattice can be used effectively as a pre-concentration step prior to all voltammetric experiments when synthetic zeolite material is incorporated into a sensing device.

Also, the selectivity of synthetic zeolite towards synthetic zeolite versus ascorbic acid is demonstrated which proves a great potential of synthetic zeolite to be used as a permselective membrane for graphite based macro/micro sensors to detect selectively DA in the presence of ascorbic acid.

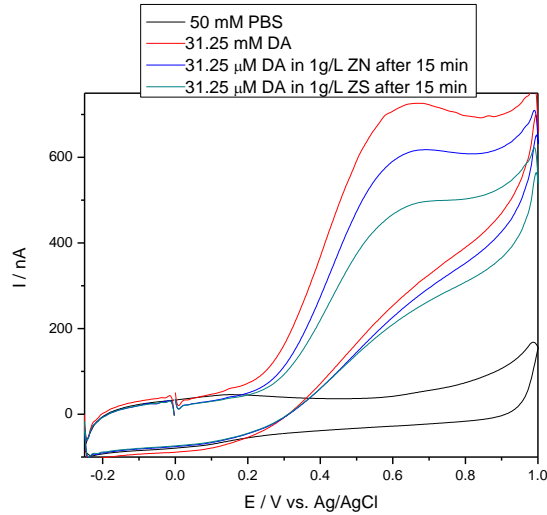


Figure 6.5 CVs recorded in 50 mL PBS of 31.25 μM concentration of dopamine before and after adding natural zeolite and synthetic zeolite in the supporting electrolyte solution, using a Boron Doped Diamond working electrode; Pt reference electrode and Ag/AgCl auxiliary electrode; scan rate 50 mV s^{-1} .

Based on these results, it can be concluded that synthetic zeolite exhibits a good sorption capacity towards DA, which makes it very suitable to be used as a permselective membrane to improve the selective detection of DA in the presence of AA. This property is due to the possibility of DA preconcentration onto synthetic zeolite incorporated onto a carbon based composite electrode improving local concentration and excluding AA presence at the electrode surface.

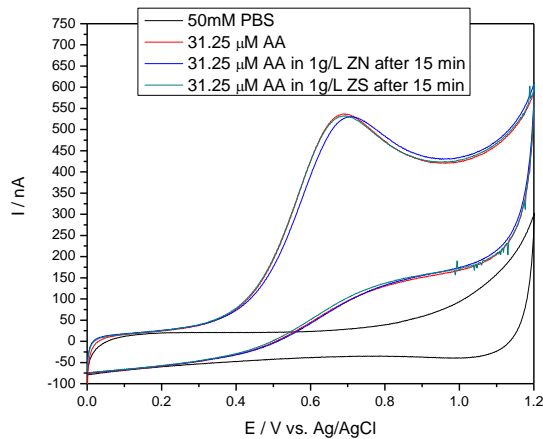


Figure 6.6 CVs recorded in 50 mL PBS of 31.25 μM concentration of ascorbic acid before and after adding natural zeolite and synthetic zeolite in the supporting electrolyte solution, using a Boron Doped Diamond working electrode; Pt reference electrode and Ag/AgCl auxiliary electrode; scan rate 50 mV s^{-1} .

6.2.2.3 Construction of modified composite sensing materials

6.2.2.3.1 Optimization of the graphite-zeolite-epoxy weight ratio for microelectrodes

Two types of zeolite materials (natural and synthetic) were introduced in the composite recipe by mechanical dispersion as presented in figure 6.7. In order to avoid a significant ohmic drop (by using too much of the insulator material that will undergo a reduction in sensor conductivity by the use of a smaller quantity of graphite) but still noticing a significant catalytic effect in detection experiments [6.41-6.42] an amount corresponding to 20% wt. zeolite was chosen to be used in this study. The optimum parameters of interest for μ -NZ-GEC and μ -SZ-GEC sensors are presented in table 6.3, where best results were obtained for μ -SZ-GEC, with a peak-to-peak separation of 0.093 V, a value close to reversible redox systems, which is considered to be 0.057 V.

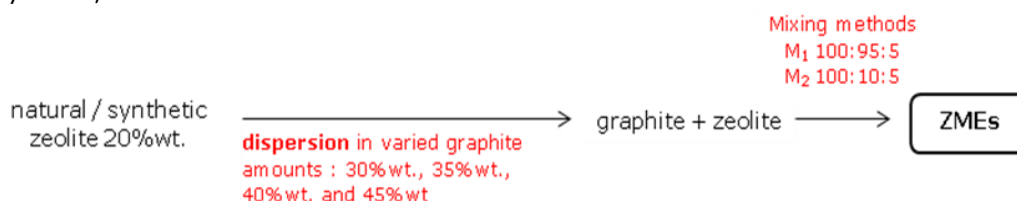


Figure 6.7 Optimization of the graphite-zeolite-epoxy weight ratio

Table 6.3: Electrochemical parameters for graphite : zeolite : epoxy composite construction; 2 mM $K_4Fe(CN)_6$ / $K_3Fe(CN)_6$ in 1M KNO_3 supporting electrolyte; scan rate 100 $mV s^{-1}$; potential range from -0.4 V to +0.8 V;

Mixing method	Resin ratio R:H:A (%wt)	Graphite (% wt.)	ΔE (V)	ΔI_a (nA)	$\Delta I_a/\Delta I_c$
M ₁ (μ -NZ-GEC)	100:95:5	45	0.343	250	0.94
M ₂ (μ -SZ-GEC)	100:10:5	45	0.093	170	1.14

6.2.2.3.2 Construction of synthetic/natural zeolite-graphite-epoxy macrosensors

The design of the macrosensors was made using a Cu wire as electrical contact inserted in an PVC tube (i.d.=2.5 cm). The geometrical area of the macrosensor surface with disk geometry was 0.196 cm^2 .

Carbon-epoxy based composites were constructed according to the following procedure:

- 1) A bare graphite-epoxy composite macroelectrode (M-GEC) sensor was firstly elaborated and considered as blank sensor, with curing conditions at 105°C for 30 min. The graphite-epoxy weight ratio, was chosen as 55% wt. graphite and 45% wt. epoxy with 100:95:5 resin:hardener:accelerator weight ratio
- 2) The second and third composite materials were modified by incorporating in the composite matrix, by mechanical dispersion, a constant 20% wt. ratio natural or synthetic zeolite, resulting in two new ZMEs: graphite 45%-natural

zeolite 20%-epoxy composite 35%, wt. (M-NZ-GEC) and graphite 45%-synthetic zeolite 20%-epoxy composite 35%, wt. (M-SZ-GEC).

6.2.2.3.3 Nafion[®] coated microelectrodes

Graphite-epoxy (μ -GEC), graphite-natural zeolite-epoxy (μ -NZ-GEC) and graphite-synthetic zeolite-epoxy (μ -SZ-GEC) disk electrodes (180 μ m diameter) were coated with Nafion[®] (Nf) via dip-coating method: dipping into Nafion solution (5 wt% solution in a mixture of lower aliphatic alcohols and water) for 5 s, action repeated for five times consequently, with pauses of 1 min between immersions. After the last dip, electrodes were dried in the air for 1 day, time for Nafion[®] membrane coated electrodes to be formed.

6.2.2.3.4 Carbon nanotubes film coated microelectrodes

Multi-walled carbon nanotubes (MWCNs) were sonicated for 6 min with tetrahydrofuran (THF) solvent in order to obtain a soluble product by avoiding agglomeration of MWCNTs particles [6.43]. The proportion of materials introduced for sonication process was 1:10 w/v.

The already made microelectrode skeletons filled with synthetic zeolite-graphite-epoxy composite materials were immersed for 5 s in the above dispersed CNTs for 3 times, time left between immersions was 10 min in order to allow the solvent to evaporate in the air. After each immersion, the Si capillary of the microsensors was carefully cleaned and allow the CNTs solution to attach only to the composite material electroactive surface.

6.3 Characterization of microelectrodes / macroelectrodes

6.3.1 Electrochemical surface characterization of unmodified graphite-epoxy composite microelectrodes

Cyclic voltammetry was used to determine the electroactive areas of all three μ -GEC, μ -NZ-GEC and μ -SZ-GEC sensors by classical potassium ferrocyanide system in 1 M KNO₃ supporting electrolyte recorded at different scan rates. Based on Randles-Sevcik equation 6.1 [6.44]:

$$I_p = 2.69 \times 10^5 AD^{1/2} n^{3/2} v^{1/2} C \quad (6.1)$$

where: A represents the area of the electrode (cm^2), n is the number of electrons participating in the reaction and is equal to 1, D is the diffusion coefficient of the molecule in solution, C is the concentration of the probe molecule in the solution and in this experimental set-up is 2 mM, and v is the scan rate (V s^{-1}), the apparent diffusion coefficient of K₃Fe(CN)₆ was determined to be $1.11 \cdot 10^{-4} \text{ cm}^2 \text{ s}^{-1}$ for the GEC sensor, $3.52 \cdot 10^{-5} \text{ cm}^2 \text{ s}^{-1}$ for NZ-GEC and $1.70 \cdot 10^{-5} \text{ cm}^2 \text{ s}^{-1}$ for the SZ-GEC sensor. All parameters values are presented in table 6.4.

By comparison with the theoretical diffusion coefficient, equal to $6.7 \cdot 10^{-6} \text{ cm}^2 \text{ s}^{-1}$ reported in literature [6.44], all sensors exhibited higher diffusion coefficients. It is known that the motion of particles in a solution, in order to reach the electrode surface and discharge themselves, can occur by convection, migration and diffusion. Based on this fact, and the increased magnitude of the apparent diffusion coefficient of the

$K_3Fe(CN)_6$, can be concluded that the effect of migration can not be considered negligible in this working conditions .

Electroactive surface area for μ -GEC , equal to $1.03 \cdot 10^{-3}$, was the highest from all sensors , value which decreased from μ -GEC to μ -ZN-GEC ($5.7 \cdot 10^{-4} \text{ cm}^2$) and μ -SZ-GEC ($3.8 \cdot 10^{-4} \text{ cm}^2$), but in all cases, the electroactive surface areas were higher than the geometric area of $2.5 \cdot 10^{-4} \text{ cm}^2$. Also, these expected results are due to the use of a decreased concentration of graphite in μ -SZ-GEC and μ -NZ-GEC sensors and increased quantity of insulating materials. Also, these results suggest that, this composite based sensors presented a large number of conducting microzones and that the majority of their surface was electroactive [6.45].

It can be observed μ -GEC microelectrode presents the higher electroactive surface, as well as the higher apparent diffusion coefficient. The behavior is considered normal, since the diffusion coefficient is a parameter characteristic of the diffusion phase reactant and not to the nature of the microelectrode.

Figures 6.8, 6.9A and 6.10A, show comparatively cyclic voltammograms of 2 mM $K_3Fe(CN)_6$ / $K_4Fe(CN)_6$ at different scan rates of all three sensors at the selected optimum composition. Literature states that for a reversible couple, the difference in peak potential has to be 0.057 V. The largest peak-to-peak separation together with less developed peaks were obtained for μ -NZ-GEC, with a $\Delta E = 0.343 \text{ V}$ (at a scan rate of 50 V s^{-1}). Lower peak-to-peak separations, 0.184 V and 0.093 V, are characteristic for μ -GEC and μ -SZ-GEC, respectively, as resulted from table 6.5 and table 6.6. This favorable behavior close to a reversible system at μ -SZ-GEC presents also well defined peaks.

Table 6.4: Apparent diffusion coefficients and electroactive surface areas of μ -GEC, μ -NZ-GEC and μ -SZ-GEC microelectrodes

Microelec- trode	Scan rate (V s^{-1})	Apparent diffusion coefficient ($\text{cm}^2 \text{ s}^{-1}$)	Theoretic al diffusion coefficient ($\text{cm}^2 \text{ s}^{-1}$)	Electroactiv e area (cm^2)	Total electroactive area (cm^2)	Geometri cal area (cm^2)
μ -GEC	0.025	$1.5 \cdot 10^{-4}$	$6.7 \cdot 10^{-6}$	$1.18 \cdot 10^{-3}$	$1.03 \cdot 10^{-3}$	$2.5 \cdot 10^{-4}$
	0.5	$1.16 \cdot 10^{-4}$		$1.04 \cdot 10^{-3}$		
	0.1	$1.24 \cdot 10^{-4}$		$1.07 \cdot 10^{-3}$		
	0.2	$1.08 \cdot 10^{-4}$		$1.0 \cdot 10^{-3}$		
	0.33	$1.01 \cdot 10^{-4}$		$9.71 \cdot 10^{-4}$		
	0.4	$9.78 \cdot 10^{-5}$		$9.55 \cdot 10^{-4}$		
	0.45	$9.69 \cdot 10^{-5}$		$9.51 \cdot 10^{-4}$		
μ -NZ- GEC	0.025	$4.79 \cdot 10^{-5}$	$6.7 \cdot 10^{-6}$	$6.68 \cdot 10^{-4}$	$5.7 \cdot 10^{-4}$	$2.5 \cdot 10^{-4}$
	0.5	$4.26 \cdot 10^{-5}$		$6.03 \cdot 10^{-4}$		
	0.1	$3.69 \cdot 10^{-5}$		$5.87 \cdot 10^{-4}$		
	0.2	$3.3 \cdot 10^{-5}$		$5.55 \cdot 10^{-4}$		
	0.33	$2.96 \cdot 10^{-5}$		$5.25 \cdot 10^{-4}$		
	0.4	$2.85 \cdot 10^{-5}$		$5.16 \cdot 10^{-4}$		
	0.45	$2.81 \cdot 10^{-5}$		$5.12 \cdot 10^{-4}$		
μ -SZ-	0.02	$6.62 \cdot 10^{-6}$	$6.7 \cdot 10^{-6}$	$2.48 \cdot 10^{-4}$	$3.8 \cdot 10^{-4}$	$2.5 \cdot 10^{-4}$

GEC	5				
	0.5	$1.05 \cdot 10^{-5}$		$3.14 \cdot 10^{-4}$	
	0.1	$1.4 \cdot 10^{-5}$		$3.62 \cdot 10^{-4}$	
	0.2	$1.8 \cdot 10^{-5}$		$4.09 \cdot 10^{-4}$	
	0.33	$2.18 \cdot 10^{-5}$		$4.51 \cdot 10^{-4}$	
	0.4	$2.33 \cdot 10^{-5}$		$4.66 \cdot 10^{-4}$	
	0.45	$2.43 \cdot 10^{-5}$		$4.76 \cdot 10^{-4}$	

At slow scan rates, the potential values, E , was slightly independent on the scan rate, confirming the lack of ohmic drop effect on the shape of cyclic voltammograms [6.46]. Although, while increasing the scan rates in CVs experiments, ΔE is independent on the scan rate. However, as noticed in figure 6.11, the measured ΔE values for reversible processes are generally higher due to uncompensated solution resistance and due to a slow electron transfer kinetics.

Table 6.5: The electrochemical parameters of the redox system (ferri/ferrocyanide) determined from the anodic branches of CVs for μ -GEC, μ -NZ-GEC and μ -SZ-GEC microelectrodes

Microelectrode type	Scan rate (V s ⁻¹)	E_a (V)	I_a (nA)	ΔI_a (nA)
μ -GEC	0.025	0.296	266.51	246.8
	0.5	0.304	335.7	305.55
	0.1	0.338	510	453.54
	0.2	0.38	700	606.8
	0.33	0.406	895.03	756.31
	0.4	0.416	954.82	797.93
	0.45	0.422	1020	849.96
μ -NZ-GEC	0.025	0.372	144.18	139.47
	0.5	0.385	194.59	186.87
	0.1	0.414	263.46	250.98
	0.2	0.453	358.6	336.47
	0.33	0.477	444.51	412.83
	0.4	0.484	482.85	445.98
	0.45	0.49	512.67	472.38
μ -SZ-GEC	0.025	0.242	82.03	55.44
	0.5	0.255	144.23	105.62
	0.1	0.258	245.43	171.38
	0.2	0.284	397.7	278.59
	0.33	0.31	568.54	391.16
	0.4	0.323	641.88	442.27
	0.45	0.334	704	486.36

By plotting ferricyanide anodic/cathodic peak current as a function of the scan rate (Figures 6.8B, 6.9B and 6.10B), resulted in a linear relationship of I vs. $v^{1/2}$ in the range of 25 - 454 mV s⁻¹, which indicated a diffusion-controlled process. The higher the slope, the better the diffusion and the faster kinetics which varied as following: μ -ZS-GEC > μ -ZN-GEC > μ -GEC. This behavior proved the catalytic effect of zeolite which for this redox system the best catalytic behavior being exhibited by the synthetic zeolite.

Voltammetric performance of the sensors in this experimental conditions can be regarded as starting point for electrochemical behavior characteristics investigation. Literature data state a hypothesis in which sensors fabricated using a mixture of graphite particles and epoxy resin, exhibit a random or ordered microelectrode ensemble behavior. From Figures 6.8A, 6.9A and 6.10A, all voltammograms at slow scan rates present a sigmoidal response consistent to a microelectrode behavior. At fast scan rates a more peak shaped response is obvious, especially at μ -SZ-GEC sensor, characteristic for solid macroelectrode behavior [6.47] and substantial hysteresis appears at all composites.

Table 6.6: The electrochemical parameters of the redox system (ferri/ferrocyanide) determined from the cathodic branches of CVs for μ -GEC, μ -NZ-GEC and μ -SZ-GEC microelectrodes

Microelectrode type	Scan rate ($V s^{-1}$)	E_c (V)	I_c (nA)	ΔI_c (nA)
μ -GEC	0.025	0.125	-292.46	-279.99
	0.5	0.12	-367.55	-342.21
	0.1	0.096	-544.78	-493.78
	0.2	0.065	-732.52	-647.99
	0.33	0.039	-933.78	-804.63
	0.4	0.026	-1034.4	-885.13
	0.45	0.021	-1097.5	-934.82
μ -NZ-GEC	0.025	0.047	-158.98	-154.96
	0.5	0.042	-206.55	-205.94
	0.1	0.021	-278.26	-266.05
	0.2	-0.0099	-376.24	-355.32
	0.33	-0.044	-464.99	-432.34
	0.4	-0.051	-501.2	-463.36
	0.45	-0.057	-530.31	-488.94
μ -SZ-GEC	0.025	0.172	-73.02	-53.96
	0.5	0.162	-124.085	-90.015
	0.1	0.146	-209.5	-147.79
	0.2	0.133	-333.91	-231.95
	0.33	0.115	-481.54	-334.52
	0.4	0.104	-547.46	-380.02
	0.45	0.096	-597.59	-407.72

$$\Delta E = E_a - E_c = 0.385 - 0.042 = 0.343 \text{ V}$$

$$\Delta I_a / \Delta I_c = 305.55 / 342.21 = 0.89$$

Theoretically, the shape of a CV for a microelectrode ensemble depends on the distance between individual microelectrode in the ensemble, and also depends on the distance relative to the thickness of the diffusion layer, which in turn, depends on the time scale of the experiment. In CV, the time scale of the experiment is determined by the scan rate and potential scan window. The shorter the spacing between individual microelectrodes, the electrochemical behavior will be similar to that of a macroelectrode for the most scan rates. While for larger spacing, sigmoidal shaped CV responses were obtained, characteristic to a microelectrode ensemble, meaning that the distance between individual graphite microelectrode is

sufficiently far that the diffusion layer does not overlap, within the time scale of the experiment [6.48].

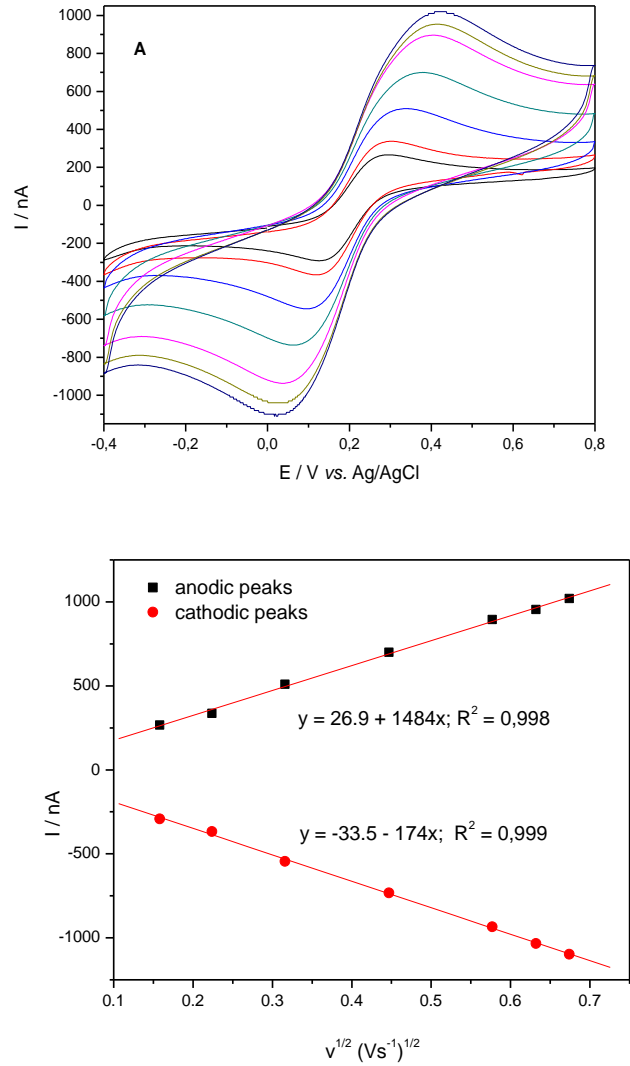


Figure 6.8 (A) Cyclic voltammograms recorded at μ -GEC, composite with 2 mM potassium ferricyanide/ferrocyanide at different scan rates : 25, 50, 100, 200, 333, 400, 454 $mV s^{-1}$ in 20 mL of 1M KNO_3 supporting electrolyte; potential range from -0.4 to +0.8 V; (B) Calibration plots of the oxidative and reductive peak currents vs. square root of scan rate without charging current subtraction.

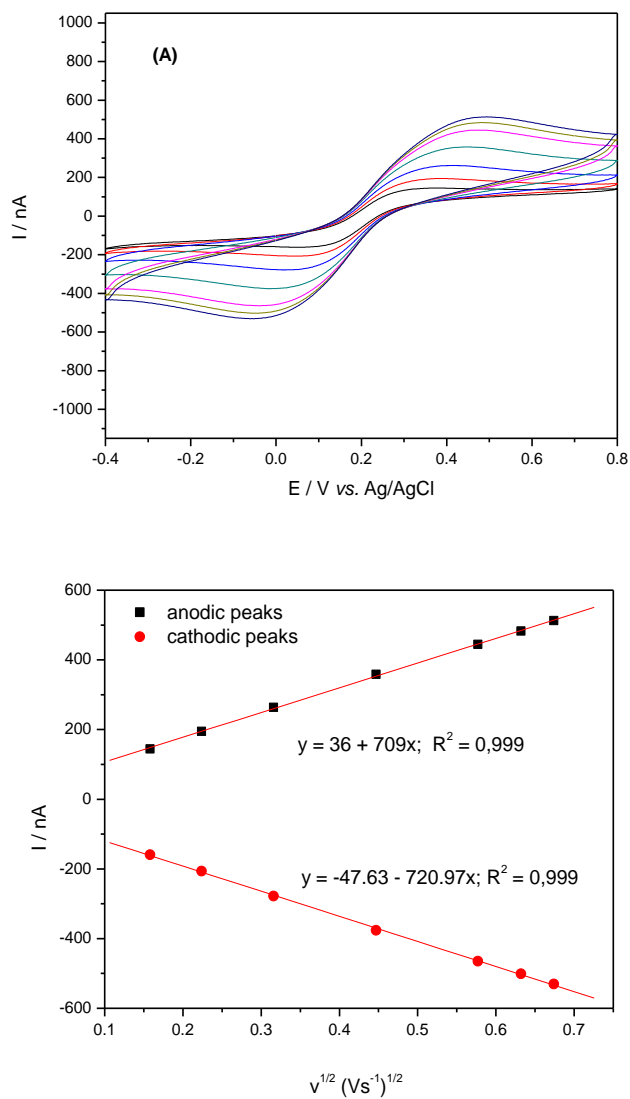


Figure 6.9 (A) Cyclic voltammograms recorded at μ -ZN-GEC composite with 2 mM potassium ferricyanide/ferrocyanide at different scan rates : 25, 50, 100, 200, 333, 400, 454 mV s^{-1} in 20 mL of 1M KNO_3 supporting electrolyte; potential range from -0.4 to +0.8 V; (B) Calibration plots of the oxidative and reductive peak currents vs. square root of scan rate without charging current subtraction.

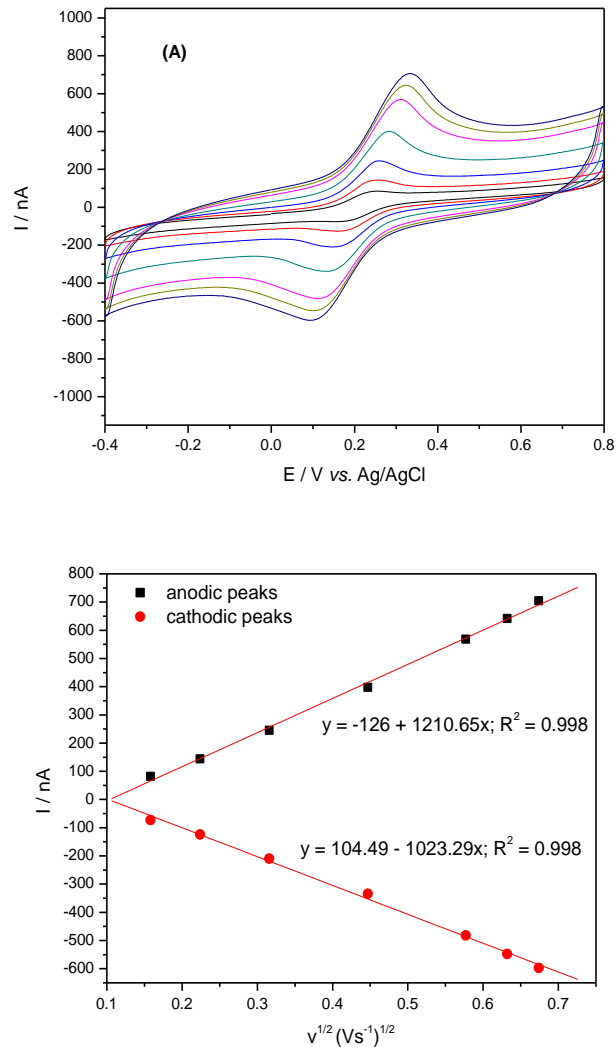


Figure 6.10 (A) Cyclic voltammograms recorded at μ -SZ-GEC composite with 2 mM potassium ferricyanide/ferrocyanide at different scan rates : 25, 50, 100, 200, 333, 400, 454 mV s^{-1} in 20 mL of 1M KNO_3 supporting electrolyte; potential range from -0.4 to +0.8 V; (B) Calibration plots of the oxidative and reductive peak currents vs. square root of scan rate without charging current subtraction.

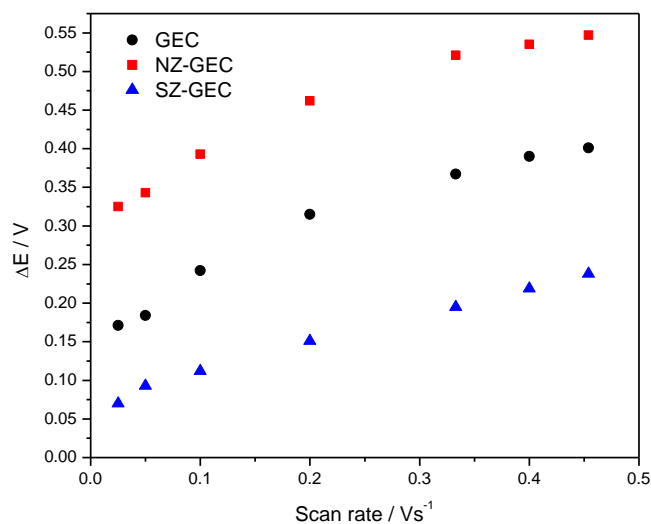


Figure 6.11 Plot of ΔE vs. scan rate parameters recorded at GEC, NZ-GEC, SZ-GEC, microelectrodes in 20 mL of 1M KNO_3 supporting electrolyte with 2 mM potassium ferricyanide/ferrocyanide at different scan rates : 25, 50, 100, 200, 333, 400, 454 mV s^{-1} ; potential range from -0.4 to +0.8 V; Ag/AgCl reference electrode and Pt auxiliary electrode.

Also, a diffusion field overlap for all composites microelectrode assemblies was noticed, aspect characteristic to a macroelectrode behavior. As well, when plotting $\log i$ vs. $\log v$, (in figure 6.12) for all three composites, slopes values of 0.475 for μ -GEC, 0.436 for μ -NZ-GEC, and 0.724 for μ -SZ-GEC are obtained. A slope lower than 0.5 is associated to a mixed linear and spherical diffusion, characteristic to a mixture of macro and microelectrode behaviour, depending on experimental time scale.

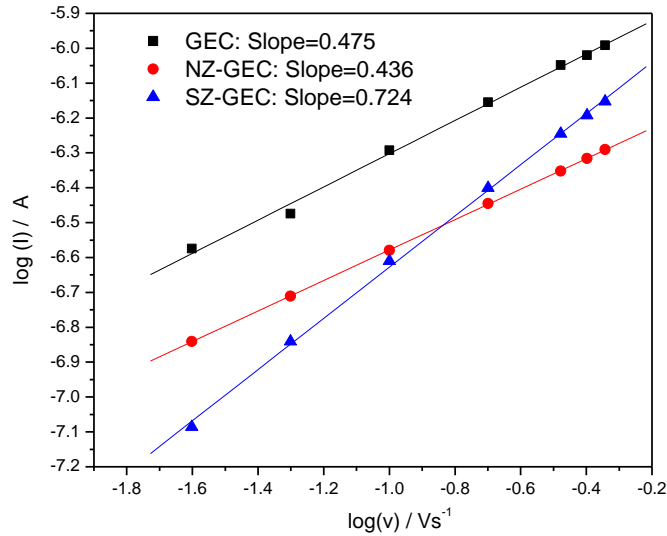


Figure 6.12 Plots of $\log(v)$ vs. $\log(i)$ parameters recorded at GEC, NZ-GEC, SZ-GEC, microelectrodes in 20 mL of 1M KNO_3 supporting electrolyte with 2 mM potassium ferricyanide/ferrocyanide at different scan rates : 25, 50, 100, 200, 333, 400, 454 mV s^{-1} ; potential range from -0.4 to +0.8 V; Ag/AgCl reference electrode and Pt auxiliary electrode.

6.3.2 Electrochemical surface characterization of film modified graphite-epoxy composite microelectrodes

Due to the fact that μ -ZS-GEC composite microelectrode presented the best results in terms of reaction reversibility, this specific microelectrode was chosen to be covered with CNT film on the surface of composite microsensor. The same experimental conditions and surface electrochemical characterization was applied for CNT film- μ -ZS-GEC microelectrode. Table 6.7 presents the results for the film covered on the microsensor compared with simple μ -SZ-GEC microelectrode.

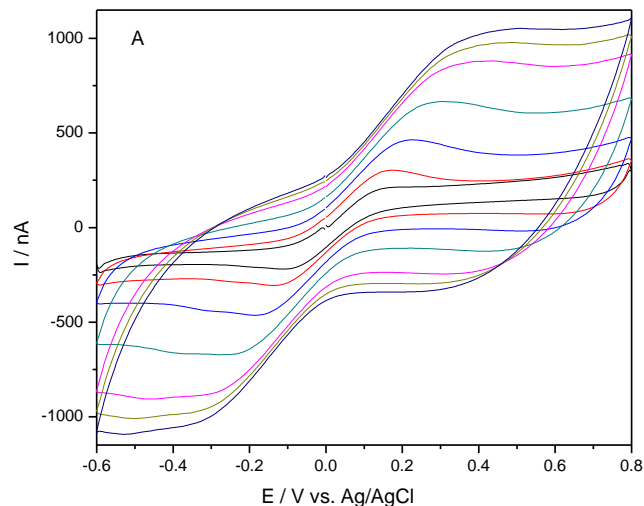
Table 6.7: Apparent diffusion coefficients and electroactive surface areas of CNT film-ZS-GEC and μ -SZ-GEC microelectrodes

Microelec- trode	Scan rate (V s^{-1})	Apparent diffusion coefficient ($\text{cm}^2 \text{s}^{-1}$)	Theoretic al diffusion coefficient ($\text{cm}^2 \text{s}^{-1}$)	Electroactiv e area (cm^2)	Total electroactive area (cm^2)	Geometri cal area (cm^2)
μ -SZ- GEC	0.02	$6.62 \cdot 10^{-6}$	$6.7 \cdot 10^{-6}$	$2.48 \cdot 10^{-4}$	$3.8 \cdot 10^{-4}$	$2.5 \cdot 10^{-4}$
	5	$1.05 \cdot 10^{-5}$		$3.14 \cdot 10^{-4}$		
	0.1	$1.4 \cdot 10^{-5}$		$3.62 \cdot 10^{-4}$		
	0.2	$1.8 \cdot 10^{-5}$		$4.09 \cdot 10^{-4}$		
	0.33	$2.18 \cdot 10^{-5}$		$4.51 \cdot 10^{-4}$		

	0.4	$2.33 \cdot 10^{-5}$		$4.66 \cdot 10^{-4}$		
	0.45	$2.43 \cdot 10^{-5}$		$4.76 \cdot 10^{-4}$		
CNT film μ -ZS- GEC	0.02 5	$6.5 \cdot 10^{-5}$	$6.7 \cdot 10^{-6}$	$7.8 \cdot 10^{-4}$	$5.88 \cdot 10^{-4}$	$2.5 \cdot 10^{-4}$
	0.5	$5.2 \cdot 10^{-5}$		$7.0 \cdot 10^{-4}$		
	0.1	$5.3 \cdot 10^{-5}$		$7.0 \cdot 10^{-4}$		
	0.2	$3.4 \cdot 10^{-5}$		$5.6 \cdot 10^{-4}$		
	0.33	$2.5 \cdot 10^{-5}$		$4.8 \cdot 10^{-4}$		
	0.4	$2.2 \cdot 10^{-5}$		$4.5 \cdot 10^{-4}$		
	0.45	$1.9 \cdot 10^{-5}$		$4.2 \cdot 10^{-4}$		

As noticed from table 6.7, the electroactive areas of the film covered microsensor is higher than for simple μ -ZS-GEC microsensor. If CNT is well dispersed, normally have to increase the electroactive surface of the microsensors, while here, values equal with $5.88 \cdot 10^{-4} \text{ cm}^2$ for CNT film- μ -ZS-GEC are comparable with the electroactive area of simple ZS-GEC microsensor, which is equal with $3.8 \cdot 10^{-4} \text{ cm}^2$. Among factors influencing the increase in electroactive surface can be considered the CNT dispersion efficiency, dipping method efficiency and the thickness of the CNT layer, and not the last, the coverage of the film on the already cured zeolite composite electrode material.

Figure 6.13A shows cyclic voltammograms of $2\text{mM K}_3\text{Fe}(\text{CN})_6 / \text{K}_4\text{Fe}(\text{CN})_6$ at different scan rates for CNT-film- μ -ZS-GEC microsensor. Compared to previous composite materials (μ -GEC, μ -ZN-GEC and μ -ZS-GEC) the film covered microsensors presented large peak-to-peak separations together with poor developed ferricyanide/ferrocyanide peaks. A value of ΔE close to 0.305 V (at a scan rate of 50 mVs^{-1}) was obtained for CNT-film- μ -ZS-GEC sensor. This ΔE values is close to the one obtained for simple μ -ZN-GEC microsensor, pointing that the film coverage has an influence in the diffusion rate providing slow kinetics.



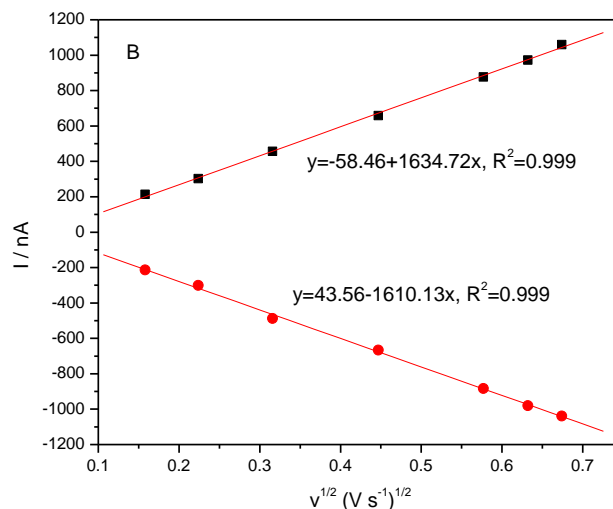


Figure 6.13 (A) Cyclic voltammograms recorded at CNT film μ -ZS-GEC composite with 2 mM potassium ferricyanide/ferrocyanide at different scan rates : 25, 50, 100, 200, 333, 400, 454 mV s^{-1} in 20 mL of 1M KNO_3 supporting electrolyte; potential range from -0.6 to +0.8 V; (B) Calibration plots of the oxidative and reductive peak currents vs. square root of scan rate without charging current subtraction.

Its electrochemical behavior in the presence of classical ferri/ferrocyanide system as linear relationship of I vs. $v^{1/2}$ in the same above presented scan rate range indicated also a diffusion-controlled process, similar as for previous simple microsensors (see figure 7.13.B).

6.3.3 Electrochemical surface characterization of modified/unmodified graphite-epoxy composite macroelectrodes

Cyclic voltammetry was used, as in previous section for microelectrodes, to determine the electroactive areas of all three M-GEC, M-NZ-GEC, M-SZ-GEC, sensors by classical potassium ferrocyanide system in 1 M KNO_3 supporting electrolyte recorded at different scan rates using Randles-Sevcik equation.

In table 6.8, all coefficients values are presented. The apparent diffusion coefficients are smaller than the theoretical one ($6.7 \cdot 10^{-6} \text{ cm}^2 \text{ s}^{-1}$), where $4.88 \cdot 10^{-6} \text{ cm}^2 \text{ s}^{-1}$ is the apparent diffusion coefficient for the M-GEC, $2.89 \cdot 10^{-6} \text{ cm}^2 \text{ s}^{-1}$ for M-NZ-GEC and $3.24 \cdot 10^{-6} \text{ cm}^2 \text{ s}^{-1}$ for M-SZ-GEC.

The calculated electroactive areas for M-GEC (0.165 cm^2), for M-NZ-GEC (0.127 cm^2) and for M-SZ-GEC (0.135 cm^2) were lower than the geometrical area of 0.196 cm^2 . The decreased electroactive surfaces for all three macroelectrodes, is due to the use of a decreased graphite concentration in the total composite matrix and an increased quantity of insulating materials, showing that for this specific composite materials they present a decreased number of conducting microzones and that the electroactive surface is not entirely active.

Table 6.8: Apparent diffusion coefficients and electroactive surface areas of M-GEC, M-NZ-GEC, M-SZ-GEC macroelectrodes

Electrode type	Apparent diffusion coefficient ($\text{cm}^2 \text{s}^{-1}$)	Theoretical diffusion coefficient ($\text{cm}^2 \text{s}^{-1}$)	Electroactive area (cm^2)	Geometrical area (cm^2)
M-GEC	$4.88 \cdot 10^{-6}$	$6.7 \cdot 10^{-6}$	0.165	0.196
M-ZN-GEC	$2.89 \cdot 10^{-6}$		0.127	
M-SZ-GEC	$3.24 \cdot 10^{-6}$		0.135	

6.4 Conclusions

Several graphite-epoxy composite microelectrodes, *i.e.*, μ -GEC, μ -ZN-GEC and μ -ZS-GEC in comparison with the same composition of macroelectrodes, *i.e.*, M-GEC, M-ZN-GEC, M-ZS-GEC were successfully prepared.

Graphite-epoxy (M-GEC), natural zeolite-graphite-epoxy (M-NZ-GEC), synthetic zeolite-graphite-epoxy (M-SZ-GEC) composite macroelectrodes were obtained as main electrochemical materials. The design of the macrosensors presented disk shaped geometry of 0.196 cm^2 .

The bare graphite-epoxy composite was considered as blank material and zeolite-graphite-epoxy composite electrode materials were constructed for highlighting the superiority of the zeolite presence in the composite matrix in further applications.

Cyclic voltammetry technique was used to determine electroactive surfaces of constructed materials. Electroactive surface area for M-GEC, equal to 0.165 cm^2 , was the highest from all sensors, value which decreased from M-GEC to M-ZS-GEC (0.135 cm^2) and M-NZ-GEC (0.127 cm^2), but in all cases, the electroactive surface areas were smaller than the calculated geometric area of 0.196 cm^2 .

Graphite-epoxy (μ -GEC), natural zeolite-graphite-epoxy (μ -NZ-GEC), synthetic zeolite-graphite-epoxy (μ -SZ-GEC) composite microelectrodes were obtained as main electrochemical materials. The design of the microsensors presented a disk shaped geometry of $2.5 \cdot 10^{-4} \text{ cm}^2$ and a final length of 5 cm. For further investigations, Nafion coated microelectrodes (Nafion- μ -GEC, Nafion- μ -ZN-GEC, Nafion- μ -ZS-GEC) and carbon nanotubes film coated microsensors (CNT-film- μ -ZS-GEC) were constructed.

The bare graphite-epoxy composite as blank material and zeolite-graphite-epoxy composite electrode materials were constructed in steps involving several optimization procedures: finding the best epoxy resin polymerization conditions, a proper mixing method of the three-epoxy component with graphite particles following the optimization of graphite-epoxy weight ratio and optimization of graphite-zeolite-epoxy weight ratio, all optimization procedures having a major importance over the sensitivity and reversibility performance of the final sensor.

The classical ferri/ferrocyanide system with cyclic voltammetry technique was used to determine electroactive surfaces of constructed materials. Electroactive surface area for μ -GEC, equal to $1.03 \cdot 10^{-3}$, was the highest from all microsensors, value which decreased from μ -GEC to μ -ZN-GEC ($5.7 \cdot 10^{-4} \text{ cm}^2$) and μ -SZ-GEC ($3.8 \cdot 10^{-4} \text{ cm}^2$), but in all cases, the electroactive surface areas were higher than the

calculated geometric area of $2.5 \cdot 10^{-4} \text{ cm}^2$, results comparable with values equal with $5.88 \cdot 10^{-4} \text{ cm}^2$ for CNT film- μ -ZS-GEC.

All sensors presented a large number of conducting microzones and the majority of their surface is electroactive. Also, a diffusion-controlled process was found based on the linear relationship of I vs. $v^{1/2}$ in the scan rate ranged from 25 to 454 mV s^{-1} .

A more detailed investigation was done for graphite-epoxy (μ -GEC), natural zeolite-graphite-epoxy (μ -NZ-GEC), synthetic zeolite-graphite-epoxy (μ -SZ-GEC) composite microelectrodes in terms of macroelectrode/microelectrode array behaviour. All voltammograms at slow scan rates presented a sigmoidal response consistent to a microelectrode behavior. At fast scan rates a more peak shaped response was obvious, especially at μ -SZ-GEC sensor, characteristic for solid macroelectrode behavior and substantial hysteresis appeared at all three composites. Also, a diffusion field overlap for all composites microelectrode assemblies was noticed, aspect characteristic to a macroelectrode behavior and slopes when plotting $\log i$ vs. $\log v$ lower than 0.5 was associated to a mixed linear and spherical diffusion, fact that arises at microelectrodes, depending on experimental time scale.

Taking into consideration that the main goal of these composite material is to detect selectively/simultaneously dopamine (DA) and ascorbic acid (AA), the sorption capacity of both natural and synthetic zeolite towards dopamine and ascorbic acid was investigated. Synthetic zeolite exhibited a good sorption capacity towards DA, which makes it very suitable to be used as a permselective membrane to improve the selective detection of DA in the presence of AA. This property is due to the possibility of DA preconcentration onto synthetic zeolite incorporated onto a carbon based composite electrode improving local concentration and excluding AA presence at the electrode surface.

6.5 References

- [6.1] T. Kuwana and W. French, "Electrooxidation or reduction of organic compounds into aqueous solutions using carbon paste electrodes," *Analytical chemistry*, vol. 24, p. 241, 1964.
- [6.2] K. Ravichandran and R. Baldwin, "Chemically modified carbon paste electrodes," *Journal of Electroanalytical Chemistry*, vol. 129, p. 293, 1981.
- [6.3] Y. Li, H. Xie, F. Zhou and H. Guo, "Determination of trace tin by anodic stripping voltammetry at a carbon paste electrode," *Electroanalysis*, vol. 18, pp. 976-980, 2006.
- [6.4] R. Ojani, J. Raouf and E. Zarei, "Acetylferrocene Modified Carbon Paste Electrode; A Sensor for Electrocatalytic Determination of Hydrazine," *Electroanalysis*, vol. 20, p. 1378-1382, 2008.
- [6.5] C. Neuhold, K. Kalcher, W. Diewald, X. Cai and G. Raber, "Voltammetric determination of nitrate with a modified carbon paste electrode," *Electroanalysis*, vol. 6, p. 227-236, 1994.
- [6.6] X. Hu and Z. Leng, "Determination of L-Ascorbic Acid by Adsorption Potentiometry with Carbon Paste Electrode," *Analytical letters*, vol. 28, pp. 2263-2274, 1995.
- [6.7] J. Lindquist, "Voltammetric determination of pyridoxine by use of a carbon

- paste electrode," *Analyst*, vol. 100, pp. 349-354, 1975.
- [6.8] J. Labuda and M. Hudokava, "Hexacyanoferrate-anion exchanger-modified carbon paste electrodes," *Electroanalysis*, vol. 9, p. 239-242, 1997.
- [6.9] A. Nezamzadeh, M. Amini and H. Faghihian, "Square-Wave Voltammetric Determination of Ascorbic Acid Based on its Electrocatalytic Oxidation at Zeolite-Modified Carbon-Paste Electrodes," *International journal of electrochemical science*, vol. 2, pp. 583-594, 2007.
- [6.10] A. Florou, M. Prodromiris, S. Tzuouwara and M. Karayannis, "ABRICATION AND VOLTAMMETRIC STUDY OF La(DCPI)₃ CHEMICALLY MODIFIED SCREEN PRINTED ELECTRODES. APPLICATION FOR THE DETERMINATION OF ASCORBIC ACID," *Analytica chimica acta*, vol. 423, pp. 107-114, 2004.
- [6.11] P. O'Connell, C. Gormally, M. Pravda and G. Guilbaut, "Development of an amperometric l-ascorbic acid (Vitamin C) sensor based on electropolymerised aniline for pharmaceutical and food analysis," *Analytica chimica acta*, vol. 431, p. 239-247, 2001.
- [6.12] E. Turkusic, V. Milicevic, H. Tahmiscija, M. Vehabovic and S. Basic, "Amperometric sensor for L-ascorbic acid determination based on MnO₂ bulk modified screen printed electrode," *Fresenius journal of analytical chemistry*, vol. 368, pp. 466-470, 2000.
- [6.13] J. Kulys and E. D'Costa, "EVALUATION OF THE ELECTRO-CATALYTIC OXIDATION OF ASCORBIC ACID, USING A PLATINUM ELECTRODE MODIFIED WITH POLY-3-METHYLTHIOPHENE," *Analytica chimica acta*, vol. 243, pp. 173-178, 1991.
- [6.14] J. Zen, D. Tsai and A. Kumar, "Recent Updates of Chemically Modified Electrodes in Analytical Chemistry," *Electroanalysis*, vol. 15, p. 1073-1087, 2003.
- [6.15] J. He, X. Lin and J. Pan, "Multi-Wall Carbon Nanotube Paste Electrode for Adsorptive Stripping Determination of Quercetin: A Comparison with Graphite Paste Electrode via Voltammetry and Chronopotentiometry," *Electroanalysis*, vol. 17, p. 1681-1686, 2005.
- [6.16] X. Lin, J. He and Z. Zha, "Simultaneous determination of quercetin and rutin at a multi-wall carbon-nanotube paste electrodes by reversing differential pulse voltammetry," *Sensors and actuators B*, vol. 119, p. 608-614, 2006.
- [6.17] G. Volikakis and C. Efstathiou, "Fast screening of total flavonols in wines, tea-infusions and tomato juice by flow injection/adsorptive stripping voltammetry," *Analytica chimica acta*, vol. 551, p. 124-131, 2005.
- [6.18] D. El-Hardy and N. El-Maal, "Selective square wave voltammetric determination of (+)-catechin in commercial tea samples using beta-cyclodextrin modified carbon paste electrode," *Microchimica acta*, vol. 161, pp. 225-231, 2008.
- [6.19] J. Wang, "Electrochemical Glucose Biosensors," *Chemical reviews*, vol. 108, pp. 814-825, 2008.
- [6.20] J. Wang, "In vivo glucose monitoring: Towards 'Sense and Act' feedback-loop individualized medical systems," *Talanta*, vol. 75, p. 636-641, 2008.
- [6.21] P. Yanfen, H. Chengguo, Z. Dongyun and H. Shengshui, "A sensitive nitric oxide microsensor based on PBPB composite film modified carbon fiber microelectrode," *Sensors and actuators B*, vol. 133, pp. 571-576, 2008.

- [6.22] A. Tatyana, K. Joyonul and C. Thomas, "Development and environmental polypyrrole films," *Sensors and actuators B*, vol. 106, pp. 512-517, 2005.
- [6.23] P. Maxime, C. Gobin, P. Thierry, F. Bedioui and D. Jacues, "Electrochemical nitric oxide microsensors: sensitivity and selectivity characterization," *Analytica chimica acta*, vol. 411, pp. 175-185, 2000.
- [6.24] J. Mitala and A. Michael, "Improving the performance of electrochemical microsensors based on enzymes entrapped in a redox hydrogel," *Analytica chimica acta*, vol. 556, pp. 326-332, 2006.
- [6.25] W. Joseph, Z. Xueji and P. Madhu, "Glucose microsensors based on carbon paste enzyme electrodes modified with cupric hexacyanoferrate," *Analytica chimica acta*, vol. 395, pp. 11-16, 1999.
- [6.26] G. Michel and C. Adrian, "Amperometric microsensor for monitoring choline in the extracellular fluid of brain," *Journal of neuroscience methods*, vol. 70, pp. 73-82, 1996.
- [6.27] A. Farook, C. Andreas, B. Martina, P. Ahmad and A. Sulaiman, "Minimizing tissue-material interaction in microsensor for subcutaneous glucose monitoring," *Biosensors and bioelectronics*, vol. 22, pp. 1625-1632, 2007.
- [6.28] C. Gianmario, R. Gaia, M. Rossana, S. Ylenia, B. Gianfranco, L. John, D. Maria and S. Pier-Andreea, "Biotelemetric monitoring of brain neurochemistry in conscious rats using microsensors and biosensors," *Sensors*, vol. 9, pp. 2511-2523, 2009.
- [6.29] B. F., "Characterization of carbon paste electrode for real-time amperometric monitoring of brain tissue oxygen," *Journal of neuroscience methods*, vol. 195, pp. 135-142, 2011.
- [6.30] O. Adrienne and O. Robert, "Effect of acid monitored with carbon paste electrodes," *Journal of neurochemistry*, vol. 62, pp. 1496-1504, 1994.
- [6.31] A. El and R. O'Neill, "Characterization in vitro of a naphthoquinone mediated glucose oxidase modified paste electrode designed for neurochemical analysis in vivo," *Electrochimica acta*, vol. 40, pp. 2791-2797, 1995.
- [6.32] C. Orha, C. Lazau, A. Pop, I. Grozescu and F. Manea, "Structural characterization and the sorption properties of the natural and synthetic zeolite," *Journal of electroelectronics and advanced materials*, vol. 15, pp. 544-549, 2011.
- [6.33] **E. Ilinoiu**, A. Pop, A. Jakab, F. Manea, R. Pode and P. Serra, "Amperometric detection of dopamine and ascorbic acid with zeolite-graphite composite microelectrode," *WIT Press Transactions on Ecology and Environment*, vol. 164, pp. 1743-3541, 2012.
- [6.34] C. Carolina, K. Renata, C. Aline, A. Luiz and C. Priscila, "Development of graphite polymer composites as electrode materials," *Materials research*, vol. 10, pp. 109-114, 2007.
- [6.35] L. Navarro, J. Trijueque, F. Vicente and H. Scholl, "Voltammetric determination of optimal conductive load proportion in graphite epoxy composite electrodes," *Journal of electroanalytical chemistry*, vol. 379, pp. 159-163, 1994.
- [6.36] J. Trijueque, L. Navarro, A. Sanmantis and F. Vicente, "Ohmic drop of prussian blue graphite epoxy electrodes," *Electrochimica acta*, vol. 45, pp. 789-795, 1999.

- [6.37] **E. Ilioiu**, L. Colar, L. Cochechi, C. Ratiu, F. Manea and R. Pode, "Kinetics and equilibrium studies of Reactive Yellow 125 adsorption on a nitrogen doped TiO₂ modified zeolite," *Environmental engineering and management journal*, vol. 10, pp. 1743-1750, 2011.
- [6.38] L. Colar, L. Cochechi, **E. Ilioiu**, F. Manea, C. Orha and R. Pode, "Adsorption of reactive yellow 125 dye from aqueous solution on a silver doped TiO₂ modified clinoptilolite," *Environmental engineering and management journal*, vol. 11, pp. 1822-1827, 2012.
- [6.39] A. Pop, **E. Ilioiu**, F. Manea, I. PISOI and G. Burtica, "Determination of organic pollutants from water by electrochemical methods," *Environmental engineering and management journal*, vol. 10, pp. 75-80, 2011.
- [6.40] W. Alain and J. Wang, "Zeolite modified carbon paste electrode for selective monitoring of dopamine," *Journal of electroanalytical chemistry*, vol. 407, pp. 183-187, 1996.
- [6.41] G. Delia, M. Andrada and W. Alain, "Ion enriched natural zeolite modified carbon paste electrode for H₂O₂ detection," *Electrochimica acta*, vol. 55, pp. 4050-5056, 2010.
- [6.42] B. Ali, Z. Mojgan, K. Balal and T. Aliereza, "Simultaneous determination of tryptophan, uric acid and ascorbic acid at iron(III) doped zeolite modified carbon paste electrode," *Colloids and surfaces B: Biointerfaces*, vol. 66, pp. 226-232, 2008.
- [6.43] R. Adriana, Multi wall carbon nanotube composite electrodes for electroanalysis applications, Timisoara: Univresitatea "Politehnica" Timisoara, 2011.
- [6.44] Y. e. al, "Implications of mechanism-based inhibition of CYP2D6 for the pharmacokinetics and toxicity of MDMA.," *Journal of Psychopharmacology*, vol. 20, pp. 842-849, 2006.
- [6.45] G. Sonia, A. Salvador, F. Cespedes and F. Robert, "Carbon composite electrodes: surface and electrochemical properties," *The analyst*, vol. 127, pp. 1512-1519, 2002.
- [6.46] M. Mazloum, Z. Akrami, H. Kazemian and H. Zare, "Electrocatalytic characteristics of uric acid oxidation at graphite-zeolite-modified electrode doped with iron III," *Journal of electroanalytical chemistry*, vol. 586, pp. 31-38, 2006.
- [6.47] O. Danny, V. Julie and W. Alison, "On the microelectrode behaviour of graphite epoxy composite electrodes," *Electrochemistry communications*, vol. 4, pp. 245-250, 2002.
- [6.48] F. Rosemary and P. Samuel, "Microfabricated ultramicroelectrode arrays: developments, advances and applications in environmental analysis," *Electroanalysis*, vol. 12, pp. 677-684, 2000.

CHAPTER 7

Applications of modified/unmodified graphite-epoxy composite macrosensors

7.1 Experimental

7.1.1 Chemicals and reagents

L-Ascorbic Acid (Sigma, Aldrich) solutions were freshly prepared prior to each experiment and dissolved in 0.01 M HCl solution, as well as protected against light exposure during experimental procedures.

Phosphate saline buffer solutions (PBS) supporting electrolyte, was prepared from di-hydrogenphosphate, sodium chloride and sodium hydroxide of analytical reagent grade (Sigma, Aldrich) and used as received. PBS solution was kept in the refrigerator when not used.

Dopamin-Hydrochloracid (Fluka) solutions were freshly prepared prior to each experiment, dissolved in PBS solution and protected against light exposure during experimental procedures.

7.1.2 Apparatus and experimental measurements

Experimental investigations were carried out using an AUTOLAB potentiostat / galvanostat PGSTAT302 (EcoChemie, Netherlands), controlled by PC and software GPES 4.9 (General Purpose Electrochemical System). All the electrochemical measurements were carried out in a Metrohm three electrode cell, equipped with a working electrode, a platinum counter electrode and respectively, a Ag/AgCl used as reference electrode. Before using, working electrodes were first cleaned mechanically using fine abrasive paper, 0.3 mm alumina powder (Metrohm, Switzerland), then were washed with distilled water for 5 minutes.

For detection experiments, the 50 mM PBS supporting electrolyte, pH of 7.4, was placed in the cell, and solutions of ascorbic acid and dopamine were employed by standard addition method solution. The scan rate employed for the detection experiments was 50 mV s⁻¹.

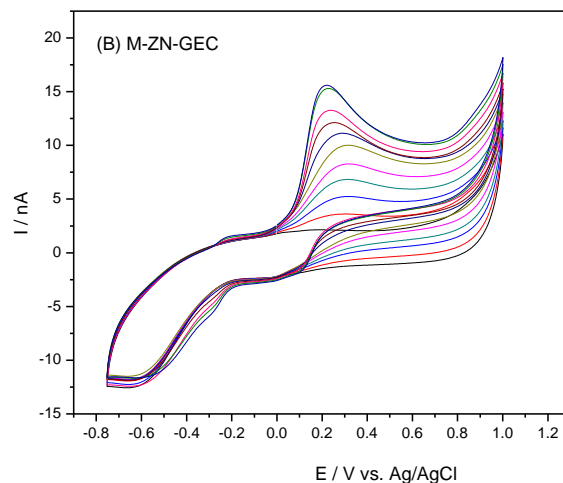
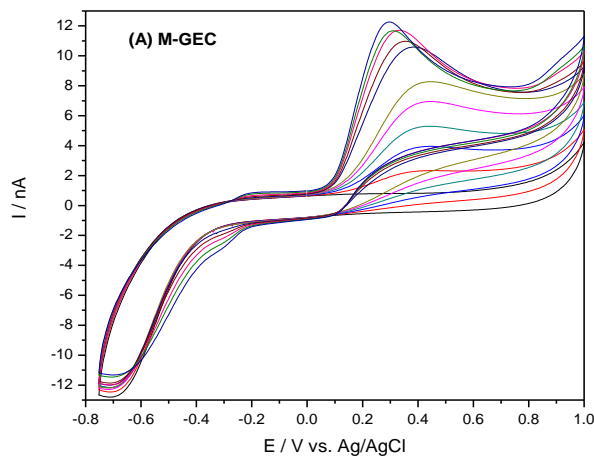
7.2 Results and discussions

7.2.1 Cyclic voltammetry of ascorbic acid/dopamine at composite macroelectrodes

It is well known that the electrochemical detection of both dopamine and ascorbic acid in the presence of each other at untreated carbon surfaces is a battle due to their proximity in their oxidation potential values.

Figure 7.1 (A), (B) and (C) depicts a series of CVs obtained for a mixture of AA and DA (dopamine being added after consecutive additions of ascorbic acid) at graphite-epoxy composite (M-GEC), graphite-natural zeolite-epoxy composite (M-ZN-GEC) and graphite-synthetic zeolite-epoxy composite (M-ZS-GEC) macroelectrodes in the concentration ranged between 100 μM – 500 μM for AA and between 10-50 μM for DA. The concentration range was chosen based on the fact that *in vivo* real concentration for AA can reach more than 500 μM and DA concentrations can reach up to 1 μM [7.1].

The results show that an irreversible oxidation process appears at first five CVs curves, due to the ascorbic acid oxidation process at carbon surface materials, while, when starting the DA standard method addition, the anodic peak corresponding to dopamine oxidation shifts to more negative potentials together with the appearance of a weak cathodic peak during reversed scans at all three composite macroelectrodes.



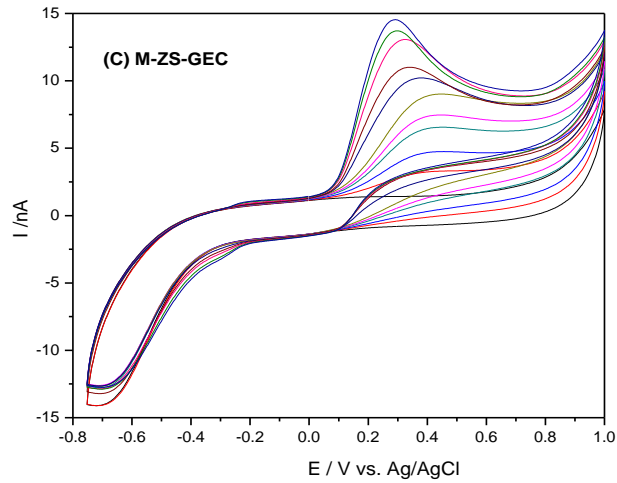
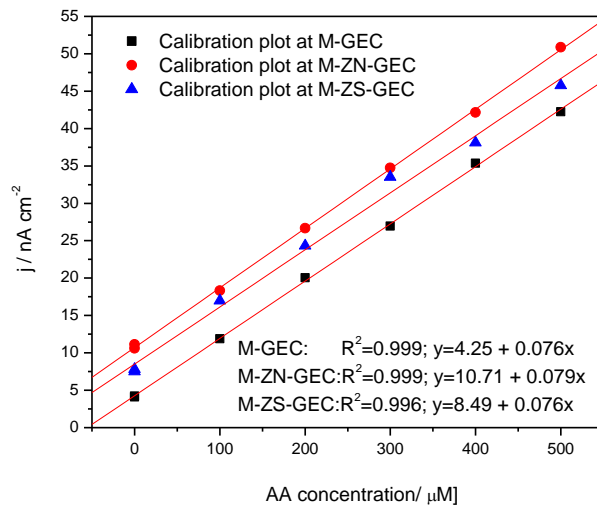


Figure 7.1 : Cyclic voltammograms (CV) recorded at (A) M-GEC, (B) M-ZN-GEC and (C) M-ZS-GEC, in 50 mL of 50 mM PBS supporting electrolyte with increasing concentrations of AA : 100 μM, 200 μM, 300 μM, 400 μM, 500 μM, followed by the addition of consecutive concentrations of DA: 10 μM, 20 μM, 30 μM, 40 μM, 50 μM ; Pt reference electrode and Ag/AgCl auxiliary electrode; potential range from -0.8 V to +1.0 V; scan rate 50 mV s⁻¹ .



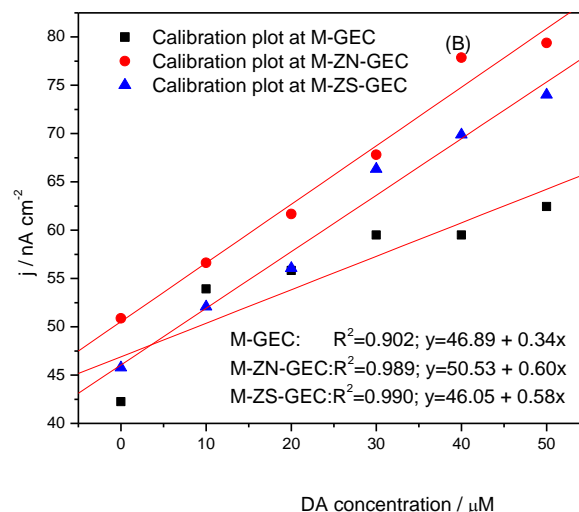


Figure 7.2 : Calibration plots of the current densities vs. (A) AA and (B) DA concentrations at M-GEC, M-ZN-GEC and M-ZS-GEC, calculated without background current subtraction;

It can be noticed that for M-ZS-GEC composite material a better peak separation between ascorbic acid and dopamine was obtained, ($\Delta E=0.164$ V), compared to bare M-GEC composite ($\Delta E=0.147$ V) and M-ZN-GEC composite ($\Delta E=0.097$ V). Although the peak separation is less than 0.200 V for all cases, larger separation potential is recommended for this particular situation, the results are promising taking into account that simultaneous detection of dopamine in the presence of ascorbic acid is very hard to achieve in normal conditions, with simple sensing devices (without improved electroactive surfaces or any protective membranes).

The electroanalytical results are gathered in Table 7.1, based on the calibration plots presented in figure 7.2 (A) and (B) for all composite materials. A linear relationship exists between AA/ DA concentrations and peak current density observed from Table 7.1

Table 7.1: Analytical parameters for CV technique for DA (concentration range between 10-50 μM) and AA (concentration range between 100-500 μM) simultaneous detection experiments;

Electrode type	Technique	AA detection			DA detection		
		Sensitivity [$\text{nA } \mu\text{M}^{-1} \text{cm}^{-2}$]	E [V]	Correlation coefficient, R^2	Sensitivity [$\text{nA } \mu\text{M}^{-1} \text{cm}^{-2}$]	E [V]	Correlation coefficient, R^2
M-GEC	CV	0.076	0.44	0.997	0.34	0.297	0.902
M-ZN-GEC		0.079	0.312	0.998	0.60	0.220	0.989
M-ZS-GEC		0.075	0.457	0.996	0.58	0.293	0.990

Very close sensitivity values were obtained for the case of AA detection at all composite macrosensors (0.076 $\text{nA } \mu\text{M}^{-1} \text{cm}^{-2}$ for M-GEC, 0.079 $\text{nA } \mu\text{M}^{-1} \text{cm}^{-2}$ for M-

ZN-GEC and $0.075 \text{ nA } \mu\text{M}^{-1}\text{cm}^{-2}$ for M-ZS-GEC) while an increase in sensitivity was noticed for DA direct detection at M-ZS-GEC as well as at M-ZN-GEC, as summarized in Table 7.1.

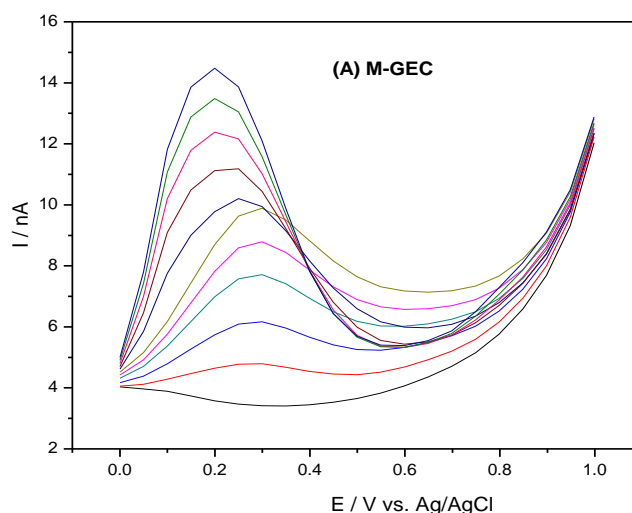
7.2.2 Pulsed voltammetric techniques

7.2.2.1 Differential-pulsed voltammetry

A second issue that can be taken into account is the fact that dopamine can be adsorbed at carbon surfaces [7.2]. This adsorption process has two main consequences for the voltammetric signal [7.3]: one is the increase in signal observed, as dopamine preconcentrates on the electrode surface between scans for very low DA concentration improving the lowest limit of detection. The other is an over time response of the electrode, and especial electrode fouling for certain DA concentrations. However, this can be overcome by the use of fast and pulsed voltammetric techniques.

The ability of a bare graphite-epoxy composite, graphite-natural zeolite-epoxy composite and graphite-synthetic zeolite-epoxy composite macroelectrodes to promote a voltammetric resolution was further investigated using differential-pulsed technique and the results are presented in figure 7.3. The differential-pulsed voltammograms show that the investigated analytes appear at different potential values, with a difference between ascorbic acid peak potential and dopamine peak oxidation potential of only 0.105 V for M-GEC, 0.110 V for M-ZN-GEC and a difference of 0.085 V for M-ZS-GEC, under the working conditions investigated of pulse amplitude 0.05 V, modulation amplitude=0.1 V, which corresponds to the scan rate of 0.25 Vs^{-1} .

Although the ascorbic acid sensitivity and peak separation between ascorbic acid and dopamine is the smallest for M-ZS-GEC than at the other two macrocomposite materials investigated, this macrocomposite exhibited increased sensitivity towards DA when differential pulse voltammetry was employed, as presented in Table 7.2.



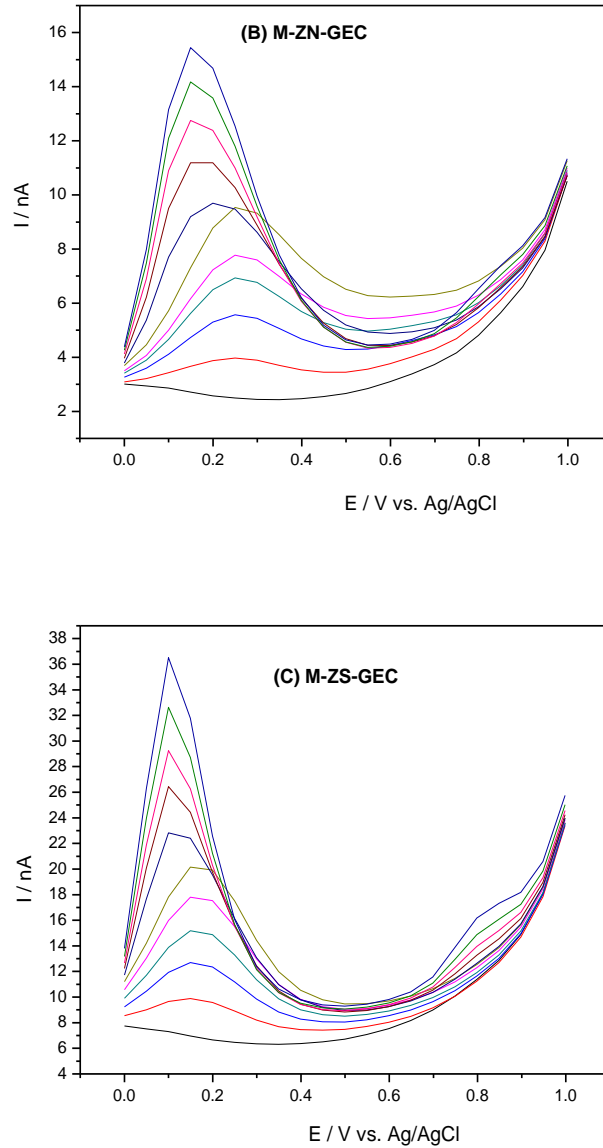


Figure 7.3: Differential-pulsed voltammograms (DPV) recorded at (A) M-GEC, (B) M-ZN-GEC and (C) M-SZ-GEC, in 50 mL of 50 mM PBS supporting electrolyte with increasing concentrations of AA: 100 μ M, 200 μ M, 300 μ M, 400 μ M, 500 μ M, followed by the addition of consecutive concentrations of DA: 10 μ M, 20 μ M, 30 μ M, 40 μ M, 50 μ M; Pt reference electrode and Ag/AgCl auxiliary electrode; potential range from 0.0 V to +1.0 V; step potential 0.05 V; modulation amplitude 0.1 V;

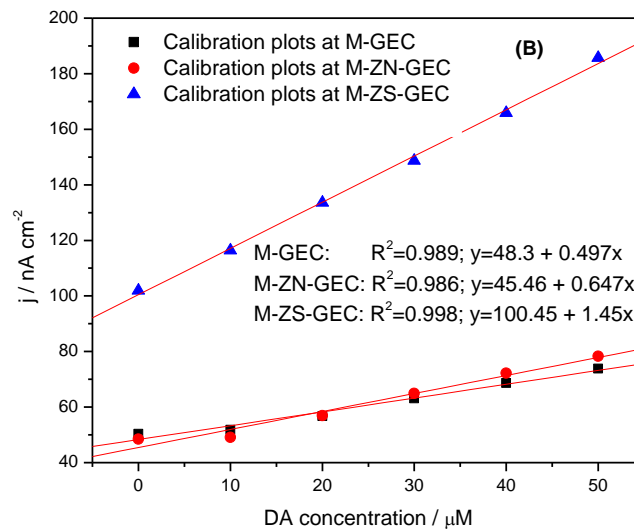
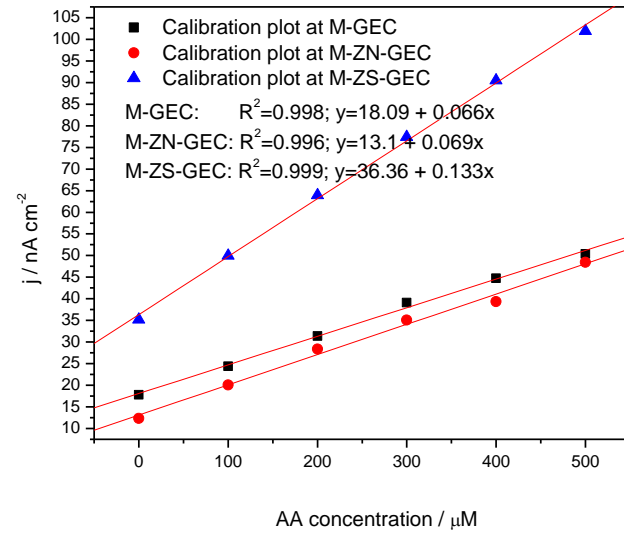


Figure 7.4: Calibration plots of (A) ascorbic acid and (B) dopamine concentrations vs. current densities recorded at M-GEC, M-ZN-GEC and M-SZ-GEC, calculated without background current subtraction.

For the same DPV technique, when the oxidation current of DA was investigated in the presence of ascorbic acid, the peak current of dopamine increased linearly with the increase in DA concentration. The dependence of the peak current density on the DA concentration is in a linear relationship in the range

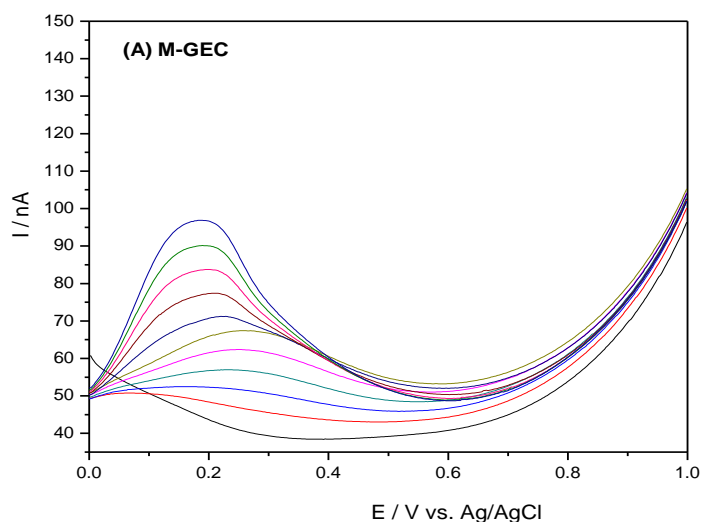
investigated of 10-50 μM at all three M-GEC, M-ZN-GEC and M-ZS-GEC macroelectrodes, as shown in figure 7.4.

As observed from the experimental determinations, the direct response of DA in cyclic voltammetric experiments, as well for the case of differential pulse voltammetric experiments, is interfered with the signal of AA, where an overlapping response is obtained from the mixture of DA and AA.

7.2.2.2 Square-wave voltammetry

Since square-wave voltammetry (SWV) allows a much higher current sensitivity and ability for peak separations than DPV, it was employed to estimate the separation capability of the two molecules [7.4]. Figure 7.5 shows the SWV voltammetric response of a mixture of AA and DA at M-GEC, M-ZN-GEC, M-ZS-GEC macroelectrodes and the analytical results of the SQW technique are presented in table 7.2. The working conditions employed for this pulsed technique are for step potential equal with 0.0025 V, for modulation amplitude a value of 0.1 V and a frequency of 50 Hz, which corresponds to the scan rate of 0.025 V s^{-1} .

As can be seen from the SWV curves, a very well-defined dopamine oxidation peak is noticed for the case of M-ZS-GEC. The analytical results show an improvement when SWV technique is employed in comparison with DPV technique, in terms of sensitivity and peak separation values. Both the sensitivity towards DA detection is improved using SWV technique (a sensitivity of only $1.5 \text{ nA } \mu\text{M}^{-1}\text{cm}^{-2}$) and the peak separation between AA and DA is around 0.219 V for M-ZS-GEC composite, fact that makes it possible the simultaneous detection of AA and DA at the surface of the M-ZS-GEC macroelectrode.



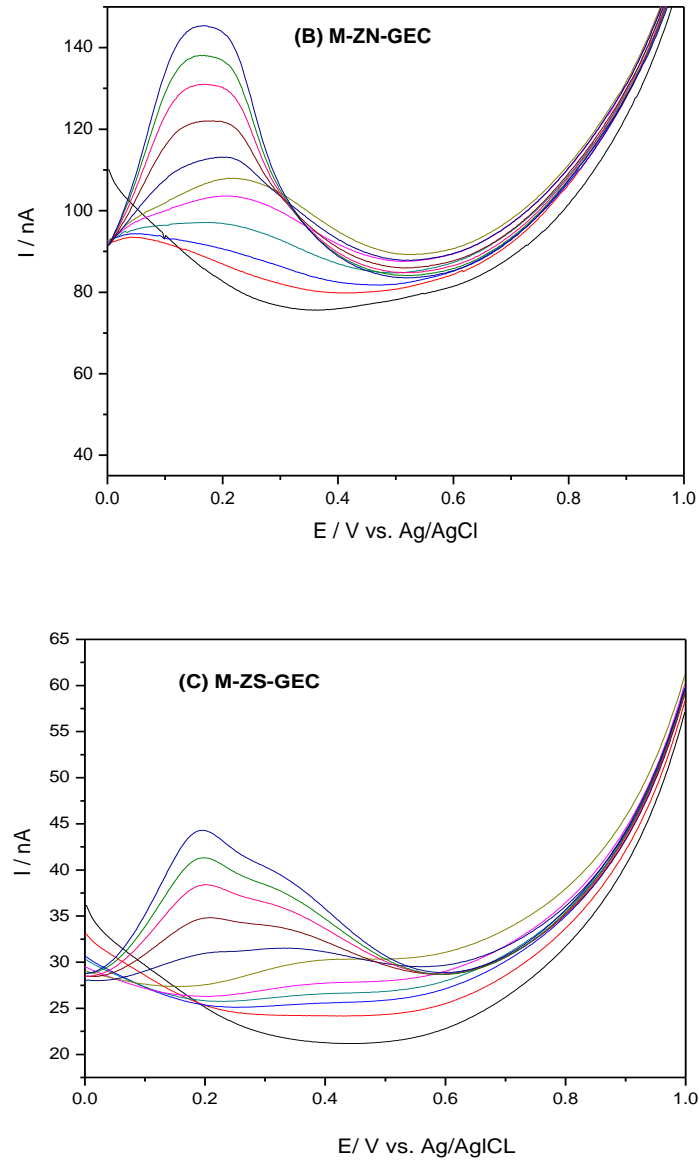


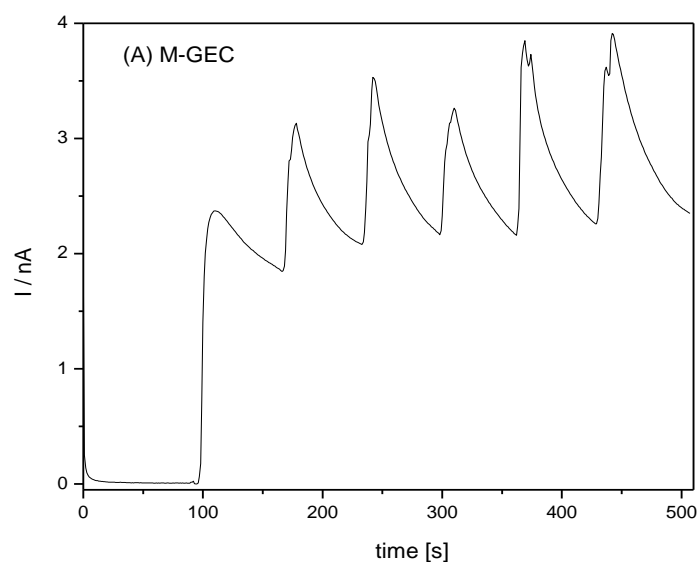
Figure 7.5: Square-wave voltammograms (SWV) recorded at (A) M-GEC, (B) M-ZN-GEC and (C) M-SZ-GEC, in 50 mL of 50 mM PBS supporting electrolyte with increasing concentrations of AA : 100 μM , 200 μM , 300 μM , 400 μM , 500 μM , followed by the addition of consecutive concentrations of DA: 10 μM , 20 μM , 30 μM , 40 μM , 50 μM ; Pt reference electrode and Ag/AgCl auxiliary electrode; potential range from 0.0 V to +1.0 V; step potential 0.05 V; modulation amplitude 0.1 V; Frequency 50Hz

Table 7.2: Analytical parameters for DPV and SWV techniques for DA (concentration range between 10-50 μ M) and AA (concentration range between 100-500 μ M) simultaneous detection experiments.

Electrode type	Technique	AA detection			DA detection		
		Sensitivity [nA μ M ⁻¹ cm ⁻²]	E [V]	Correlation coefficient R ²	Sensitivity [nA μ M ⁻¹ cm ⁻²]	E [V]	Correlation coefficient R ²
M-GEC	DPV	0.066	0.303	0.998	0.497	0.198	0.989
M-ZN-GEC		0.069	0.263	0.996	0.647	0.153	0.986
M-ZS-GEC		0.133	0.182	0.999	1.66	0.097	0.989
M-GEC	SWV	0.265	0.270	0.999	3.06	0.187	0.996
M-ZN-GEC		0.290	0.229	0.997	3.94	0.167	0.996
M-ZS-GEC		0.081	0.411	0.982	1.5	0.192	0.991

7.2.3 Cronoamperometric detection experiments

Constant-potential amperometry (CPA) is a very useful technique for practical applications and offers the best temporal resolution among available techniques. Taking into consideration that in the extracellular fluid of the central nervous system, DA concentrations are present at a level from nanomolar to micromolar range (0.01-1 μ M) CPA should be regarded as the most viable.



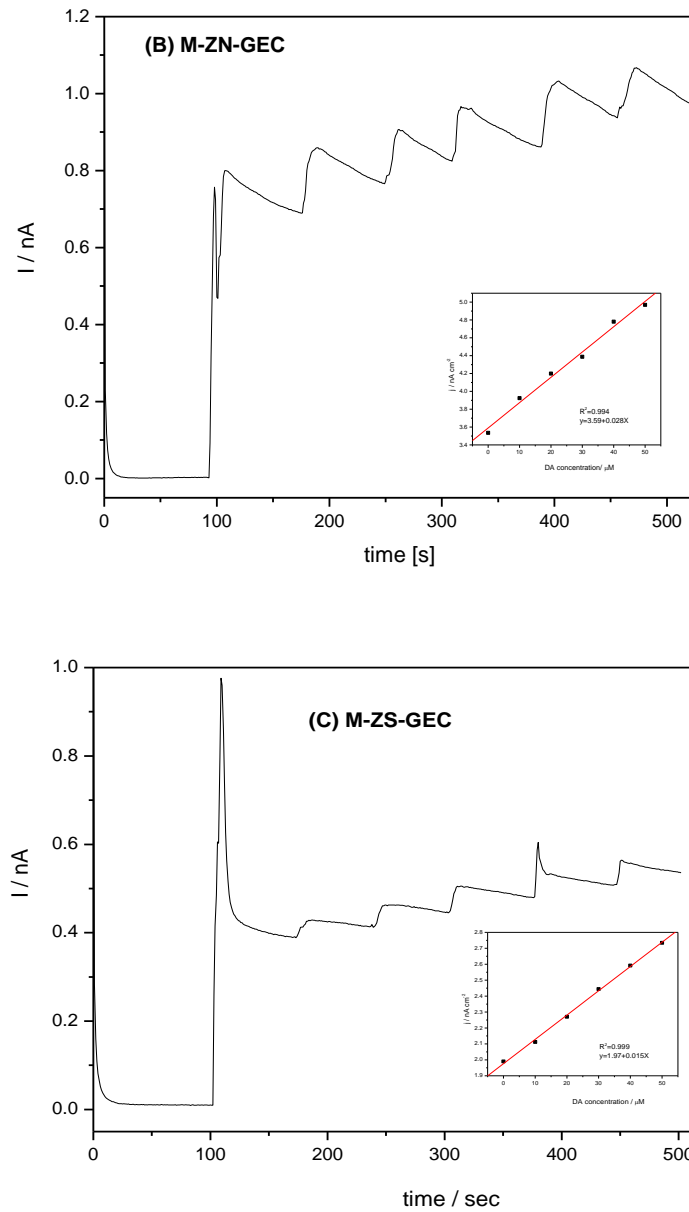


Figure 7.6: CPA recorded at (A) M-GEC, (B) M-ZN-GEC and (C) M-ZS-GEC in 50 mL of 50 mM PBS supporting electrolyte with adding 500 μ M AA followed by increasing concentrations of Dopamine : 10 μ M, 20 μ M, 30 μ M, 40 μ M, 50 μ M, Pt reference electrode and Ag/AgCl auxiliary electrode; Potential value +0.100 V; inset: calibration plots for current densities vs. DA concentration calculated without background current substraction.

Figure 7.6 presents the amperometric measurements of dopamine in the presence of 500 μM AA (DA concentration range between 10-50 μM) recorded at M-GEC, M-ZN-GEC and M-SZ-GEC macroelectrode composites without any protective membrane at an applied constant potential of +0.100 V. M-GEC electrode exhibits a plateau at a DA concentration of 30 μM , which should be explained by the electrode fouling. Even if AA detection signal is more evidenced for M-ZS-GEC, the best shape of the signal corresponds to DA detection.

In-vitro detection of low dopamine concentrations must be regarded as starting point for improving the microsensors for further in vivo experiments. Serious interactions may occur at implantation due to the exposure to brain tissue and the study of SZ-GEC microsensor to DA response when covered with specific membranes to assure selectivity has to be taken into consideration for future studies.

Table 7.3 : Analytical parameters for CV technique for DA (concentration range between 10-50 μM) and AA (concentration range between 100-500 μM) simultaneous detection experiments;

Electrode type	Technique	DA detection		
		Sensitivity [$\text{nA } \mu\text{M}^{-1}\text{cm}^{-2}$]	E [V]	Correlation coefficient, R^2
M-GEC	CA	-*	0.100	-
M-ZN-GEC		0.028		0.994
M-ZS-GEC		0.014		0.999

*No linear calibration was found

7.3 Conclusions

The voltammetric techniques, *i.e.*, cyclic voltammetry, differential-pulsed voltammetry and square-wave voltammetry, tested for the simultaneous detection of ascorbic acid dopamine on composite macroelectrodes allowed the detection of both analytes with better sensitivity for DA detection using synthetic zeolite-modified graphite- epoxy composite macroelectrode. Also, at this electrode the peak separation value of minimum 200 mV was reached using square-wave voltammetry under the optimize conditions of 0.0025 V step potential, 0.1 V modulation amplitude and 50 Hz frequency.

Under the above-presented experimental conditions, the catalytic effect towards dopamine detection was proved for synthetic zeolite-modified graphite-epoxy composite microelectrode, allowing increasing the sensitivity and selectivity for this analyte detection, besides a possible electrostatic attraction between dopamine cation and the negative surface of the synthetic zeolite and electrostatic repulsion with ascorbic acid anion.

Also, synthetic zeolite-modified graphite-epoxy composite macroelectrode gave the best electroanalytical parameters for dopamine detection using chronoamperometry, the most useful technique for the practical applications.

7.4 References

- [7.1] C. Martinez, M. Cerro, S. Ferro, A. De Battisti and M. Quiroz, "Electrochemical behaviour of dopamine at Nafion modified boron doped diamond electrode: preliminary results," *Canadian journal of analytical sciences and spectroscopy*, vol. 52, pp. 325-333, 2007.
- [7.2] J. Baur, E. Kristensen, L. May, D. Widemann and R. Wightman, "Fast scan cyclic voltammetry of biogenic amines," *Analytical chemistry*, pp. 1268-1272, 1988.
- [7.3] B. Bath, D. Michael, B. Trafton, J. Joseph and P. Runnels, "Subsecond adsorption and desorption of dopamine at carbon fiber microelectrodes," *Analytical chemistry*, pp. 5994-6002, 2000.
- [7.4] **E. Ilinoiu**, F. Manea, P. Serra and R. Pode, "Simultaneous/selective detection of dopamine and ascorbic acid at synthetic-modified/graphite-epoxy composite macro/microelectrodes," *Sensors*, IN PRESS.

CHAPTER 8

Applications of modified/unmodified graphite-epoxy composite microsensors

8.1 Preliminary studies regarding ascorbic acid and dopamine detection

8.1.1 Ascorbic acid

Vitamin C or L-ascorbic acid (AA), a water-soluble vitamin, is an important molecule for physiological process in human metabolism, being distributed in skin, liver, leukocytes, as well in the central nervous system [8.1]. It is present in many biological systems and in multivitamin preparation which are commonly used to supplement inadequate dietary intake and as anti-oxidants [8.2-8.3].

The concentration of AA in foodstuffs, beverages and pharmaceuticals can be an index of quality [8.3]. Also, the concentration of ascorbic acid in the extracellular fluid of the central nervous system [8.4-8.5], is at a level of 10^{-4} mol L⁻¹. Therefore it is essential to develop simple and rapid methods for determination of these biological molecules in routine analysis.

Many methods by which AA may be detected and measured in foods and pharmaceuticals (e.g., titration, spectrophotometry [8.6-8.7], potentiometry [8.8] and amperometry [8.9] have been reported in the literature.

AA is an electroactive compound, so, the development of voltammetric sensors for determination of AA in human fluids, food processing, pharmaceuticals, and clinical analysis has received considerable interest in recent years. Furthermore, AA is of particular importance because it accompanies dopamine in biological samples. What is still a challenging task for electroanalytical research, is the detection of AA in the presence of dopamine and vice versa. Dopamine and ascorbic acid are oxidized at nearly the same potential at almost carbon-based or metal electrodes, and an overlapping response of a mixture of DA and AA is usually obtained, reason for which both sensitivity and selectivity are the same important in the development of an appropriate sensor system for each target analyte.

Miniaturization of sensing devices promotes and facilitates the possibility of rapid analysis even in small scale environments and the possibility to use modified electrodes can increase the electron transfer rate and also, the sensitivity.

8.1.2 Experimental

8.1.2.1 Chemicals and materials

L-Ascorbic Acid (Sigma, Aldrich) solutions were freshly prepared prior to each experiment and dissolved in 0.01 M HCl solution, as well as protected against light exposure during experiments.

Most of the experiments were performed using sodium phosphate saline buffer solutions (PBS) supporting electrolyte, prepared from di-hydrogenphosphate,

sodium chloride and sodium hydroxide of analytical reagent grade (Sigma, Aldrich) and used as received. PBS solution was kept in the refrigerator when not used.

8.1.2.2 Apparatus and experimental measurements

All voltammetric experiments were carried out at room temperature (25°C) using an eDAQ QuadStat four-channel Potentiostat (Australia) controlled with an eChem software for cyclic voltammetry in a three-electrode electrochemical cell, carbon composite working electrodes, Ag/AgCl reference electrode and Pt auxiliary electrode. A magnetic stirrer provided the convective transport during the voltammetric experiments.

For detection experiments, the 50 mM PBS supporting electrolyte at pH 7.4 was placed into the cell, and solutions of ascorbic acid and dopamine were employed by standard addition method solution. The scan rate for the detection experiments was 250 mV s⁻¹.

8.1.3 Results and discussions

8.1.3.1 Cyclic voltammetry of ascorbic acid

Electrochemical behaviour of AA was investigated by CV recorded in a 50 mM phosphate buffer supporting electrolyte at all carbon composite microsensors, namely bare graphite-epoxy composite (μ -GEC) as blank material in comparison with sensors containing natural zeolite (μ -ZN-GEC) and synthetic zeolite (μ -SZ-GEC), as well as CNT-film- μ -ZS-GEC microelectrode, at a scan rate of 250 mV s⁻¹. For all cyclic voltammograms presented in Figure 8.1A, 8.2A, 8.3A and 8.4A an anodic peak is observed during the positive scans and no cathodic peak during the negative scans, showing an irreversible AA oxidation process at all three electrode materials.

The oxidation peak current response was directly proportional to AA concentrations, and linear calibrations with good correlation coefficients were obtained in the range of 125 μ M - 1.5 mM AA. The sensitivity values of 963 nA μ M⁻¹cm⁻² for μ -GEC, 1091 nA μ M⁻¹cm⁻² for μ -ZN-GEC, 554 nA μ M⁻¹cm⁻² for μ -SZ-GEC and 2145 nA μ M⁻¹cm⁻² for CNT-film μ -SZ-GEC were determined. The best sensitivity was obtained for the electrode material containing CNT film, followed by the μ -ZN-GEC, with a value close to the μ -GEC electrode material, while for μ -ZS-GEC-composite material a lower sensitivity was found.

According to [8.14], a sensitivity equal with 230 nA μ M⁻¹cm⁻² was obtained for AA detection at a natural zeolite-carbon nanotube-epoxy macrosensor (NZ-CNT-epoxy). The superiority of the graphite-natural zeolite-epoxy microsensors was proven vs. another composite having natural zeolite in its matrix, as well as the superiority of the carbon nanotube -film-modified microsensors.

Also, the electrochemical oxidation of AA at μ -GEC (oxidation potential of 0.365 V), μ -ZN-GEC (oxidation potential of 0.303 V) and CNT-film μ -SZ-GEC (oxidation potential of 0.220 V) presented more sharpened oxidation peaks compared to the broadened peaks encountered at μ -SZ-GEC (oxidation potential at 0.521 V). The more negative potential value for AA oxidation at μ -NZ-GEC in comparison with the μ -GEC microsensors, can be due to the catalytic effect of the zeolite material incorporated in the carbon composite matrix but the less negative oxidation potential was encountered at CNT-film μ -SZ-GEC, mostly due to the catalytic effect of the carbon nanotube. The catalytic effect can be evaluated through the enhancement of the peak current intensity or by lowering the target analyte overpotential.

In the same time, it was observed a shifting of the peak current of AA to a more positive potential value at SZ-GEC compared with the same GEC sensing device. Detection of ascorbic acid at similar carbon composite materials was achieved at approximately 0.5 V vs. SCE at a carbon paste electrode [8.10], at 0.5 V vs. SCE at a carbon ceramic electrode [8.11], and around 0.65V at a ferrocene carboxylic acid modified carbon paste electrode [8.12]. The investigated micro-sensors investigated here presented good peculiarities towards AA detection.

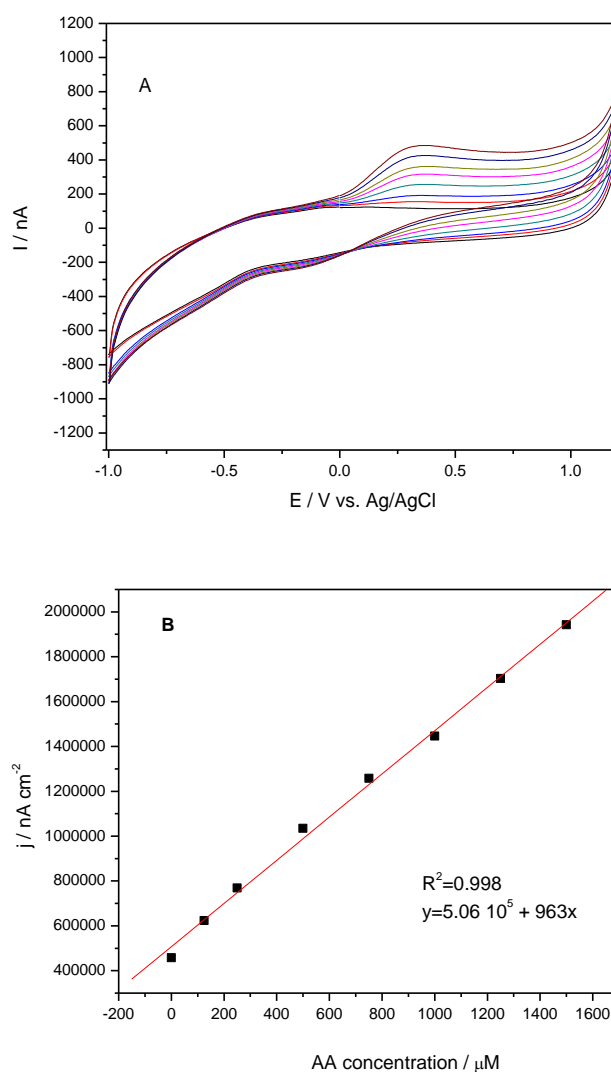


Figure 8.1 : Cyclic voltammograms recorded at (A) μ -GEC in 20 mL of 50 mM PBS supporting electrolyte with increasing concentrations of AA : 125 μ M, 250 μ M, 500 μ M, 750 μ M, 1 mM, 1,25 mM, 1.5 mM; Pt reference electrode and Ag/AgCl auxiliary electrode; potential range from -1.0 V to +1.2 V; scan rate 250 mV s⁻¹. (B) Calibration plot of the anodic currents densities recorded at E=+0.365 V vs. AA concentration, calculated without background current subtraction.

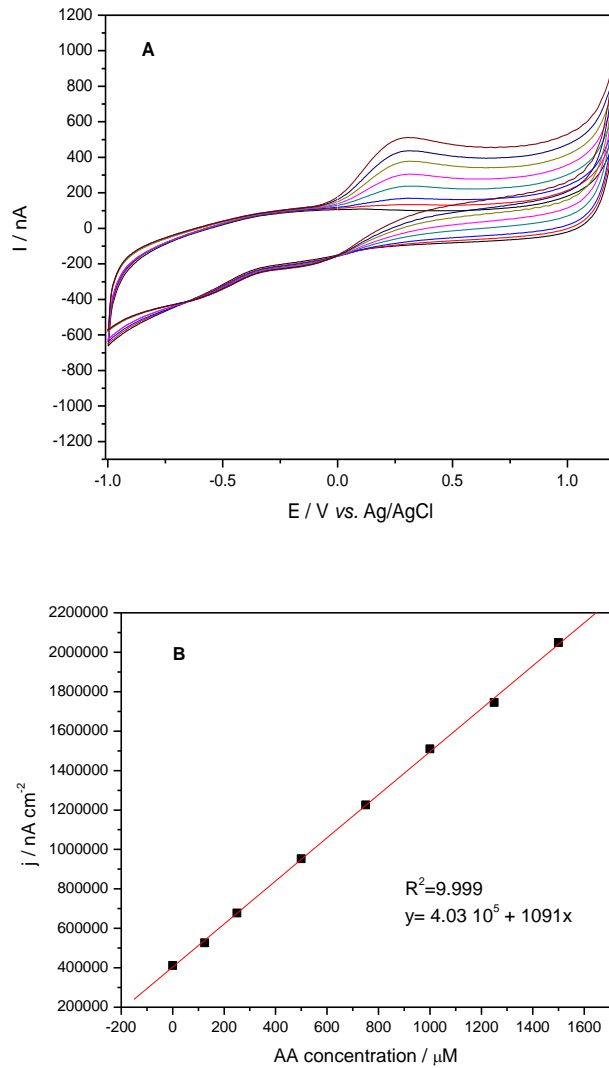


Figure 8.2 : Cyclic voltammograms recorded at (A) μ -ZN-GEC in 20 mL of 50 mM PBS supporting electrolyte with increasing concentrations of AA : 125 μ M, 250 μ M, 500 μ M, 750 μ M, 1 mM, 1,25 mM, 1.5 mM; Pt reference electrode and Ag/AgCl auxiliary electrode; potential range from -1.0 V to +1.2 V; scan rate 250 mV s^{-1} . (B) Calibration plot of the anodic current densities recorded at $E = +0.303$ V vs. AA concentration, calculated without background current subtraction.

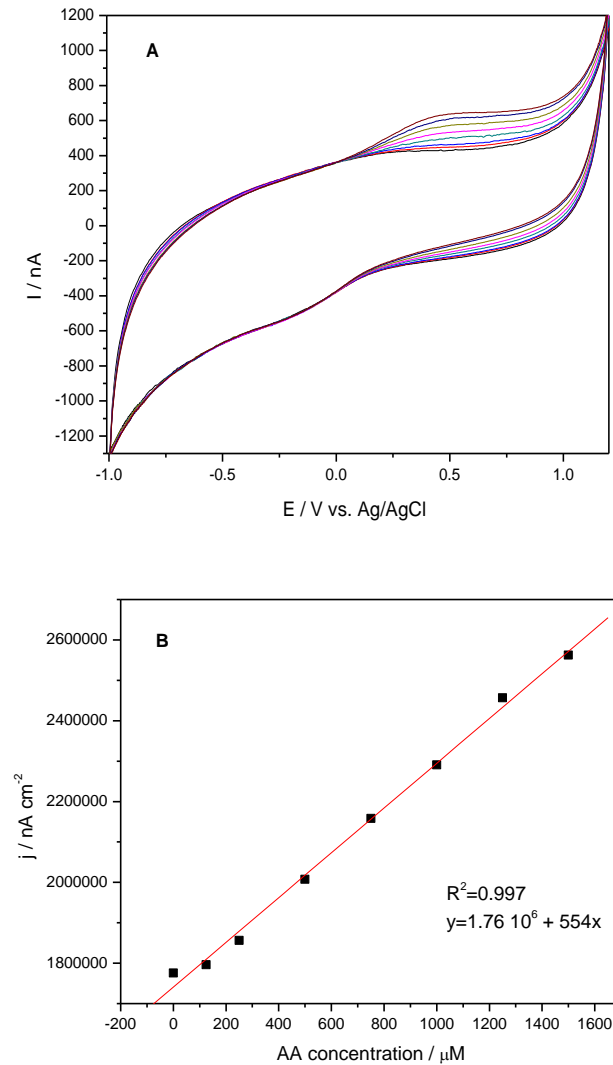


Figure 8.3 : (A) Cyclic voltammograms recorded at (A) μ -SZ-GEC in 20 mL of 50 mM PBS supporting electrolyte with increasing concentrations of AA : 125 μ M, 250 μ M, 500 μ M, 750 μ M, 1 mM, 1,25 mM, 1.5 mM; Pt reference electrode and Ag/AgCl auxiliary electrode; potential range from -1.0 V to +1.2 V; scan rate 250 mV s⁻¹. (B) Calibration plot of the anodic current densities recorded at E=+0.521 V vs. AA concentration, calculated without background current subtraction.

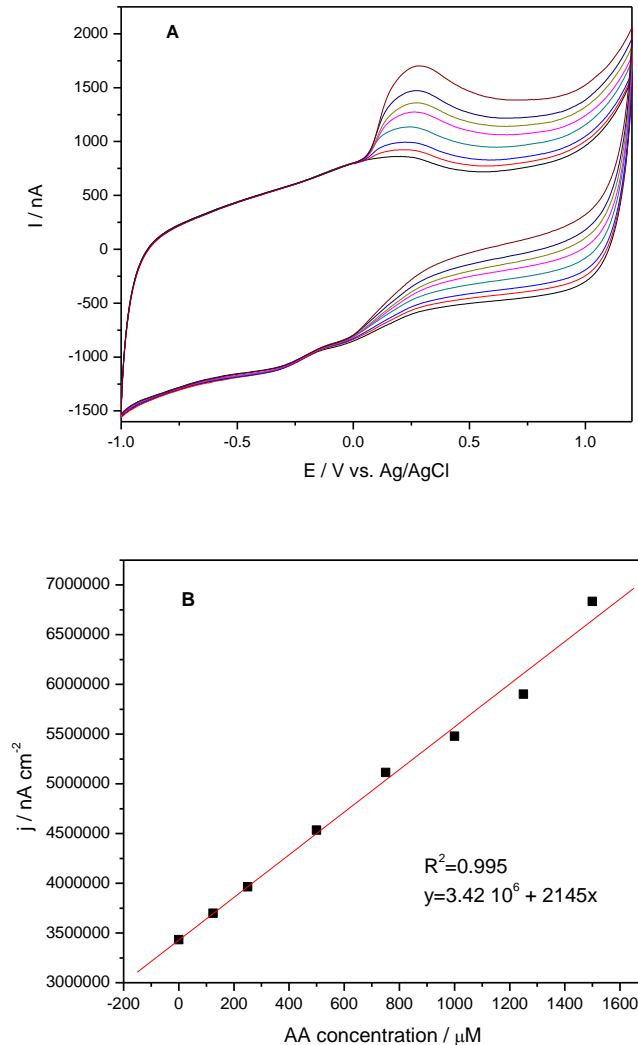


Figure 8.4 : (A) Cyclic voltammograms recorded at (A) CNT-Film- μ -SZ-GEC in 20 mL of 50 mM PBS supporting electrolyte with increasing concentrations of AA : 125 μ M, 250 μ M, 500 μ M, 750 μ M, 1 mM, 1.25 mM, 1.5 mM; Pt reference electrode and Ag/AgCl auxiliary electrode; potential range from -1.0 V to +1.2 V; scan rate 250 mV s⁻¹. (B) Calibration plot of the anodic current densities recorded at E=+0.521 V vs. AA concentration, calculated without background current subtraction.

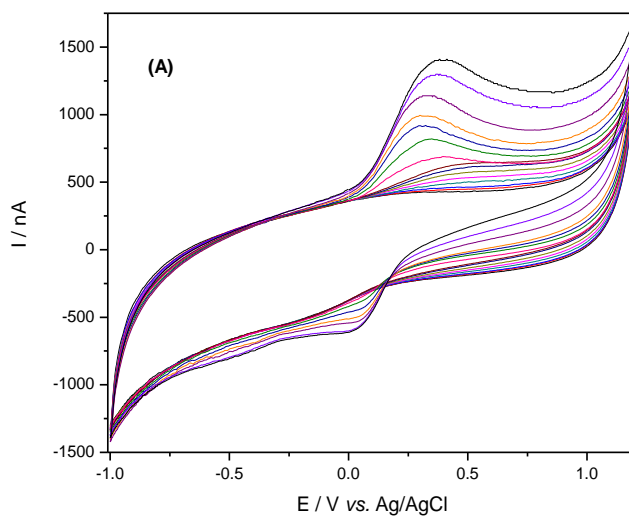
Taken into consideration the final application of the designed carbon composite materials, the fact that SZ-GEC sensor presented a slightly decreased sensitivity towards AA detection, without any protective membranes at the electroactive sensing surface, makes this material a candidate for further investigations related to the selective response towards dopamine molecule in the presence of ascorbic acid as main interfering compound.

8.1.3.2 Cyclic voltammetry of a mixture of ascorbic acid and dopamine

AA and DA coexist in the extra-cellular fluid of the central nervous system and exhibit similar oxidation potentials at carbon based materials, and the selective determination of these biomolecules is a great problem due to the overlapped signals. A real challenge is given by the *in vivo* measurement of dopamine in the presence of ascorbic acid, without a significant interference, which requires certain preliminary electrochemical tests.

As preliminary electrochemical tests, in order to notice the dopamine electrochemical response at μ -SZ-GEC, cyclic voltammetry experiments were carried out in the presence of 1.5 mM AA, by adding increasing concentrations of DA until a maximum concentration of 1.5 mM DA was reached. The voltammograms are presented in figure 8.5, and more defined peaks are noticed for DA oxidation. Also, a cathodic peak occurred at reversed scanning in the presence of DA, and a difference between anodic and cathodic peak potential equal to 0.360 V, is characteristics to a quasi-reversible redox process.

In comparison with AA oxidation potential value of 0.521 V, the oxidation process of DA occurred at a lower potential value of 0.385 V, which informs that DA oxidation on the electrode surface is favoured against AA electrooxidation. This aspects is confirmed also by a greater sensitivity reached for DA detection ($2046 \text{ nA } \mu\text{M}^{-1}\text{cm}^{-2}$) in comparison with AA detection ($554.11 \text{ nA } \mu\text{M}^{-1}\text{cm}^{-2}$) using CV.



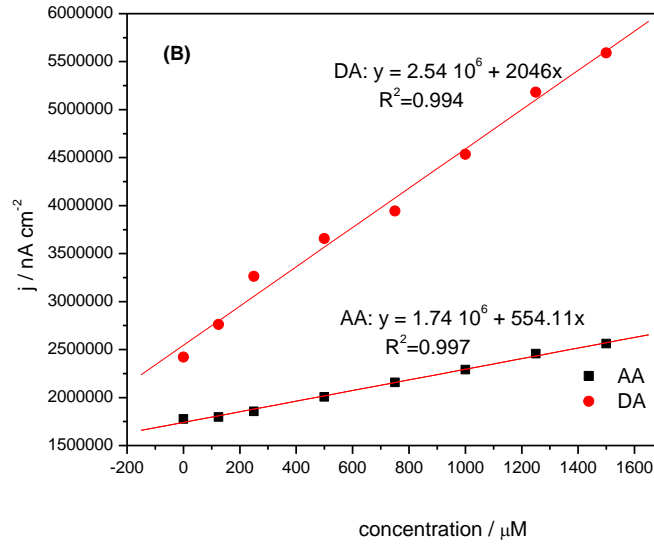
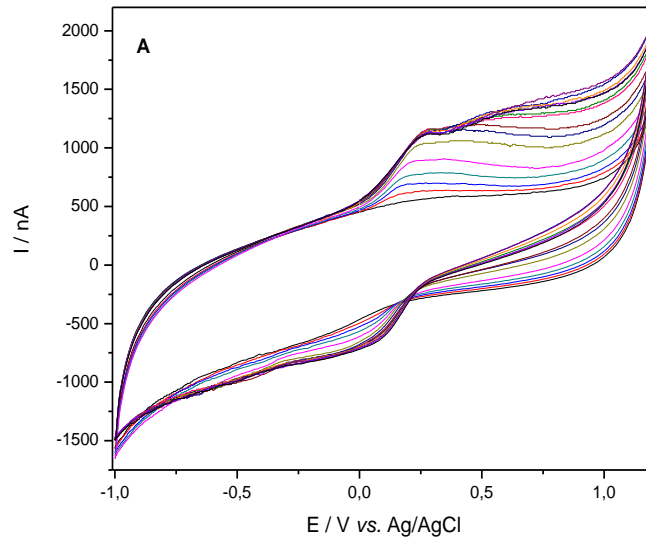


Figure 8.5 : **A**-Cyclic voltammograms recorded at μ -SZ-GEC, in 20 mL of 50 mM PBS supporting electrolyte with increasing concentrations of AA followed by increasing concentrations of DA: 125 μM , 250 μM , 500 μM , 750 μM , 1 mM, 1.25 mM, 1.5 mM; **B**- Calibration plots of the current densities vs. DA concentration at a potential value of $E = +0.385$ V and AA concentration at a potential value of $E = +0.521$ V ; calculated without background current subtraction ; Pt reference electrode and Ag/AgCl auxiliary electrode; potential range from -1.0 to +1.2 V; scan rate 250 mV s^{-1} ;



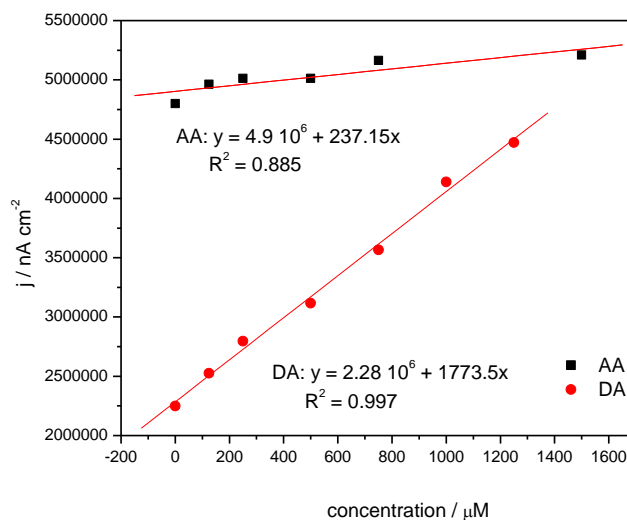


Figure 8.6: **A** - Cyclic voltammograms recorded at μ -SZ-GEC, in 20 mL of 50 mM PBS supporting electrolyte with increasing concentrations of DA followed by increasing concentrations of AA: 125 μM , 250 μM , 500 μM , 750 μM , 1 mM, 1.25 mM, 1.5 mM; **B** - Calibration plots of the current densities vs. DA concentration at a potential value of $E = +0.275$ V and AA concentration at a potential value of $E = +0.521$ V; calculated without background current subtraction; Pt reference electrode and Ag/AgCl auxiliary electrode; potential range from -1.0 to +1.2 V; scan rate 250 mV s^{-1} .

A similar experiment was carried out to explore the electrochemical behaviour of the electrode, first in the presence of same DA concentrations range, and then AA concentrations were added up to 1.5 mM AA.

Based on CVs recorded and presented in figure 8.6, the sensitivities for the simultaneous DA and AA detection were determined as 1773.5 $\text{nA } \mu\text{M}^{-1}\text{cm}^{-2}$ for DA detection and respective, 237.15 $\text{nA } \mu\text{M}^{-1}\text{cm}^{-2}$ for AA detection. For AA detection no good correlation coefficient was obtained, which informed that no AA detection is possible under these working conditions. Also, it must be noticed a small difference between the sensitivities for DA detection under both working conditions. A better DA detection sensitivity was reached under the working conditions characterised by the presence of 1.5 mM AA (2046 $\text{nA } \mu\text{M}^{-1}\text{cm}^{-2}$) in comparison with AA absence (1773.5 $\text{nA } \mu\text{M}^{-1}\text{cm}^{-2}$), which means that about 13 % of the sensitivity is owing to AA presence. This aspect should be explained by the fact that in homogeneous solutions, AA can reduce the DA oxidation product back to DA, improving the local concentration of DA at the electrode surface [8.13]. To avoid AA interference for DA detection in the practical application, a permselective Nafion membrane should be proposed.

8.1.4 Conclusions

Electrochemical behaviour of AA was investigated by CV at all carbon composite microsensors, namely bare graphite-epoxy composite (μ -GEC) as blank material in comparison with microsensors containing natural zeolite (μ -ZN-GEC) and

synthetic zeolite (μ -SZ-GEC), as well as CNT-film- μ -ZS-GEC microelectrode offering an image of their sensitivity towards ascorbic acid. CNT-film- μ -ZS-GEC exhibited the highest sensitivity of $2145 \text{ nA } \mu\text{M}^{-1}\text{cm}^{-2}$ and the less positive oxidation potential of 0.220 V , while μ -SZ-GEC microsensor presented the lowest sensitivity and the most positive oxidation potential value, equal to 0.521 V .

The catalytic effect of the carbon nanotubes was obvious as well as for the natural zeolite material, which had improved sensitivity values and improved oxidation potential values compared to bare μ -GEC microsensor.

For further applications regarding the selective detection of dopamine in the presence of ascorbic acid, a slightly decreased sensitivity towards AA is desired, fact that was encountered at μ -SZ-GEC microsensor (sensitivity equal to $554.11 \text{ nA } \mu\text{M}^{-1}\text{cm}^{-2}$ and $E=0.521 \text{ V}$). Moreover, to avoid AA interference for DA detection in the practical application, a permselective Nafion membrane can be also investigated.

8.2 Microsensors optimization for dopamine detection

8.2.1 Dopamine

Dopamine (DA) is a major chemical responsible for transmitting signals between the nerve cells (neurons), being implicated in several cognitive abilities and behaviors. It is known that the lack of dopamine can cause disorders at nervous system level, like Parkinson [8.14] and schizophrenia [8.15], as well as disorders at renal, hormonal and vascular systems levels.

Methods for dopamine quantification are of practical importance in chemical, clinical, biological or environmental fields and represents the subject of present investigations. Neuroscientists are using microdialysis technique [8.16], although the resulting low volume and dilute samples can be challenging to analyze, requiring further highly sensitive analytical systems. High performance liquid chromatography (HPLC) technique might seem an easy, precise and reliable method for analyzing neurotransmitters including DA [8.17]. Among other techniques, e.g., potentiometric [8.18], or chemiluminescence [8.19].

Since DA is an electroactive molecule, electrochemical methods are another very promising alternative for its quantification and even present some advantages over other techniques. Combining the advantageous properties of microelectrodes [8.20], and biotelemetry technique [8.21], small devices can be implanted in living organisms obtaining a real-time monitoring of the investigated molecules. Though, the detection of DA by electrochemical methods is a challenging task, due to AA interference in real solutions. This task is difficult to achieve for chemists, since they require both sensitive and selective sensing devices. Research for *in vivo* and *in vitro* detection of DA was employed at carbon based microelectrodes, but due to the overlapping signal of AA that complicates the detection of DA especially at carbon-based electrodes, the sensing devices were usually employed in various forms. Using carbon-based sensing devices, a possible adsorption step might occur and cause differences in kinetic response, as observed for carbon-fiber microelectrodes [8.22].

8.2.2 Experimental

8.2.2.1 Chemicals and materials

Dopamin-Hydrochloracid (Fluka) solutions were freshly prepared prior to each experiment, dissolved in PBS and protected from light exposure during experimental procedures. As supporting electrolyte, a 50 mM PBS solution was used, which was kept in the refrigerator when not used.

Nafion solutions came in the form of 5% Nafion in a mixture of lower aliphatic alcohols and water (Sigma, Aldrich).

8.2.2.2 Apparatus and experimental measurements

All voltammetric experiments were carried out at room temperature (25°C) using an eDAQ QuadStat four-channel Potentiostat (Australia) controlled with an eChem software for cyclic voltammetry in a three-electrode electrochemical cell, carbon composite working electrodes, Ag/AgCl reference electrode and Pt auxiliary electrode. A magnetic stirrer provided the convective transport during the voltammetric experiments.

For detection experiments, the 50 mM PBS supporting electrolyte at pH 7.4 was placed into the cell, and solutions of dopamine were employed by standard addition method solution. The scan rate for the detection experiments was 250 mVs⁻¹.

The coating procedure of the microsensors with Nafion membrane was described previously in chapter 6.

8.2.3 Results and discussions

8.2.3.1 Cyclic voltammetry of dopamine

8.2.3.1.1 Cyclic voltammetry of dopamine at microelectrodes without Nafion[®] membrane

Because dopamine is an oxidizable compound, its detection can be achieved by electrochemical methods based on anodic oxidation. As can be seen in figure 8.7A, 8.7B and 8.7C, by adding increasing concentrations of DA, an increase in anodic peak oxidation is observed at all carbon based composite microelectrodes : graphite-epoxy, graphite-natural zeolite-epoxy and graphite-synthetic zeolite-epoxy (peak no.1). A considerable positive shifting of oxidation potential is observed for μ -SZ-GEC microelectrode, where DA oxidation occurs at a potential value of $E_a = 0.161$ V with a peak separation of $\Delta E = E_a - E_c = 0.069$ V. According to the literature data, this redox pair, peak 1/peak 2, is associated with a reversible process [8.23]. Although, a quasi-reversible behavior was noticed for μ -GEC and μ -NZ-GEC microelectrodes, where the anodic peak potential shifted to a much more positive values, $E = 0.281$ V at both μ -GEC and at μ -NZ-GEC, with larger ΔE .

It can be noticed the shape of the anodic peak, a clearly defined for the case of SZ-GEC microelectrode, proving that the DA oxidation process occurred without inhibition, in comparison with the voltammogram shapes in figure 8.7 A and B, where the DA oxidation peaks are less defined.

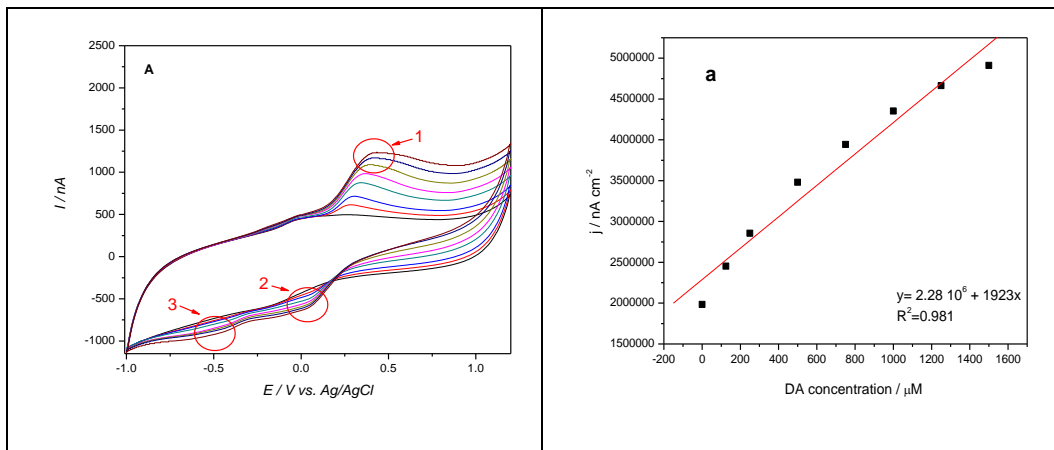
For the reversed scan direction, two reduction peaks occur, better revealed for μ -ZS-GEC microelectrode and μ -GEC microelectrode, peak no.2 and peak no.3, while for μ -NZ-GEC only peak no.2 is obvious. Based on literature data [8.24]. The

number of electrons consumed for DA oxidation varies from two to four, depending on the catalytic activity. Thus, according to equations from scheme 1, [8.25], dopamine oxidation (peak 1) (eq.8.1) forms dopamine-o-quinone, which is reduced in peak 2 or suffers a ring closure and forms leucodopaminechrome (eq. 8.2) which can be oxidized further again to dopaminechrome. A similar behavior is explained for epinephrine [8.25], although the oxidation of leucodopamine to dopaminechrome in this case does not occur. From the shape of dopamine detection voltammograms, it is observed that the early starting potential of dopamine oxidation at μ -SZ-GEC might correspond as well with the oxidation of leucodopaminechrome. The dopaminechrome could polymerize to nucleolus like compounds on the electrode surface leading to electrode fouling and as consequence, the electron transfer reaction inhibition in DA oxidation.

All voltammetric experiments were performed in a PBS supporting electrolyte of pH =7.4, and it is known that dopamine, at this pH value is in its protonated form ($pK_b = 8.87$) [8.26] and the presence of synthetic zeolite lattice in the composite matrix might favorize the adsorption of dopamine-quinone⁺ specie on the surface of the electrode.

For these reasons, the catalytic effect of DA oxidation was proved at μ -SZ-GEC, where the use of zeolite modified electrodes can increase the selectivity and sensitivity towards this analyte detection.

All analytical parameters (LOD, sensitivity, correlation coefficients, relative standard deviation and limit of quantification) obtained with cyclic voltammetry (CV) technique are summarized in Table 8.1. For all tested microelectrodes, within the concentration range investigated (125 μ M – 1.5 mM DA), linear dependences were obtained (see Table 8.1), responses characteristic for diffusion-controlled processes, which are imposed for voltammetric determinations. The best sensitivity was encountered at μ -SZ-GEC, 2027 μ M nA⁻¹cm⁻². The same graphite-synthetic zeolite-epoxy composite microelectrode, allowed to reach the best LOD value of 7.03 μ M.



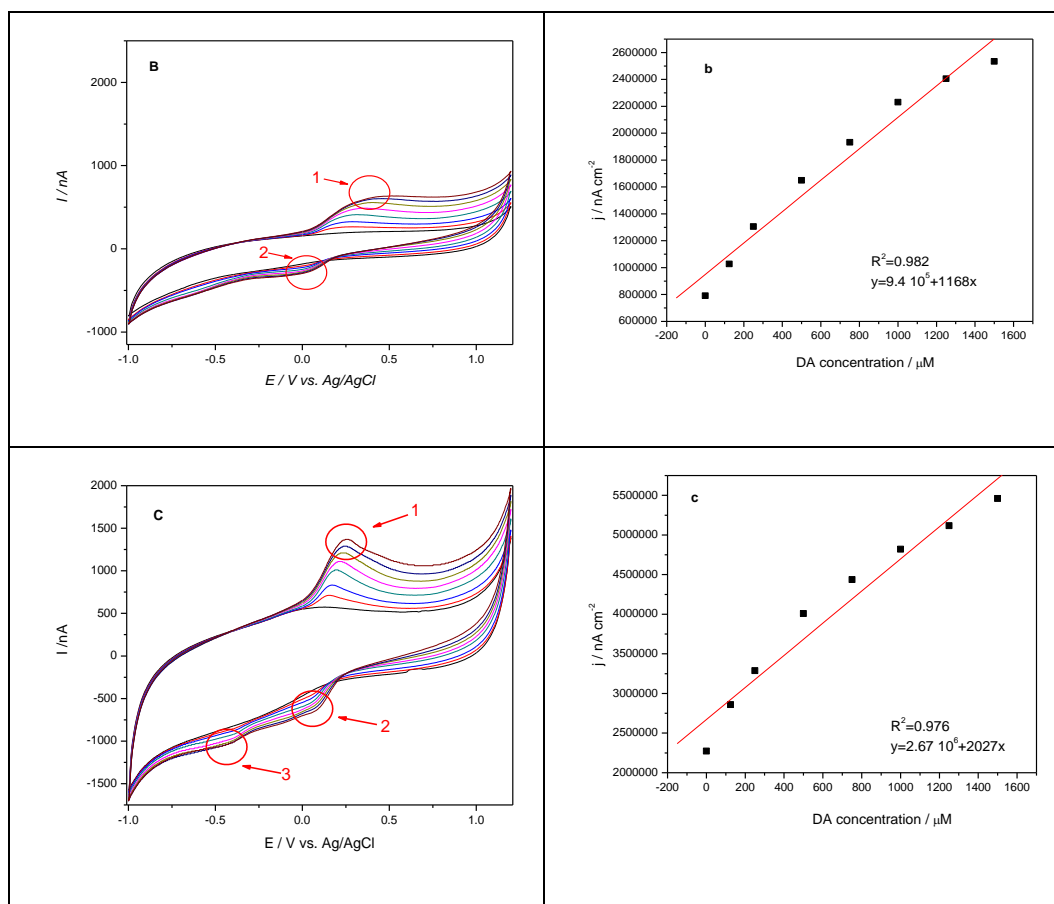
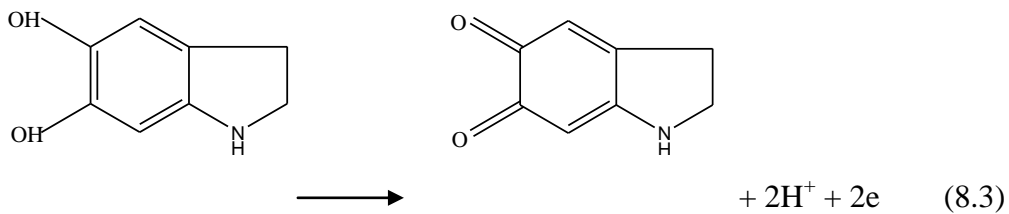
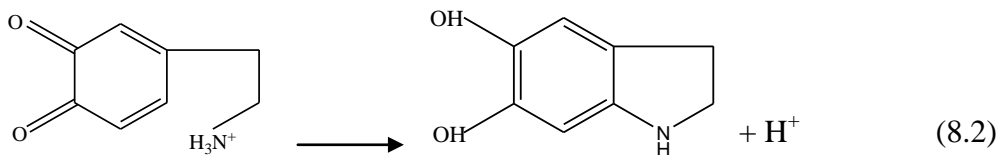
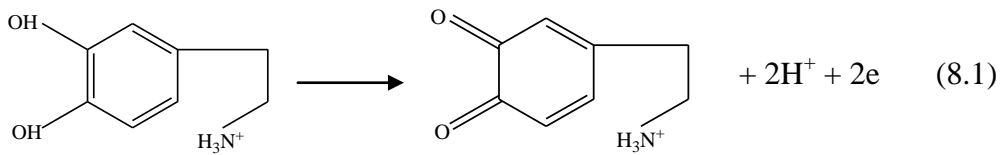


Figure 8.7: Cyclic voltammograms recorded at (A) μ -GEC, (B) μ -ZN-GEC, (C) μ -SZ-GEC, in 20 mL of 50 mM PBS supporting electrolyte with increasing concentrations of DA : 125 μ M, 250 μ M, 500 μ M, 750 μ M, 1 mM, 1.25 mM, 1.5 mM; Pt reference electrode and Ag/AgCl auxiliary electrode; potential range from -1.0 V to +1.2 V; scan rate 250 mV s^{-1} ; and (a) Calibration plot of the anodic current densities recorded at $E=+0.281$ V vs. DA concentration, calculated without background current subtraction (b) Calibration plot of the anodic current densities recorded at $E=+0.281$ V vs. DA concentration, calculated without background current subtraction and (c) Calibration plot of the anodic current densities recorded at $E=+0.161$ V vs. DA concentration, calculated without background current subtraction.



Scheme 1: Possible reaction scheme of DA on the electrode surface [8.23]

LOD were calculated by using the approach on the standard deviation of the regression based on equation 8.4:

$$LOD = \frac{3.3 S}{b} \quad (8.4)$$

where: S = relative standard deviation;
 b = the slope of the calibration plot.

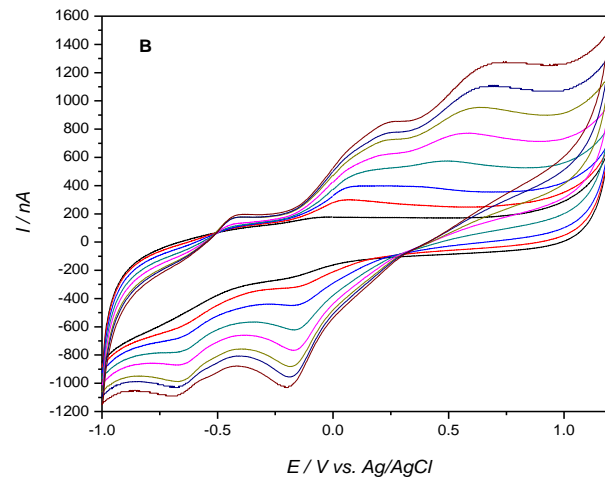
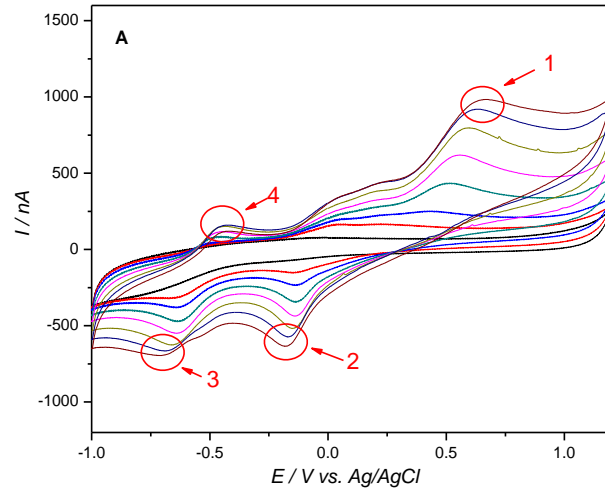
The low RSD values, which varied between 0.38 and 1.84 % at all three microelectrodes under investigation, concluded that the sensing devices can be consequently used for DA detection, with good repeatability of the analytical signal [8.27].

Taking into consideration that DA suffers from ascorbic acid, DOPAC, uric acid interference in the voltammetric determinations, due to the vicinity of their oxidation potentials, the improved response at μ -Z-GEC microelectrode, opens new approaches in DA detection. To note that such improvement was achieved without any membrane barrier on the electrode surface.

Table 8.1: Analytical parameters for CV technique for dopamine detection at microelectrodes without any protective membrane

Electrode type	Tehnique	E [V]	Sensitivity [nA $\mu\text{M}^{-1}\text{cm}^{-2}$]	Correlation coefficient, R^2	LOD [μM]	RSD [%]	LQ
μ -GEC	CV	+0.281	1923	0.981	11.86	0.380	39.54
μ -ZN-GEC		+0.281	1168	0.982	36.91	1.84	122.75
μ -SZ-GEC		+0.161	2027	0.976	7.03	0.81	32.06

8.2.3.1.2 Cyclic voltammetry of dopamine at microelectrodes with Nafion® membrane



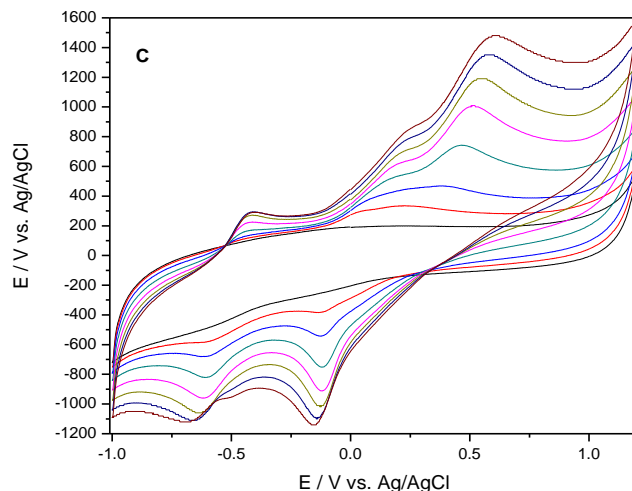


Figure 8.8: Cyclic voltammograms recorded at (A) μ -GEC, (B) μ -ZN-GEC, (C) μ -SZ-GEC with Nafion membrane, in 20 mL of 50 mM PBS supporting electrolyte with increasing concentrations of DA : 125 μ M, 250 μ M, 500 μ M, 750 μ M, 1 mM, 1.25 mM, 1.5 mM; Pt reference electrode and Ag/AgCl auxiliary electrode; potential range from -1.0 V to +1.2 V; scan rate 250 mV s^{-1} .

Similar cyclic voltammetric experiments with increasing concentrations of DA were performed at all three Nafion[®] (Nf) coated graphite based composites, by immersing the microelectrodes in a 5%wt. Nafion alcohol solution for 5 times. From Figure 8.8, was observed that the dopamine oxidation peak current, peak 1, shifted to more positive potential values, 0.666 V for Nf- μ -GEC, 0.706 V Nf- μ -NZ-GEC and 0.605 V for Nf- μ -SZ-GEC, respectively.

An increase in peak separation potential (ΔE) was calculated for Nf- μ -GEC equal to 0.843 V, a value of 0.905 V for Nf- μ -NZ-GEC, and the smallest value was recorded at Nf- μ -SZ-GEC equal to 0.757 V. The presence of irreversible (cathodic-to-anodic peak separations higher than 0.4 V [8.28] is due to the decrease in electron transfer between DA and the electrode. When the surface of an electrochemical sensing device is covered with a membrane, the immediate effect is the decrease in electrode conductivity, and as consequence, a larger ohmic drop, reason for existence of larger peak separations in the CV curves. Nf films are rich in negative charges and it is a strong cation exchanger, but has no electrocatalytic ability in DA oxidation, and the results are observed in the blocking effect [8.29].

In comparison with the composite materials without Nafion films, where the cathodic peaks are almost inexistent, except for μ -GEC and μ -SZ-GEC microelectrodes, after Nafion[®] coverage, the reduction peak no. 2 and peak no.3 occurred more obvious. The cathodic peaks are attributed to the reduction of dopamine-quinone and leucodopaminechrome, respectively. The difference consists in a fourth peak appearance, corresponding to the oxidation to dopaminochrome, as mentioned in 8.2.3.1.1 section.

Even the layer structure of Nafion has slowed the kinetics, increase in sensitivity is noticed at all three Nafion coated materials where linear calibrations were obtained with good correlation coefficients in the range 125 μ M- 1.5 mM (Table

8.2). This aspect could be explained by a premise according to which Nf entraps DA cations that leads to a higher local concentrations of DA on the electrode surface with a direct effect in improving DA electrochemical signal.

Even if Nafion is widely involved in electro analysis, because it can repel anions successfully, in this specific case, the graphite-synthetic zeolite-epoxy without Nafion membrane is highlighted as being the best material for DA detection.

When the permeability of the Nafion film is calculated after Gorski formula [8.25] in equation 8.5:

$$P = \left(\frac{I_{film}}{I_{bare}} \right) \times 100 \quad (8.5)$$

where: I_{film} and I_{bare} are DA voltammetric peak currents recorded at the Nafion-coated composite electrodes and the bare composites;

The smallest permselectivity ($P=108\%$) was obtained at Nf- μ -GEC and the highest at Nf- μ -NZ-GEC ($P=189\%$), while the Nf- μ -ZS-GEC had a permeability of 129%. The electronegative field given by the zeolite presence in the composite matrix is accentuated for the case of synthetic zeolite where the permselectivity is lower than for the case of natural zeolite.

It is clear that Nafion membrane leads to an increase on both anodic and cathodic currents of DA, although the sensitivity response is correlated to the film thickness, and in some cases, the DA signal might be reduced if the thickness is too high [8.30]. Normally, DA cations are accumulated in the hydrophilic regions or in the ion channels of Nafion, causing the sensitivity increase [8.27], but Nf contains a low content of ion-exchange groups, so, to have enough ion-exchangeable groups, the thickness of the layers has to be high, fact that turns into a retarded kinetic process [8.28]. The process of Nf coverage at all three composite microsensors was similar, and the concentrations of DA cations in PBS supporting electrolyte ready to be exchanged in Nafion film were kept constant. However, the analytical parameters presented in Table 8.2, showed improved electroanalytical parameters, i.e., LOD, sensitivity, and LQ. Also, a good repeatability is reflected by the lower RSD values.

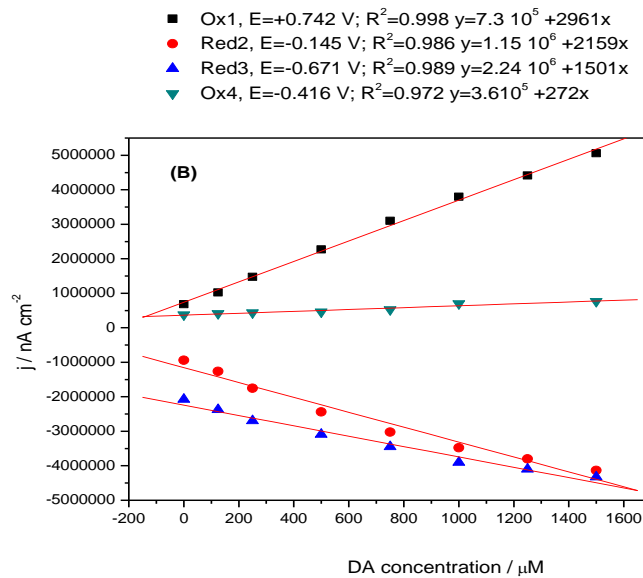
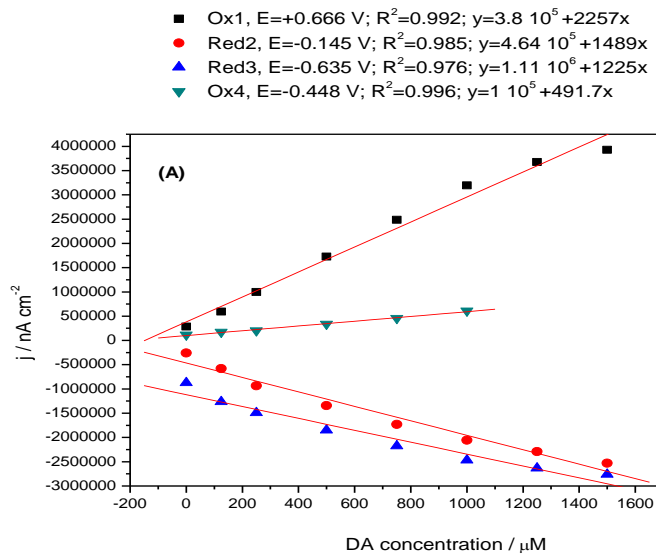
Table 8.2: Analytical parameters for CV technique for dopamine detection (peak no.1) at microelectrodes with Nafion membrane

Electrode type	Technique	E [V]	Sensitivity [nA $\mu\text{M}^{-1}\text{cm}^{-2}$]	Correlation coefficient , R^2	LOD [μM]	RSD [%]	LQ
Nf- μ -GEC	CV	+0.666	2575	0.992	7.13	2.11	23.79
Nf- μ -NZ-GEC		+0.742	2961	0.998	5.63	0.75	18.78
Nf- μ -SZ-GEC		+0.605	3623	0.990	4.82	0.70	16.08

If taking into consideration the possibility of indirect detection due to the appearance of the well defined peaks in the reduction scan, when the microsensors are covered with Nafion film, results from Table 8.3 should be analyzed. The necessity of possible consideration of this aspect is determined by the high potential

values at which DA oxidation peak appears, knowing the high level of interferences at this potential value.

Analyzing Table 8.3, it can be noticed that for both reduction peaks, peak no.2 and peak no.3, are obtained good sensitivities, for all three categories of sensors, although better results are observed for μ -SZ-GEC microsensors, where the values of sensitivities are as high as for the case when the sensors are not covered with Nafion film.



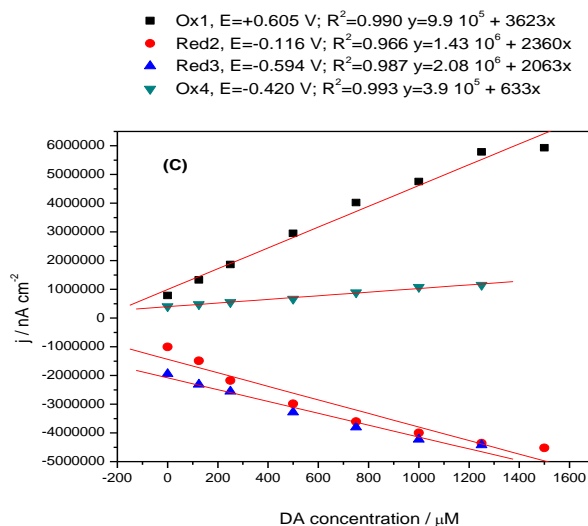


Figure 8.9: Calibration plots of the anodic/cathodic current densities recorded at (A) μ -GEC, (B) μ -ZN-GEC, (C) μ -ZS-GEC microsensors covered with Nafion membrane vs. DA concentration, calculated without background current subtraction.

Table 8.3: Calibration plot parameters for all peaks at sensors covered with Nafion film

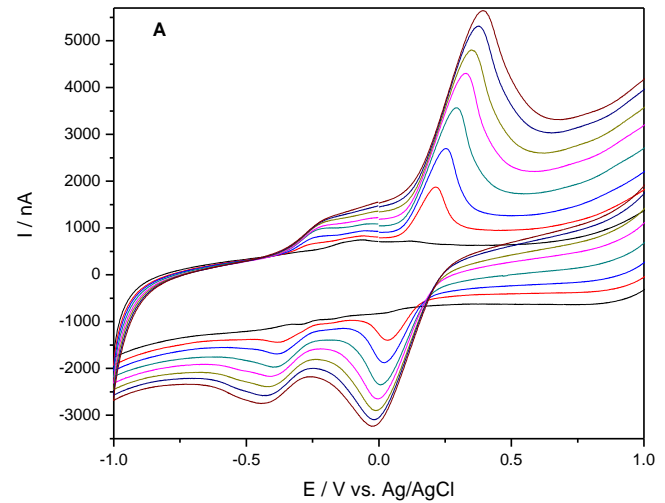
Sensor type	Peak no.	Potential value [V]	Sensitivity [$\text{nA } \mu\text{M}^{-1} \text{cm}^{-2}$]	Correlation coefficient, R^2
μ -GEC	Ox.1	+0.666	2575	0.992
	Red.2	-0.145	1489	0.982
	Red.3	-0.635	1225	0.976
	Ox.4	-0.448	491.7	0.996
μ -ZN-GEC	Ox.1	+0.742	2961	0.998
	Red.2	-0.145	2159	0.986
	Red.3	-0.671	1501	0.989
	Ox.4	-0.416	272	0.972
μ -ZS-GEC	Ox.1	+0.605	3623	0.990
	Red.2	-0.116	2360	0.966
	Red.3	-0.594	2063	0.987
	Ox.4	-0.420	633	0.993

8.2.3.1.3 Cyclic voltammetry of dopamine at microelectrodes with CNT film membrane

If not for *in-vivo* applications but for *in-vitro* applications, the response to DA at CNT-film- μ -ZS-GEC microsensor was also investigated. It can be noticed all four oxidation/reduction defined peaks in the shape of the voltammogram (see Figure 8.10 A) informs about a DA oxidation process without any inhibition. The sensitivity was calculated for all peaks (see Table 8.4), with regards to sensitivity of $12321 \text{ nA } \mu\text{M}^{-1} \text{cm}^{-2}$ at $E=0.216 \text{ V}$, which proved to be the highest from all types of microsensors investigated before, even for the ones covered with Nafion membrane.

The catalytic activity was noticed not only from the increased sensitivity towards dopamine detection but as well from the value of the oxidation potential

($E=0.216$ V) and a peak separation of $\Delta E= 0.186$ V (potential peak no.1-potential peak no.2).



- Ox 1, $E= +0.216$ V; $R^2=962$ $y=6.09 \cdot 10^6 + 1.23 \cdot 10^4 x$
- Red 2, $E=-0.247$ V; $R^2=949$ $y=2.62 \cdot 10^6 + 1799 x$
- ▲ Red 3, $E=-0.380$ V; $R^2=981$ $y=5.24 \cdot 10^6 + 4137x$
- ▼ Ox 4, $E= +0.030$ V; $R^2=945$ $y=5.05 \cdot 10^6 + 6005x$

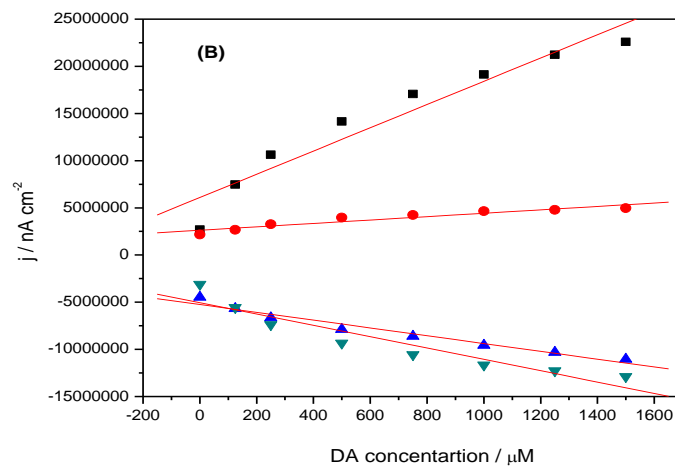


Figure 8.10: (A) Cyclic voltammograms recorded at CNT-film- μ -SZ-GEC, in 20 mL of 50 mM PBS supporting electrolyte with increasing concentrations of DA : 125 μ M, 250 μ M, 500 μ M, 750 μ M, 1 mM, 1.25 mM, 1.5 mM; Pt reference electrode and Ag/AgCl auxiliary electrode; potential range from -1.0 V to +1.0 V; scan rate 250 mV s^{-1} ; (B) Calibration plots of the anodic/cathodic current densities vs. dopamine concentrations, calculated without background current subtraction.

Table 8.4: Calibration plot parameters for all peaks at CNT-Film- μ -ZS-GEC microsensors

Sensor type	Peak no.	Potential value [V]	Sensitivity [$\text{nA } \mu\text{M}^{-1}\text{cm}^{-2}$]	Correlation coefficient, R^2
CNT-Film- μ -ZS-GEC	Ox.1	+0.216	12321	0.962
	Red.2	-0.247	1799	0.949
	Red.3	-0.380	4137	0.981
	Ox.4	-0.030	6005	0.945

8.2.3.2 Effect of the scan rate in cyclic voltammetric measurements

The amount of DA^+ cations that can be trapped into the Nf film depends on a series of factors, e.g. charge and size of the dopamine cation, its concentration in the electrolyte solution, concentration of competing Na^+ ions of the Nafion film, Nf membrane thickness (which determines the amount of sulphonate groups in the film), diffusion of DA in the film. In order to check some mechanism aspects regarding DA oxidation process on composite microelectrode with/without Nafion, the scan rate was varied in CVs experiments (0.110 V s^{-1} to 0.450 V s^{-1}) with $500 \mu\text{M}$ of DA in the PBS supporting electrolyte.

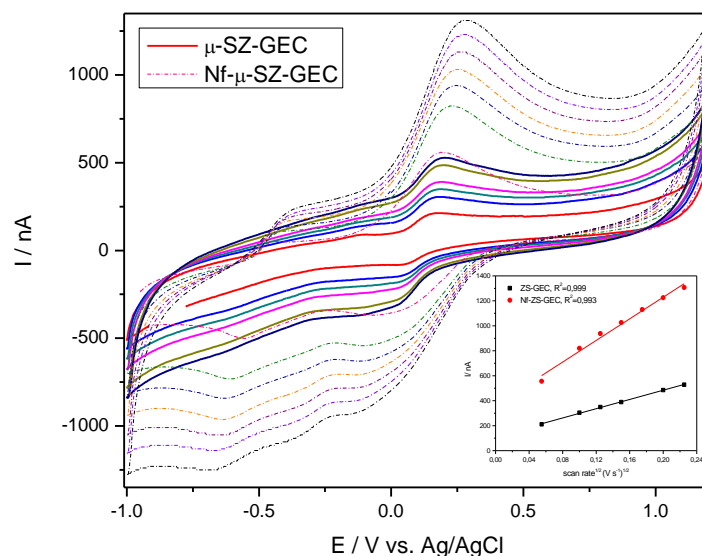


Figure 8.11: CVs for $500 \mu\text{M}$ DA in 50 mM PBS supporting electrolyte at different scan rates at μ -SZ-GEC : 0.110 V s^{-1} ; 0.2 V s^{-1} ; 0.25 V s^{-1} ; 0.3 V s^{-1} ; 0.4 V s^{-1} ; 0.45 V s^{-1} ; Inset: Plot of the anodic current (I_a) vs. square root of the scan rate (V s^{-1}) $^{1/2}$ at the same experimental conditions; Pt reference electrode and Ag/AgCl auxiliary electrode; potential range from -1.0 V to $+1.2 \text{ V}$;

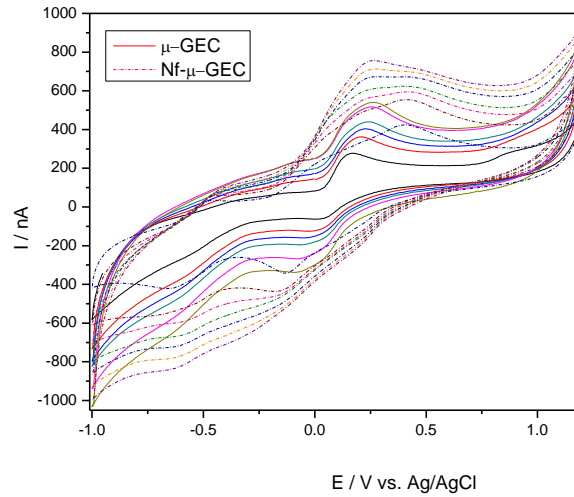


Figure 8.12: CVs for 500 μM DA in 20 mL of 50 mM PBS supporting electrolyte at different scan rates at $\mu\text{-GEC}$: 0.110 Vs^{-1} ; 0.2 Vs^{-1} ; 0.25 Vs^{-1} ; 0.3 Vs^{-1} ; 0.4 Vs^{-1} ; 0.45 Vs^{-1} ; Inset: Plot of the anodic current (I_a) vs. square root of the scan rate (V s^{-1})^{1/2} at the same experimental conditions; Pt reference electrode and Ag/AgCl auxiliary electrode; potential range from -1.0 V to +1.2 V;

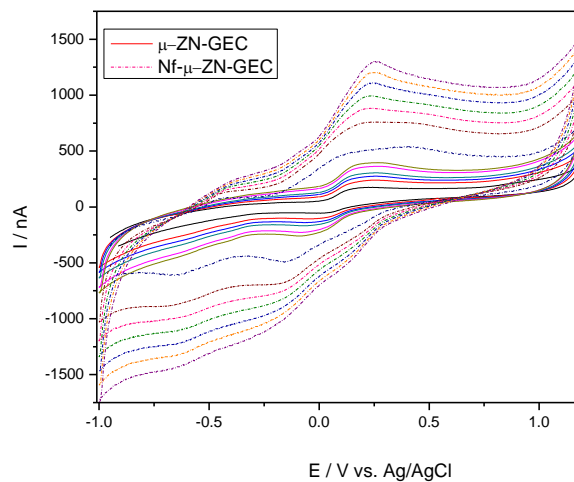


Figure 8.13: CVs for 500 μM DA in 20 mL of 50 mM PBS supporting electrolyte at different scan rates at $\mu\text{-ZN-GEC}$: 0.110 Vs^{-1} ; 0.2 Vs^{-1} ; 0.25 Vs^{-1} ; 0.3 Vs^{-1} ; 0.4 Vs^{-1} ; 0.45 Vs^{-1} ; Inset: Plot of the anodic current (I_a) vs. square root of the scan rate (V s^{-1})^{1/2} at the same experimental conditions; Pt reference electrode and Ag/AgCl auxiliary electrode; potential range from -1.0 V to +1.2 V;

Figure 8.11 presents the comparison of a series of cyclic voltammograms at different scan rates at $\mu\text{-SZ-GEC}$ microelectrode (solid line representing the response of bare $\mu\text{-SZ-GEC}$ at different scan rates and dotted line at the same

microelectrode that has the Nf film applied). The linear dependancies of anodic current densities (j) vs. square root of the scan rate ($v^{1/2}$), highlights a typical diffusion-controlled electrochemical process, are proved by the good correlation coefficient presented in table 8.5. The same diffusion characteristics are encountered at all three graphite based composites microelectrodes that are covered or not with Nafion film, results being summarized in Table 8.5.

Table 8.5: Effect on the scan rate in cyclic voltammetric measurements

Electrode type	Without Nf film		With Nf film	
	Slope [nA $\mu\text{M}^{-1}\text{cm}^{-2}$]	Correlation coefficient, R^2	Slope [nA $\mu\text{M}^{-1}\text{cm}^{-2}$]	Correlation coefficient, R^2
μ -GEC	$6.268 \cdot 10^6$	0.997	$1.512 \cdot 10^7$	0.990
μ -ZN-GEC	$5.108 \cdot 10^6$	0.998	$1.792 \cdot 10^7$	0.998
μ -SZ-GEC	$7.396 \cdot 10^6$	0.999	$1.732 \cdot 10^7$	0.993
CNT-film- μ -ZS-GEC	$2.914 \cdot 10^7$	0.999	-	-

Furthermore, the slopes of the plots I_a vs. $v^{1/2}$ for uncoated microelectrodes are smaller than for Nf coated electrodes, proving that a higher load of DA is incorporated inside the Nafion films compared to that accumulated from solution. This aspect is proved especial by no zero intercept of linear curves, which informed that sorption or surface-controlled process are significant (higher value was determined for Nafion-coated microsensors).

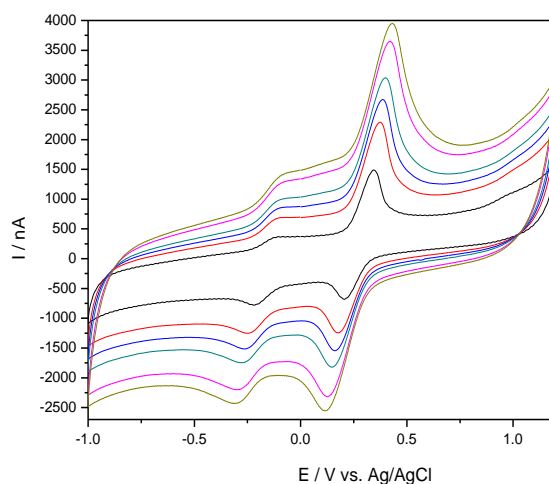


Figure 8.14: CVs for 500 μM DA in 20 mL of 50 mM PBS supporting electrolyte at different scan rates at CNT-film- μ -SZ-GEC : 0.110 Vs^{-1} ; 0.2 Vs^{-1} ; 0.25 Vs^{-1} ; 0.3 Vs^{-1} ; 0.4 Vs^{-1} ; 0.45 Vs^{-1} ;

8.2.3.3 Constant potential amperometry experiments

Constant-potential amperometry (CPA) is a very useful technique for practical applications and offers the best temporal resolution among available

techniques. Taking into consideration that in the extracellular fluid of the central nervous system, DA concentrations are present at a level from nanomolar to micromolar range (0.01-1 μ M) CPA should be regarded as the most viable.

Figure 8.15 presents the amperometric measurements of dopamine recorded at μ -SZ-GEC microelectrode without Nafion membrane at an applied potential of +0.150 V and with Nafion membrane at an applied potential of +0.430 V (see figure 8.16), while all electroanalytical parameters recorded as well at μ -GEC and μ -NZ-GEC microelectrodes are gathered in Table 8.6. The best results were obtained for Nf- μ -SZ-GEC in relation to the electroanalytical parameters, i.e., a limit of detection of 0.21 μ M, a sensitivity of 540 nA μ M⁻¹cm⁻² and an RSD value of 3.55 %.

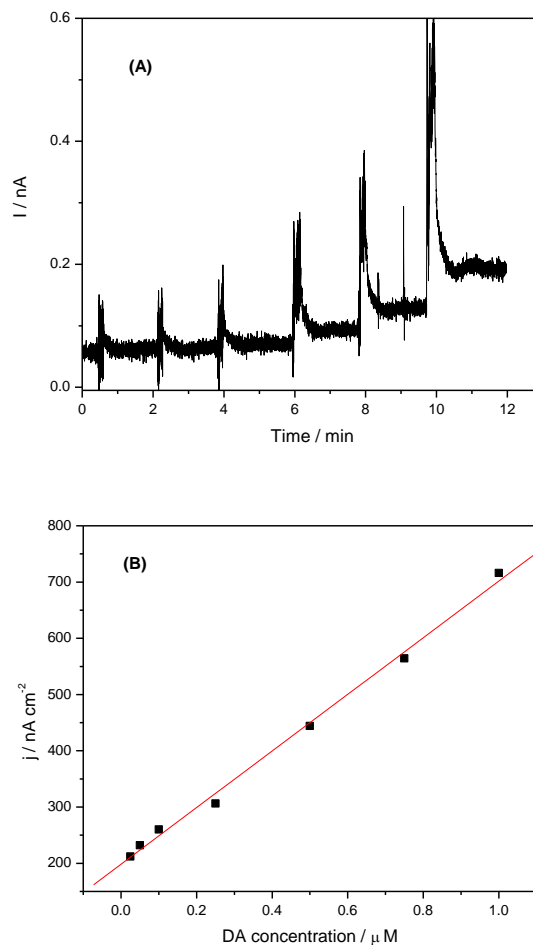


Figure 8.15: (A) CPA recoded at μ -SZ-GEC microelectrode without Nafion film in 20 mL of 50 mM PBS supporting electrolyte with increasing concentrations of Dopamine : 25 nM, 50 nM, 100 nM, 250 nM, 500 nM, 750 nM, 1 μ M; Pt reference electrode and Ag/AgCl auxiliary electrode; Potential value +0.150 V; (B) Calibration plots of the anodic/cathodic current densities vs. dopamine concentrations, calculated without background current subtraction

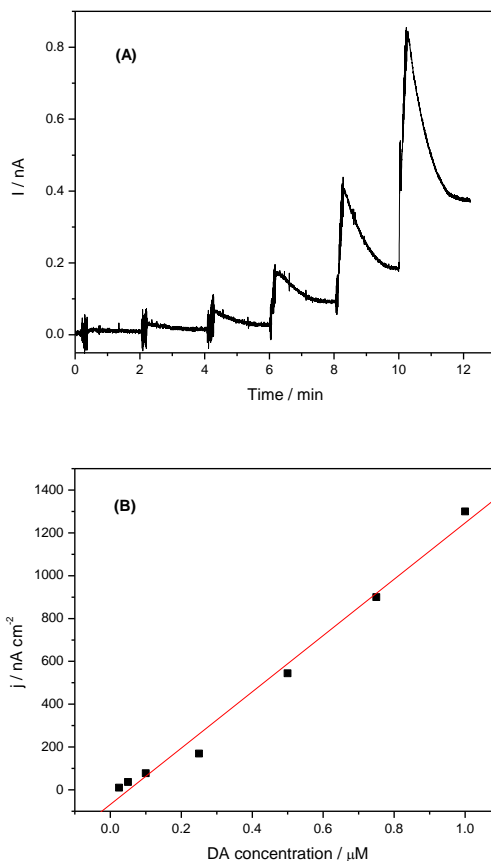


Figure 8.16: (A) CPA recorded at μ -SZ-GEC microelectrode with Nafion membrane in 20 mL of 50 mM PBS supporting electrolyte with increasing concentrations of Dopamine : 25 nM, 50 nM, 100 nM, 250 nM, 500 nM, 750 nM, 1 μ M; Pt reference electrode and Ag/AgCl auxiliary electrode; Potential value 0.430 V; (B) Calibration plots of the anodic/cathodic current densities vs. dopamine concentrations, calculated without background current subtraction.

Table 8.6: Analytical parameters for CPA technique for dopamine detection at microelectrodes with/without Nafion film

Electrode type	Without Nf film			With Nf film		
	μ -GEC	μ -NZ-GEC	μ -SZ-GEC	μ -GEC	μ -NZ-GEC	μ -SZ-GEC
Potential value [V]	+0.250		+0.150	+0.430		
Sensitivity [$\text{nA } \mu\text{M}^{-1} \text{cm}^{-2}$]	197.2	292	540	1772	1128	1500
Correlation coefficient, R^2	0.989	0.997	0.997	0.992	0.997	0.994
LOD [μM]	101.1	39.9	0.21	0.28	0.17	0.14
RSD [%]	67.47	30.55	3.55	8.6	5.17	14.10
LQ [μM]	336.71	133	0.729	0.94	0.56	0.58

For the CNT-film- μ -ZS-GEC microsensor the response of DA with CPA technique was assessed at two different potential values, namely at +0.250 V and at +0.150 V (see results Table 8.7), with the mentioning that at the positive potential a better sensitivity was obtained ($2.867 \cdot 10^4 \text{ nA } \mu\text{M}^{-1}\text{cm}^{-2}$), almost double that the one obtained in CV technique, the sensitivity obtained at +0.150 V is comparable with the one obtained for simple μ -ZS-GEC microsensor without Nf film.

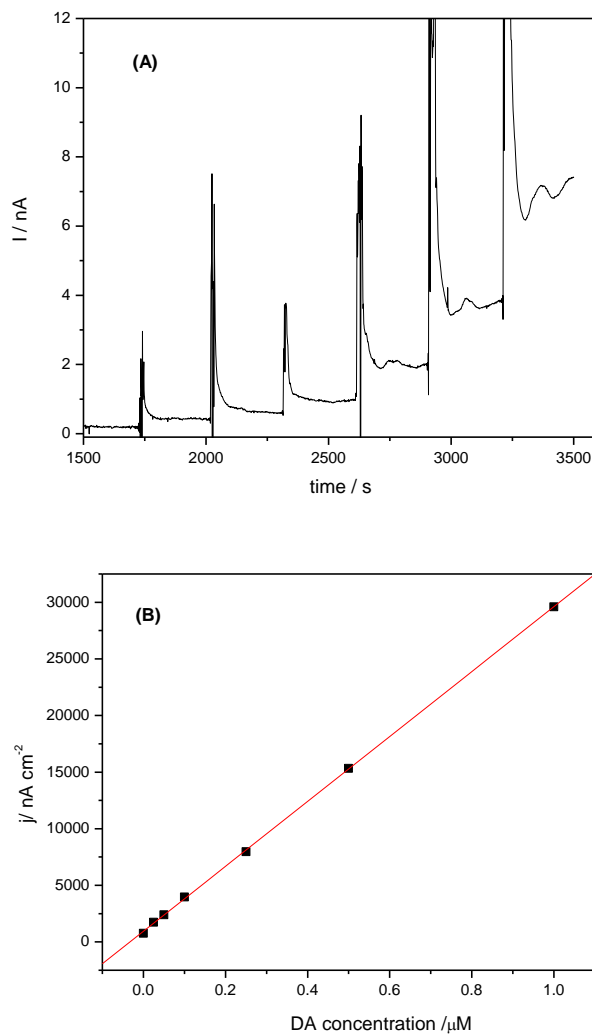


Figure 8.17: (A) CPA recorded at CNT-Film- μ -SZ-GEC microelectrode membrane in 20 mL of 50 mM PBS supporting electrolyte with increasing concentrations of Dopamine : 25 nM, 50 nM, 100 nM, 250 nM, 500 nM, 750 nM, 1 μ M; Pt reference electrode and Ag/AgCl auxiliary electrode; Potential value 0.250 V; (B) Calibration plots of the anodic/cathodic current densities vs. dopamine concentrations, calculated without background current subtraction

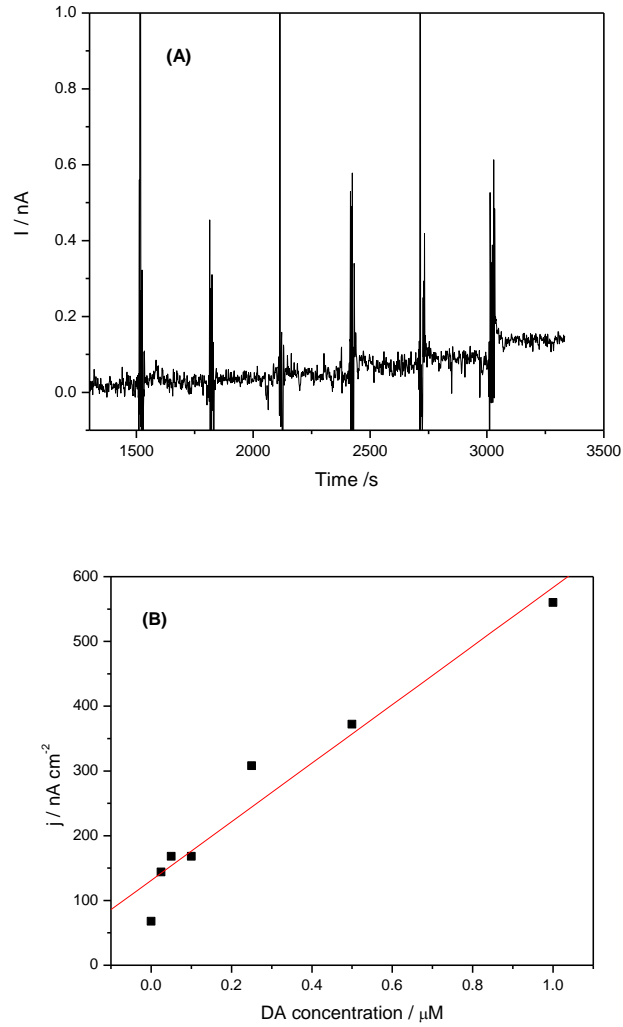


Figure 8.18: (A) CPA recorded at CNT-Film- μ -SZ-GEC microelectrode membrane in 20 mL of 50 mM PBS supporting electrolyte with increasing concentrations of Dopamine : 25 nM, 50 nM, 100 nM, 250 nM, 500 nM, 750 nM, 1 μ M; Pt reference electrode and Ag/AgCl auxiliary electrode; Potential value 0.150 V; (B) Calibration plots of the anodic/cathodic current densities vs. dopamine concentrations, calculated without background current subtraction

Table 8.7: Analytical parameters for CPA technique for dopamine detection at CNT-film-ZS-GEC microelectrode

Sensor type	CNT-film- μ -ZS-GEC	
Potential value [V]	+0.250	+0.150
Sensitivity [$\text{nA } \mu\text{M}^{-1}\text{cm}^{-2}$]	$2.867 \cdot 10^4$	452.2
Correlation coefficient, R^2	0.999	0.973

In-vitro detection of low dopamine concentrations must be regarded as starting point for improving the microsensors for further in vivo experiments. Serious interactions may occur at implantation due to the exposure to brain tissue and the study of μ -SZ-GEC microsensor to DA response when covered with specific membranes to assure selectivity has to be taken into consideration for future studies.

8.2.4 Conclusions

The direct detection of DA on simple μ -GEC, μ -ZN-GEC and μ -ZS-GEC with CV technique revealed that μ -ZS-GEC microsensor presented good sensitivity ($2027 \text{ nA } \mu\text{M}^{-1} \text{ cm}^{-2}$), improved oxidation potential ($E=0.161 \text{ V}$) with a peak separation of $\Delta E= 0.069 \text{ V}$ and the best LOD value ($7.03 \text{ } \mu\text{M}$) compared with μ -GEC and μ -ZN-GEC microsensors.

When compared the bare graphite-synthetic zeolite-epoxy composite microsensor with the one covered with CNT film, the analytical parameters show improved results in terms of sensitivity ($12321 \text{ nA } \mu\text{M}^{-1} \text{ cm}^{-2}$) but not also when compared the oxidation potential of dopamine, which for CNT-film- μ -ZS-GEC was attained at $E=0.216 \text{ V}$.

The microelectrodes consisted of the same composition as macroelectrodes allowed achieving better sensitivities for DA detection. The sensitivity of $2044 \text{ nA } \mu\text{M}^{-1} \text{ cm}^{-2}$ was achieved with synthetic zeolite-modified graphite-epoxy composite microelectrodes versus $0.58 \text{ nA } \mu\text{M}^{-1} \text{ cm}^{-2}$ the same composition macroelectrode.

This results obtained for the case of direct dopamine detection can open new approaches for its analytical quantification. In this direction, the above mentioned microsensors were covered with a layer of Nafion.

Although Nf is used widely in electroanalysis, in this particular conditions, bare μ -ZS-GEC is highlighted as being the best material for DA detection. Worth mentioning, that when microsensors are covered with Nafion, an indirect detection can be considered, due to the appearance of the well defined peaks in the reduction scan, fact which is also available for CNT-film- μ -ZS-GEC microsensor.

The constant potential amperometry (CPA), the most practical technique employed for the direct detection of dopamine, revealed the best results obtained for bare μ -ZS-GEC (in comparison with μ -GEC and μ -ZN-GEC) but comparable with CNT-film- μ -ZS-GEC microsensor, especially at the oxidation potential of 0.150 V . When Nafion membrane was attached, the amperometry result are considerable better in terms of sensitivity and limits of detection, taking into consideration that the oxidation potential was at $+0.430 \text{ V}$ but not above CNT-film- μ -ZS-GEC microsensor at an oxidation potential of $+0.250 \text{ V}$.

8.3 Interference studies

8.3.1 Introduction

Works that deal with sensing devices in the clinical sector are dedicated mostly for the detection of neurotransmitters, proteins, biomolecules, pathogenic bacteria and cancer biomarkers.

Neurotransmitters are endogenous chemical messengers that transmit, enhance, and transform specific signals between a neuron and other cells. Brain

neurotransmitters include catecholamines, namely dopamine, norepinephrine and epinephrine, glutamate, acetylcholine and choline [8.31].

According to Zhou et al. [8.32], the major problem of electrochemical detection of dopamine in real biological matrix is the coexistence of many interfering compounds. Among these, ascorbic acid is particularly important. In the extracellular fluid of the central system, DA exists in the range from 0.01 to 1 μM [8.33], while the concentration of AA is much higher, in the range from 100 to 500 μM [8.34], making ascorbic acid the main interferent. Nevertheless, another compound is also considered of great interference, namely dopamine metabolite, DOPAC.

Glutamate is the most widespread excitatory neurotransmitter in the mammalian central nervous system (CNS) [8.35-8.36], and plays a major role in a broad range of brain functions. The normal human-blood-glutamate concentration is around 10 μM [8.37].

The use of polymeric films such as the cation exchanger Nafion constitutes until now one of the best strategies to protect the surface of working electrode from interference of anions.

According to this information, preliminary cyclic voltammetric experiments were carried out for testing the response of ascorbic acid after microsensors were covered with Nafion membrane.

8.3.2 Experimental

Preparation of Nafion coated electrodes is previously described in detail in Chapter 6, via dip coating method.

All voltammetric experiments were carried out at room temperature (25°C) using an eDAQ QuadStat four-channel Potentiostat (Australia) controlled with an eChem software for cyclic voltammetry in a three-electrode electrochemical cell, carbon composite working electrodes, Ag/AgCl reference electrode and Pt auxiliary electrode. A magnetic stirrer provided the convective transport during the voltammetric experiments.

For detection experiments, the 50 mM PBS supporting electrolyte at H 7.4 was placed in the cell, and solutions of ascorbic acid, DOPAC and uric acid were employed by standard addition method solution. The scan rate employed for the detection experiments was 250 mV s^{-1} for the cyclic voltamograms experiments and a constant potential of 430 mV for the CPA experiments.

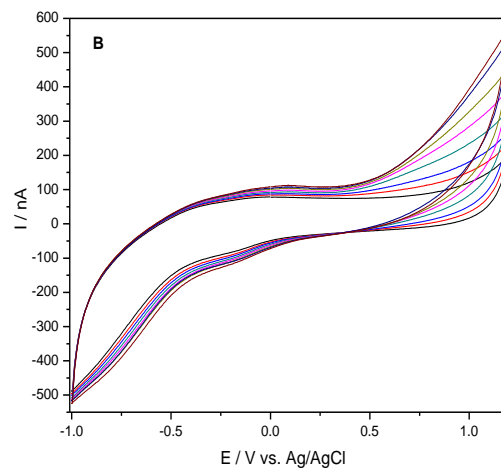
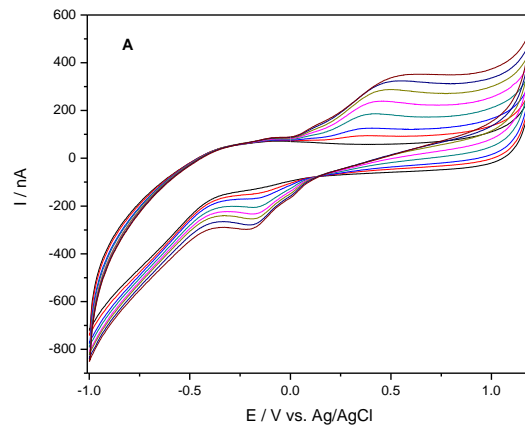
8.3.3 Results and discussions

A good electrochemical sensor require not only sensitivity to the analyte of interest, but also selectivity to that compound. The brain environment contains many active and oxidizable compounds that may interfere in dopamine detection experiments.

Although, the synthetic zeolite exhibited selectively towards DA versus AA based on the charge neutrality, its presence into zeolite-modified carbon-epoxy composite microelectrode did not assure a complete repulsion of AA due to the available graphite island towards ascorbic acid detection. For this reason and to avoid the interference of AA and the other electroactive compounds, Nafion membrane covered microsensors were tested by cyclic voltammetric experiments.

DOPAC voltammetric curves are presented in figure 8.19 for $\mu\text{-GEC}$, $\mu\text{-ZN-GEC}$, $\mu\text{-SZ-GEC}$ without Nf coverage. It can be seen that for $\mu\text{-GEC}$ DOPAC

oxidation can be considered an important interfering agent since the starting oxidation potential is around 0.100 V, with a peak current value at 0.500 V, the signal of DA and DOPAC at this microelectrode being overlapped. The same situation is present for μ -ZN-GEC microsensor, where the peak potential for DOPAC occurs at 0.600 V and for μ -SZ-GEC microsensor at 0.520 V.



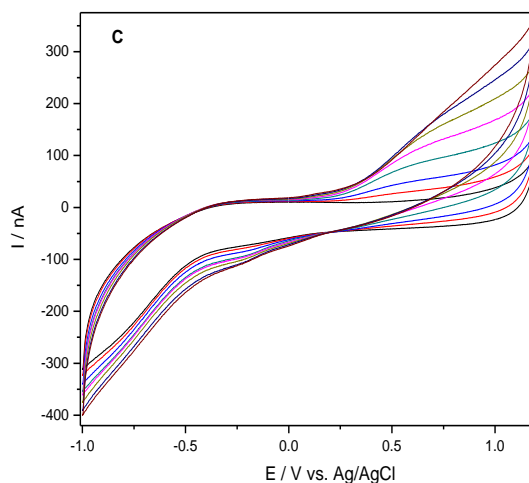


Figure 8.19 CVs recorded at (A) μ -GEC, (B) μ -ZN-GEC, (C) μ -SZ-GEC without Nafion membrane, in 20 mL of 50 mM PBS supporting electrolyte with increasing concentrations of DOPAC : 125 μ M, 250 μ M, 500 μ M, 750 μ M, 1 mM, 1.25 mM, 1.5 mM; Pt reference electrode and Ag/AgCl auxiliary electrode; potential range from -1.0 V to +1.2 V; scan rate 250 mV s^{-1} .

Table 8.8 summarizes the sensitivities values for DOPAC and the rest of interferences encountered by cyclic voltammetric techniques.

Table 8.8 Sensitivity values for main interferences occurred by cyclic voltammetry

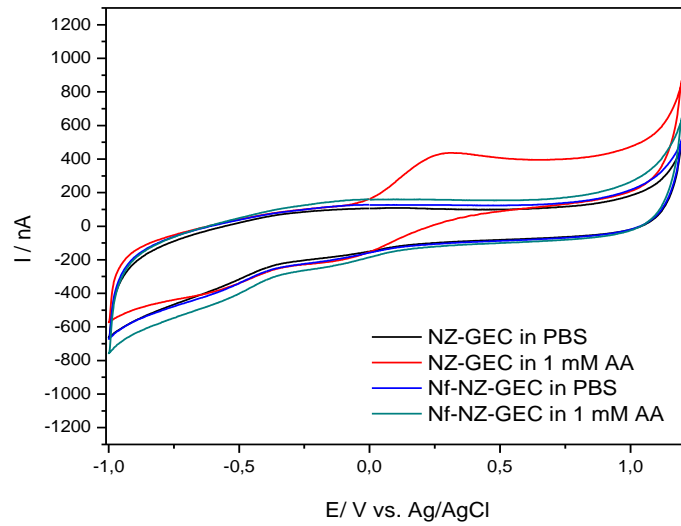
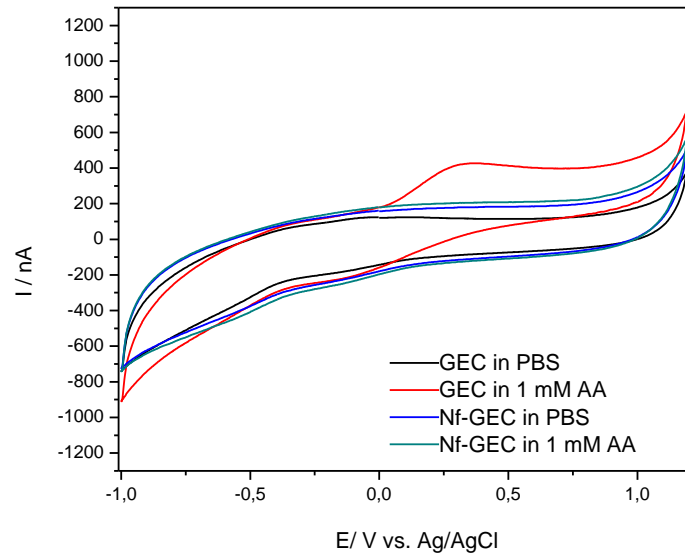
Analyte	Electrode type	Sensitivity [$\text{nA } \mu\text{M}^{-1}\text{cm}^{-2}$]
DA	μ -GEC	963
	μ -ZN-GEC	1091
	μ -SZ-GEC	554
AA	μ -GEC	1923
	μ -ZN-GEC	1168
	μ -SZ-GEC	2027
DOPAC	μ -GEC	759
	μ -ZN-GEC	300
	μ -SZ-GEC	448

Due to the reason that AA and DOPAC have close sensitivities, Nafion film was selected to cover all microelectrodes and check again the response to AA.

Figure 8.20 shows the rejection effect of Nf film towards the negative AA⁻, a significant reduction in AA detection signal being obtained after the membrane coverage. In Nafion, a key property are the sulphonic acidic groups, SO_3H^+ , which are highly hydrophilic and in the presence of water they are strongly hydrated, moment when H^+ became weakly attracted to the SO_3^- groups and move. For this reason, a strong electrostatic interaction between DA cation and Nf film is present and a strong electrostatic repulsion to AA anionic form is encountered, suppressing the oxidation of AA at electrode surface. The red voltammogram curves at all tree

128 Applications of modified/unmodified graphite-epoxy composite microsensors - 8

materials, represents the response of 1 mM AA in PBS supporting electrolyte compared to the background voltammogram shape (black line). A 94.95 % signal reduction was obtained for μ -SZ-GEC, a 93.72 % at μ -GEC and the smallest reduction of 92.25 % was noticed at μ -NZ-GEC composite microelectrode.



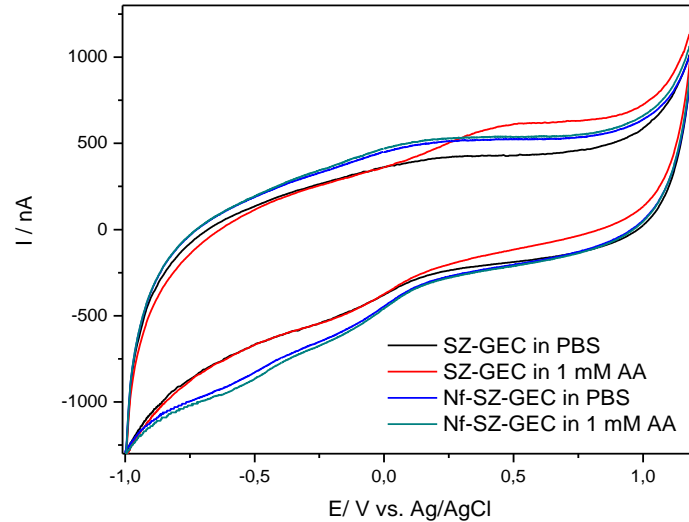


Figure 8.20 CVs recorded at (A) μ -GEC, (B) μ -ZN-GEC, (C) μ -SZ-GEC **without/with Nafion membrane**, in 20 mL of 50 mM PBS supporting electrolyte in the presence of 1 mM AA; Pt reference electrode and Ag/AgCl auxiliary electrode; potential range from -1.0 V to +1.2 V; scan rate 250 mV s⁻¹.

No significant interference signals were noticed on exposing composite microsensors covered with Nf film, to the electroactive molecules present in the striatal extracellular fluid even at pharmacologically relevant concentrations (the response of AA was tested for a concentration of 500 μ M, DOPAC for 10 μ M, UA for 2.97 μ M, and for DA for 1 μ M) (Table 8.9) by CPA technique, at a potential value of 0.430 V, chosen to assure the potential value at which all components should be oxidized , and as consequence, the maximum potential to interfere DA detection.

Table 8.9 Effects of some electroactive molecules (AA, DOPAC, UA) present in the striatal extracellular fluid on the amperometric response of graphite based microsensors

Interferent	μ -GEC [nA μ M ⁻¹ cm ⁻²]	μ -SZ-GEC [nA μ M ⁻¹ cm ⁻²]	μ -SZ-GEC [nA μ M ⁻¹ cm ⁻²]
AA	5.6 10 ⁻³	3.2 10 ⁻³	4.0 10 ⁻³
DOPAC	19.2 10 ⁻²	4.7 10 ⁻²	4.0 10 ⁻³
UA	9.28 10 ⁻¹	3.56	13.44 10 ⁻³
DA	1.77 10 ³	1.19 10 ³	1.5 10 ³

8.3.4 Conclusions

These preliminary results show the advantage of Nafion polymer modified microsensors to be selective over the most important interference molecule for further in vivo measurements. The potential to use these microsensors, especially ZS-GEC microsensor which presented the highest repulsion percentage for ascorbic

acid (94.95%) calculated from the CV technique, requires although further investigations when it comes to a detailed detection of dopamine.

8.4 Real-time monitoring of brain tissue oxygen

8.4.1 Introduction

Combining electrochemistry with *in vivo* applications, requires the use of some amperometric/voltammetric sensors, therefore, the detection of some electro-active molecules can be easily assessed. This achievement can be obtained by the use of biomedical telemetry [8.38], that involves data transmission from the implanted device to an external one. In time, data transmission by electrical wires was replaced by means of wireless transmission system [8.39], due to the fact that is less susceptible to interference with the ambient electric noise [8.40].

Neurochemically compounds can be detected by implanting an electrochemical micro-sensor in specific brain regions, which is polarized at a suitable potential, and the variations of sensor current response can give in real-time information related to concentrations of target molecules [8.41]. The working electrode can be metallic (gold, silver or platinum) or carbon-based sensing material, the latter being employed more often in biological studies [8.42], and reasons for which carbon based electrodes are used for O₂ detection are explained in [8.43].

The present study, focuses on using graphite-epoxy composite sensors for *in vivo* monitoring of dissolved brain O₂ using Constant Potential Amperometry (CPA) technique, O₂ being the most important oxidative substrate for biochemical reactions and for the production of brain energy. The concentrations of extra-cellular brain oxygen was stimulated by the injection of 1-methyl-4-phenyl-1,2,3,6-tetrahydropyridine (MPTP), which is known to induce oxidative neuronal stress [8.44].

8.4.2 Experimental

8.4.2.1 Regents and solutions

All chemicals were analytical reagent grade, used as supplied. Colloidal solution (4% cellulose nitrate in ethanol/diethyl ether from Fluka) was purchased from Sigma-Aldrich. The phosphate-buffer saline (PBS) supporting electrolyte solution was made using NaCl, Na₂HPO₄ and NaOH from Sigma, then adjusted to pH 7.4. Ultrapure (<99.9%) oxygen and nitrogen were purchased from Sapio s.r.l. Special Gases Division.

8.4.2.2 Working electrode (WE) preparation

The implantable sensing materials (graphite-epoxy based composites with/without zeolite prepared exactly as the optimized recipe in section 6) were filled inside a Teflon-insulated silver wire (using the same construction procedure and dimensions of the geometrical area of the micro-sensor as described in Chapter 6). The diameter of the sensing surface of 180 μm guarantees the detection of brain tissue oxygen, and not the small blood vessels oxygen [8.45]. Here, the silver wire guaranteed the electrical contact and the final O₂ micro-sensor dimensions had a length of approximately 1.2 cm. After curing, the electro-active area of the sensors were immersed (1 dip) in cellulose nitrate colloidal solution and left to dry over

night at room temperature (25°C). This colloidal solution is highly hygroscopic and small charged molecules (ions) and gases (O_2) can permeate the membrane which acts as a barrier for bigger organic molecules such as proteins, reducing a possible poisoning of the WE surface [8.45].

8.4.2.3 Apparatus and measurements

8.4.2.3.1 Experiments *in vitro*

Experiments *in vitro* were performed in a standard three-electrode electrochemical cell containing 10 mL PBS supporting electrolyte at room temperature (25°C). An Ag/AgCl electrode was used as reference, and a Pt wire served as the auxiliary electrode. All *in vitro* calibrations were performed 24h after sensor manufacturing, the same day for the *in vivo* implantation (day 0, pre-calibration), and repeated after rat sacrifice (day 8, post-calibration). The difference between a three-electrode system for *in vitro* experiments compared to *in vivo* ones is exemplified in figure 8.21, where the PBS supporting electrolyte for *in vitro* procedures is replaced with brain extracellular fluid.

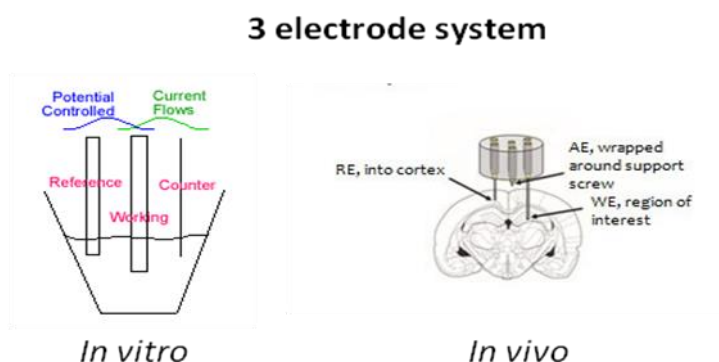


Figure 9.21 Comparatively presentation of the set-up for *in vitro*/ *in vivo* experimental procedure.

1) Cyclic voltammetry (CV) experiments

O_2 reduction at all three WE (μ -GEC, μ -NZ-GEC and μ -SZ-GEC) was experimentally demonstrated using CV technique, at a scan rate of 250 mV/s. Blank voltamograms were recorded in PBS supporting electrolyte, and after purging continuously for 15 min pure O_2 , PBS-100% O_2 solutions were obtained, and all WEs were scanned again in order to observe the O_2 reduction potential. Only one sensing material was selected for *in vivo* application, sensing material which requested further *in vitro* pre/post-calibrations.

2) Constant potential amperometry (CPA) experiments

CPA was used for *in vitro* pre/post-calibrations and *in vivo* experiments, fixing the O_2 reduction potential at -350 mV/s vs. Ag/AgCl reference electrode. All *in*

in vitro calibrations were performed in freshly prepared N_2 and O_2 solutions under standard conditions of pressure and temperature.

For *pre calibrations* experiments, the WE was used 1 day after fabrication. The experiment begun with the settling down of the WE in 10 mL of PBS supporting electrolyte under the applied potential of -350mV/s vs. Ag/AgCl, until a stable baseline level was attained. To obtain effective deaeration, into the PBS solution was vigorously purged O_2 -free N_2 for 15 min until stabilization was reached again, moment for the saturation achieved. Calibrations were performed involving $0\text{--}250\mu\text{M}$ O_2 , when known volumes ($+200\mu\text{L}$, $+204\mu\text{L}$, $+208\mu\text{L}$, $+212\mu\text{L}$, $+216\mu\text{L}$) of a saturated (100%) O_2 solution were added into the N_2 -purged PBS.

Post calibrations experiments were conducted in the same experimental manner, for low oxygen concentrations, after rat sacrifice and extraction of the sensors.

8.4.2.3.2 Experiments *in vivo*

The WE that was selected for *in vivo* implantation was connected to the biotelemetric device, as well as Ag/AgCl reference/auxiliary electrode.

1) *Electronic Set-Up*

The proposed set-up consists in three main parts: 1. A mobile unit (a circuit that includes an amperometric and a digital section); 2. Receiving USB device, and 3. A computer for signal acquisition and analysis as exemplified in figure 8.22.

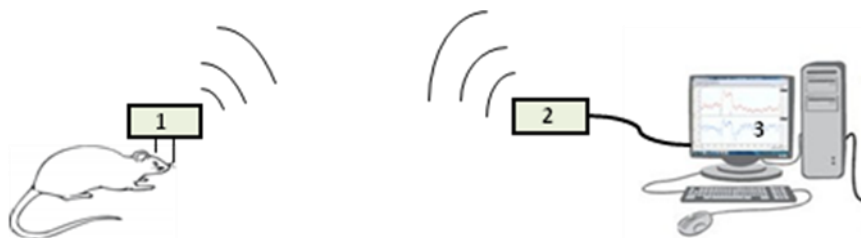


Figure 8.22 System for acquisition, transmission and elaboration of electrochemical signals.

The power supply for the mobile unit fixed to the rat's scalp is provided by a thin lithium battery, and all the experimental measurements begin as soon as the battery is added. The circuit from the mobile unit polarizes the WE with a constant working potential (-350 mV) and reads the sensor current that contains information regarding the concentration of the compound in the brain area under investigation. The resulted sensor currents are converted into digital values and then transformed in serial data for the wireless interfering with the PC, via USB. The computer performs the signal acquisition, plots and displays the received data with the help of a customized software. Detailed information about the electronics, firmware and software are explained in [8.46].

2) Stereotaxic surgery

Stereotaxic surgery was performed under chloral hydrate anesthesia. The rat skull was drilled and the O₂ WE micro-sensors were implanted in the right and left striatum. The reference/auxiliary electrodes were implanted in the left parietal cortex (200 μm silver wire), and two screws were inserted in the skull for reinforcing the biotelmtric device adhesion (Figure 8.23A,B). The 'basement' portion of the device (without battery) was fixed to the skull using dental cement, and the electrodes were connected and the skin was sutured (Figure 8.23 C,D).

3) *In vivo* procedures

After surgery, the animals were housed in large plastic bowls and maintained in a temperature and light controlled environment, with free access to food and water. The O₂ micro-sensor was polarized 24h after surgery (day 1) by insertion of a battery in the "basement". The oxygen monitoring in the brain tissue, started with the animal in its home bowl, where the rat was subjected to a pharmacological 7 days treatment with MPTP administration at a dosage of 18 mg/kg (day 1), 13 mg/kg (day 2), 8 mg/kg (day 3) and a challenge dose of 15 mg/kg (day 7). The changes of brain tissue O₂ were calculated as absolute variations versus the corresponding baseline, and monitored using CPA technique. Constant potential amperometry, where the detecting electrode is held at a constant potential sufficient to detect the reduction of the target substance, was used for O₂ detection at NZ-GEC micro-sensor being held at -350 mV. The advantage of CPA was that it has lower background currents *in vivo*, but is limited to the detection of one analyte.

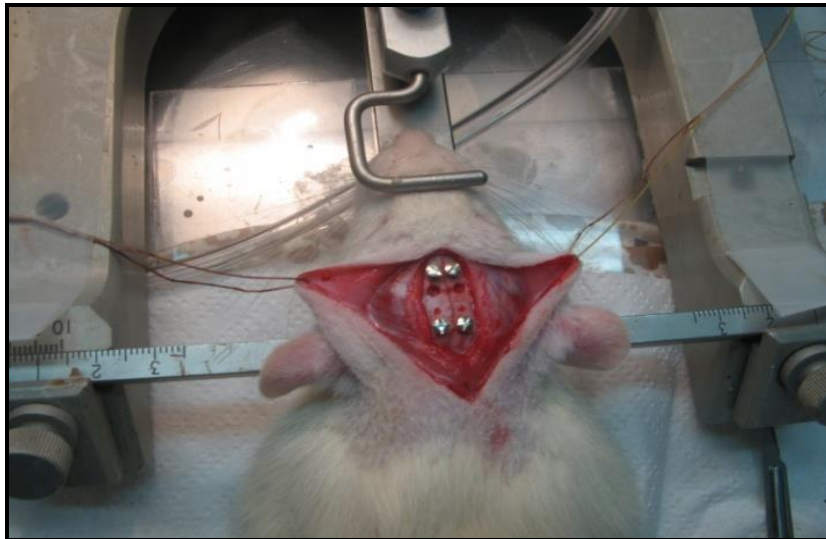


Figure 8.23 A: holes drilled for WE, ref/aux and screws implantation

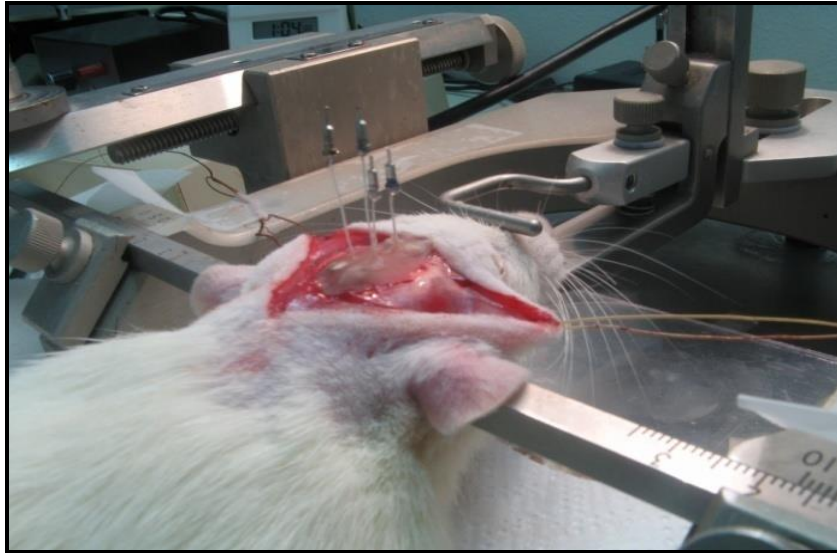


Figure 8.23 B: sensors implantation

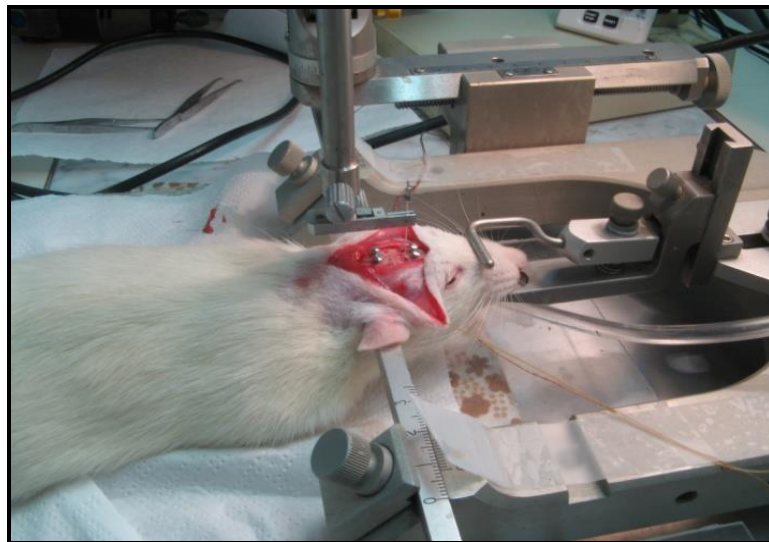


Figure 8.23 C: fixing the 'basement' to the skull



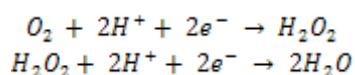
Figure 8.23 D: suturing the skin

8.4.3 Results and discussions

8.4.3.1 Micro-sensors response to oxygen

Cyclic voltammetry (CV) experiments

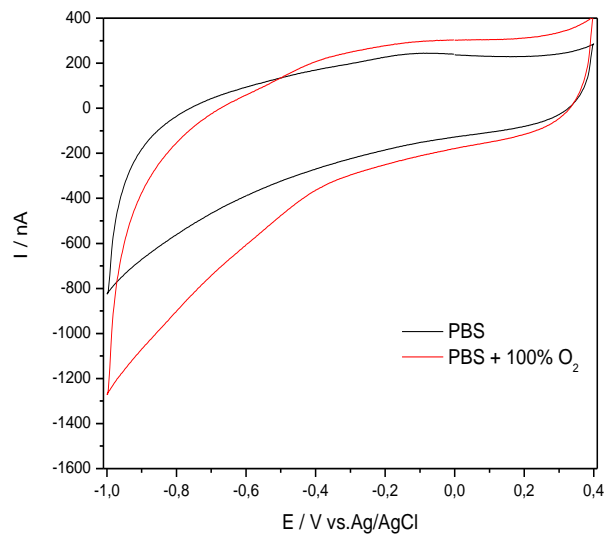
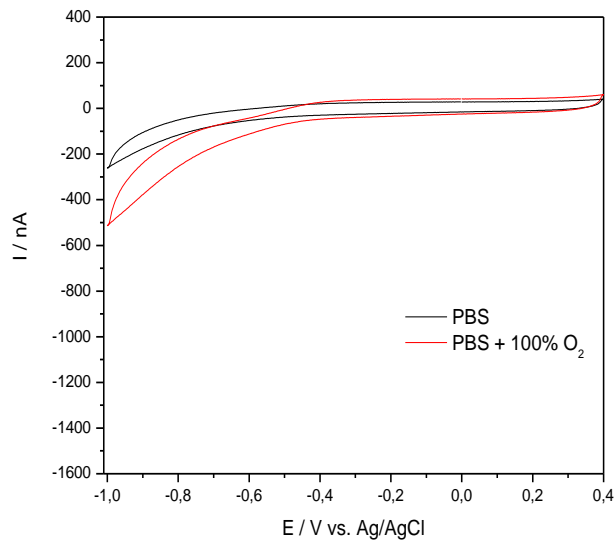
Oxygen reduction at carbon electrodes occurs as a two-electron process [8.47]:



Oxygen sensor selection for implantation was performed connecting μ -GEC, μ -NZ- μ GEC, μ -SZ-GEC micro-electrodes to the three-electrode electrochemical system and exposing them to a standard PBS supporting electrolyte, as blank voltammograms, and to a saturated 100% O_2 PBS solution, as illustrated in Figure 8.24. Cyclic voltammetry, performed at pH 7.4, showed the best O_2 response at a potential value of -365 mV for μ -NZ-GEC micro-electrode, with a sensitivity of 0.0912 nA/ μ M, while the bare GEC presented the smallest sensitivity for O_2 reduction. All results are presented in Table 9.9. The reduction potential of O_2 was obtained in other research groups at -650 mV for a carbon paste electrode [8.43], and at a potential value of -400 mV for a bare graphite-epoxy micro-sensor in [8.45].

The optimum material considered for implantation was GEC due to its increased sensitivity towards O_2 and its reduction potential value, although the background current registered in PBS supporting electrolyte was bigger compared to the blank voltammogram of GEC micro-sensor.

The decreased sensitivity of 0.0242 nA/ μ M for μ GEC sensing device was expected, taking into consideration that the electrochemical reduction of oxygen at carbon electrodes is slower than at traditional electrodes like Pt or Gold [8.47] an overview of the elch.red of O₂-articles implantation], reason for what, the use of catalytic materials, (e.g. zeolites in this study), improved the oxygen reduction potential, improvement observed as well in the case of μ -SZ-GEC micro-electrode.



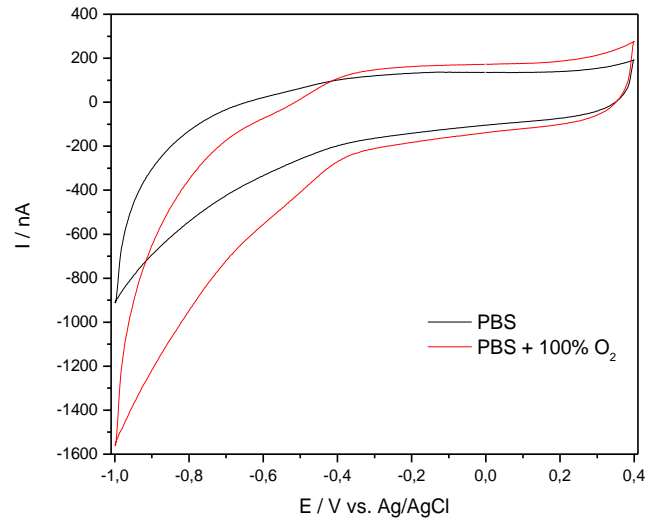


Figure 8.24 : Cyclic voltammograms recorded at (A) μ -GEC, (B) μ -NZ-GEC and (C) μ -SZ-GEC, microelectrode covered with 4% cellulose nitrate solution (1 dip and left overnight) in 10 mL of 50 mM PBS supporting electrolyte and 100% O_2 for O_2 response; scan rate 250mVs^{-1} ; potential range -1.0V to $+0.4\text{V}$; Ag/AgCl reference electrode and Pt auxiliary electrode;

Table 8.9: CV's data for O_2 detection at μ -GEC, μ -NZ-GEC, μ -SZ-GEC

Electrode type	Starting O_2 reduction potential [mV]	Sensitivity [nA/ μM]
μ -GEC	-465	0.0242
μ -NZ-GEC	-365	0.0912
μ -SZ-GEC	-400	0.0609

Constant potential amperometry (CPA) experiments

The pre-calibration experiments at μ -NZ-GEC micro-sensor for low O_2 concentrations using CPA technique is presented in Figure 8.25. The concentrations of O_2 solution were taken as $0\ \mu\text{M}$ (N_2 -saturated) and maximum $250\ \mu\text{M}$ (air-saturated). The graphite-natural zeolite-epoxy sensing material displayed a good linearity of 0.994 and a sensitivity of $0.083\ \text{nA}/\mu\text{M}$, while the post-calibration experiments revealed a small reduction in linearity, $R^2=0.974$, but an increase in sensitivity, up to $0.146\ \text{nA}/\mu\text{M}$ (inset Figure 9.27), behavior that can be due to the possible removal of nitrate cellulose coverage.

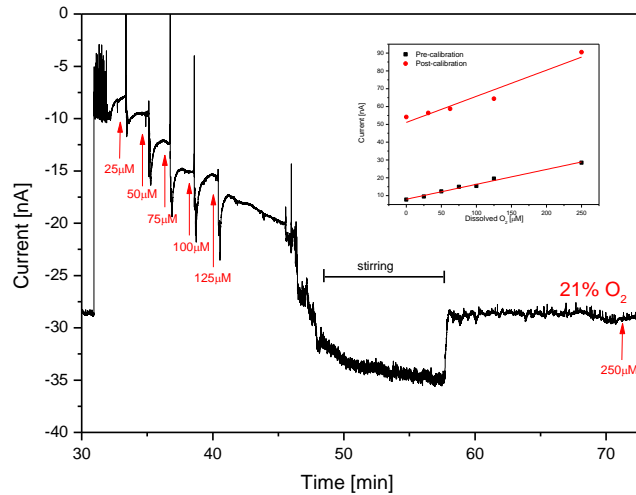


Figure 8.25: In vitro **pre-calibration** of oxygen micro-sensor using CPA performed at -350 mV vs. Ag/AgCl reference electrode with low concentrations of O₂; the oxygen sensor response was tested by exposing them to known volumes (200 μ L, +204 μ L, +208 μ L, +212 μ L, +216 μ L) of saturated O₂ solution (1.25mM) to a 10 mL saturated nitrogen PBS. *Inset*: In vitro **pre/post calibration** plots of the current *I* vs. dissolved O₂ concentration at NZ-GEC response characteristic for O₂ reduction.

Compared to previous results obtained in the same research department, [8.41] where a conical shape bare graphite-epoxy micro-sensor was implanted, the pre-calibration results obtained in the present study are improved.

8.4.3.2 Baseline levels of striatal O₂

Baseline striatal currents were recorded daily starting from day 1. The initial micro-sensor stabilization was obtained after 150 min. The time necessary for sensors to stabilize the current level (at the beginning of each experiment) was between 150 min and 100 min, time after which, the pharmacological treatment was administrated. The calculated oxygen baseline current in day 1 was around 23 nA and further fluctuations of baseline levels were recorded day by day, as noticed in Table 8.10.

Table 8.10 Determination of dissolved O₂ concentration according to MPTP administration

Treatment day	Absolute baseline levels (\approx 150 min stabilization) [nA]	Δ I increase after MPTM administration [nA]	Dissolved O ₂ concentration determined after MPTP administration [μ M]
Day 1	23.4	27.7	237.5
Day 2	41.1	13.6	67.7
Day 3	57.3	6.5	20.24
Day 7	32.5	25.2	207.5

8.4.3.3 Effect on striatal O_2 current changes after pharmacological treatments

The effect of the pharmacological treatment is briefly explained in Figure 8.26, exemplified for the day 7. To explore the potential of the microsensor, MPTP neurotoxin was administrated as intraperitoneal injections to the rat for three days consequently at different dosages, and a challenge dose in day 7. Confirmation that μ -NZ-GEC micro-sensor, operating at -350mV, responds rapidly to changes in brain tissue O_2 *in vivo*, was verified by the increase with a 27.7 nA (from baseline level) (day 1) after MPTP administration at a dosage of 18 mg/kg. An increase of striatal O_2 current was observed in each day of experiments, when the maximum oxygen variations vs. baseline was achieved in 50-100 min after the neurotoxin injection. The maximum increase was obtained in day 1, and the minimum current increase was attained in day 3 with a variation of only 6.3 nA, as can be noticed in Figure 9.29. The challenge dose of 15 mg/kg administrated in day 7, had an increase in dissolved O_2 , similar to the one that occurred in day 1, with a current increase vs. baseline level of 25.2 nA.

Systemic administration of MPTP, induced a sustained increase of striatal oxygen, due to the fact that once MPTP administrated and transformed in MPP^+ (after crossing the brain barrier), inside the dopaminergic neurons can block the electron transport chain, therefore, enhancing the production of reactive oxygen species.

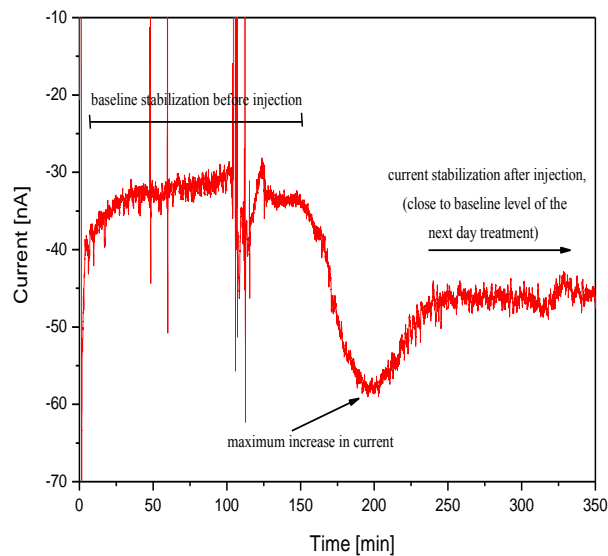


Figure 8.26: Effect of pharmacological treatments on striatal dissolved oxygen. (A) example for day 7 ;

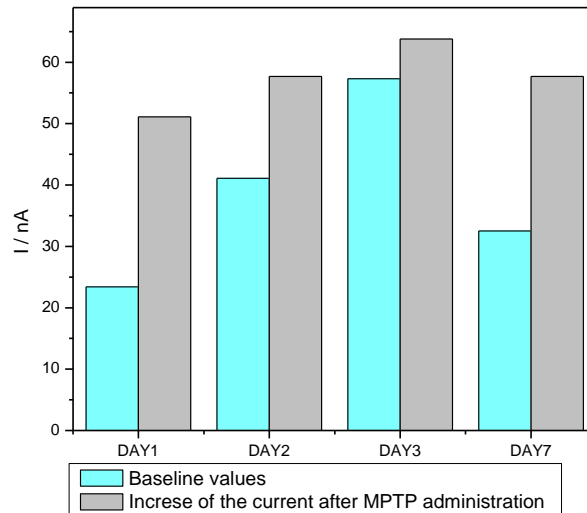


Figure 8.27: Current increase in day 1, 2, 3 and 7 of implantation when MPTP neurotoxin was administrated at a dosage of 18, 13, 8 and respectively 15 mg/kg after baseline stabilization; applied potential is -350mV.

Using *in vitro* or *in vivo* calibrations, it is possible that the concentration of dissolved O_2 , after MPTP administration, to be estimated. The maximum concentration values found for each treatment day were as expressed in Table 9.10 compared to previously reported O_2 concentrations of 40-80 μ M [6][2-sassari doc]. Values that indicate normal levels of tissue oxygen seem to vary although between the available monitoring systems, possibly because of the different technologies used, causing some confusions among users. As well, concentrations of oxygen may vary depending on the depth of measurement [8.48] and the heterogeneity of the tissue [8.49].

8.4.4 Conclusions

Using *in vitro* or *in vivo* calibrations, it was possible that the concentration of dissolved O_2 , after MPTP administration, to be estimated. The *in-vivo* procedure using a new zeolite-graphite-epoxy composite microsensors was successfully applied in the detection of extracellular brain oxygen and the molecular oxygen concentration based on pre/post calibrations.

8.4.5 References

- [8.1] M. Reiger, "Oxidative reactions in and on the skin:mechanism and prevention," *Cosmetical toillery*, vol. 108, pp. 43-56, 1993.
- [8.2] B. Fox and A. Cameron, *Food science, nutrition and health*, London: E. Arnold, 1989.
- [8.3] A. Yu and H. Chen, "Electrocatalytic oxidation and determination of ascorbic acid at poly(glutamic acid) chemically modified electrode," *Analytica chimica acta*, vol. 344, p. 181-185, 1997.

- [8.4] A. Ciszewski and G. Milczarek, "Polyeugenol-Modified Platinum Electrode for Selective Detection of Dopamine in the Presence of Ascorbic Acid," *Analytical chemistry*, vol. 71, p. 3203–3209, 1999.
- [8.5] J. Zheng and X. Zhou, "Sodium dodecyl sulfate-modified carbon paste electrodes for selective determination of dopamine in the presence of ascorbic acid," *Bioelectrochemistry*, vol. 70, p. 408–415, 2007.
- [8.6] G. Szepesi and Z. Fresenius, "New method for the spectrophotometric determinations of ascorbic acid and dehydroascorbic acid," *Analytical chemistry*, vol. 265, pp. 334–336, 1973.
- [8.7] K. Verna, A. Jain and A. Chaurasia, "Determination of ascorbic acid in soft drinks, preserved fruit juices and pharmaceuticals by flow injection spectrophotometry: matrix absorbance correction by treatment with sodium hydroxide," *Talanta*, vol. 42, pp. 779–787, 1995.
- [8.8] P. Janda, J. Weber, L. Dunsch and A. Lever, "Detection of ascorbic acid using a carbon fiber microelectrode coated with cobalt tetramethylpyridoporphyrazine," *Analytical chemistry*, vol. 68, pp. 960–965, 1996.
- [8.9] G. Greenway and P. Ongomo, "Determination of L-ascorbic acid in fruit and vegetables juice by flow injection with immobilized ascorbate oxidase," *Analyst*, vol. 115, pp. 1297–1299, 1990.
- [8.10] A. Salimi, M. Hussein and R. Hallaj, "Simultaneous determination of ascorbic acid, uric acid and neurotransmitters with a carbon ceramic electrode prepared by sol-gel technique," *Talanta*, vol. 70, pp. 823–832, 2006.
- [8.11] C. Miaw-Ling and C. Chur-Min, "Simultaneous voltammetric determination of ascorbic acid and its derivatives in cosmetics using epoxy-carbon composite electrodes," *Journal of food and drug analysis*, vol. 13, pp. 205–211, 2005.
- [8.12] R. Jahan-Bakhsh, O. Reza and K. Abolfazl, "Carbon paste electrode spiked with ferrocene carboxylic acid and its application to the electrocatalytic determination of ascorbic acid," *Journal of electroanalytical chemistry*, vol. 515, pp. 45–51, 2001.
- [8.13] B. Anamaria, R. Adriana, **I. Elida**, M. Florica, J. Stephen and S. Joop, "Carbon nanotube composite for environmental friendly sensing," *Environmental engineering and management journal*, vol. 11, pp. 239–246, 2012.
- [8.14] P. Damier, E. Hirsch, Y. Agid and A. Graybiel, "The substantia nigra of the human brain II: Patterns of loss of dopamine containing neurons in Parkinson's disease," *Brain*, vol. 122, pp. 1437–1448, 1999.
- [8.15] F. Seeman and K. Shitij, "More dopamine, more D2 receptors," *National academy of science*, vol. 97, 2000.
- [8.16] B. Gianfranco, A. Biossa, D. Farina, Y. Spissu, S. Dedola, G. Calia, G. Puggini, G. Rocchitta, R. Migheli, M. Desole and P. Serra, "Dual asymmetric flow microdialysis for in vivo monitoring of brain neurochemicals," *Talanta*, p. in press, 2011.
- [8.17] W. Wilson, S. Mietling and J. Hong, "Automated HPLC analysis of tissue levels of dopamine, serotonin and several prominent amine metabolites in extracts from various brain regions," *Journal of liquid chromatography*, vol. 6, pp. 871–886, 1983.
- [8.18] A. Othman, N. Rizka and M. El-Shahawi, "Potentiometric determination of dopamine in pharmaceutical preparations by crown ether-PVC membrane sensors," *Analytical sciences*, vol. 20, pp. 651–655, 2004.

- [8.19] S. Zhao, Y. Huang, M. Shi, R. Liu and Y.-M. Liu, "Chemiluminescence resonance energy transfer based detection for microchip electrophoresis," *Analytical chemistry*, vol. 82, pp. 2036-2041, 2010.
- [8.20] X. Xie, D. Stueben and Z. Berner, "The application of microelectrodes for the measurements of trace metals in water," *Analytical letters*, vol. 38, pp. 2281-2300, 2007.
- [8.21] D. Robinson, B. Venton, L. Heien and M. Wightman, "Detecting subsecond dopamine release with fast-scan cyclic voltammetry in vivo," *Clinical chemistry*, vol. 49, pp. 1763-1773, 2003.
- [8.22] D. Gligor, L. Muresan, A. Dumitru and I. Popescu, "Electrochemical behaviour of carbon paste electrodes modified with methylene green immobilized on two different X type zeolites," *Journal of applied electrochemistry*, vol. 37, pp. 261-267, 2007.
- [8.23] C. Martinez, M. Cerro, S. Ferro, A. De Battisti and M. Quiroz, "Electrochemical behaviour of dopamine at Nafion modified boron doped diamond electrode: preliminary results," *Canadian journal of analytical sciences and spectroscopy*, vol. 52, pp. 325-333, 2007.
- [8.24] H. Shurong, N. Zheng, H. Feng, X. Li and Z. Yuan, "Determination of dopamine in the presence of ascorbic acid using poly(3,5-dihydroxy benzoic acid) film modified electrode," *Analytical biochemistry*, vol. 179, pp. 179-184, 2008.
- [8.25] J. Chou, S. Ilgen, S. Gordon, D. Asanga, W. McFarland, H. Metiu and S. Buratto, "Investigation of the enhanced signals from cations and dopamine in electrochemical sensors coated with Nafion," *Journal of electroanalytical chemistry*, vol. 632, p. 970101, 2009.
- [8.26] A. Babei, M. Zendejdel, B. Khalilzadeh and A. Taheri, "Simultaneous determination of tryptophan, uric acid and ascorbic acid at iron(III) doped zeolite modified paste electrode," *Colloids and surfaces B: Biointerferences*, vol. 66, pp. 226-232, 2008.
- [8.27] L. Rocha and H. Carapuca, "Ion-exchange voltammetry of dopamine at Nafion-coated glassy carbon electrodes," *Bioelectrochemistry*, vol. 69, pp. 258-266, 2006.
- [8.28] Xian-Qin, K. Guang-FenG and C. Ying, "A nafion and choline bi-layer modified carbon fiber electrode for in vivo detection of dopamine in mouse cerebrum," *Chinese journal of analytical chemistry*, vol. 36, pp. 157-161, 2008.
- [8.29] X. Kang, Z. Mai, X. Zou, P. Cai and J. Mo, "A sensitive nonenzymatic glucose sensor in alkaline media with a copper nanocluster/multiwall carbon nanotube-modified glassy carbon electrode," *Analytical biochemistry*, vol. 363, pp. 143-150, 2007.
- [8.30] J. Huang, H. Fang, C. Liu, E. Gu and D. Jiang, "A Novel Fiber Optic Biosensor for the Determination of Adrenaline Based on Immobilized Laccase Catalysis," *Analytical letters*, vol. 41, pp. 1430-1442, 2008.
- [8.31] Y. Zhou, R. Tian and J. Zhi, "Amperometric biosensor based on tyrosinase immobilized on a boron-doped diamond electrode," *Biosensors and bioelectronics*, vol. 22, p. 822-828, 2007.
- [8.32] P. Capella, B. Ghasemzadeh, K. Mitchell and R. Adams, "Nafion coated carbon fiber electrodes for neurochemical studies in brain tissue," *Electroanalysis*, pp. 175-182, 1990.
- [8.33] R. D. O'Neill, "Microvoltammetric techniques and sensors for monitoring neurochemical dynamics in vivo. A review," *Analyst*, vol. 5, pp. 767-779, 1994.

- [8.34] M. Perry, Q. Li and R. Kennedy, "Review of recent advances in analytical techniques for the determination of neurotransmitters," *Analytica chimica acta*, vol. 635, p. 1-22, 2009.
- [8.35] S. Chakraborty and C. Raj, "Mediated electrocatalytic oxidation of bioanalytes and biosensing of glutamate using functionalized multiwall carbon nanotubes-biopolymer nanocomposite," *Journal of electroanalytical chemistry*, vol. 609, p. 155-162, 2007.
- [8.36] G. Babu, M. Bawari, V. Mathur, J. Kalita and U. Mishra, "Blood glutamate levels in patients with motor neuron disease," *Clinica chimica acta*, vol. 273, p. 195-200, 1998.
- [8.37] A. Kiourti, "Biomedical telemetry: communication between implanted devices and the external world," *Opticon*, vol. 1826, pp. 1-6, 2010.
- [8.38] P. Serra, "Wireless transmission of fast-scan cyclic voltammetry at a carbon-fiber microelectrode: proof of principle," *Journal of neuroscience methods*, vol. 140, pp. 103-115, 2004.
- [8.39] S. Kwang, "A miniaturized low-power remote environmental monitoring system based on electrochemical analysis," *Sensors and actuators B*, vol. 140, pp. 153-161, 2004.
- [8.40] J. Lowry, "Real time monitoring of brain energy metabolism in vivo using microelectrochemical sensors: the effects of anesthesia," *Bioelectrochemistry*, vol. 54, pp. 39-47, 2001.
- [8.41] B. F., "Characterization of carbon paste electrode for real-time amperometric monitoring of brain tissue oxygen," *Journal of neuroscience methods*, vol. 195, pp. 135-142, 2011.
- [8.42] M. Desole, M. Miele, G. Esposito, L. Fresu, R. Migheli, D. Zangani, S. Sircana and S. Grella, "Neuronal antioxidant system and MPTP-induced oxidative stress in the striatum of brain stem of the rat," *Pharmacology biochemistry and behaviour*, vol. 51, pp. 581-592, 1995.
- [8.43] B. Gianfranco, G. Giuia, D. Sonia, C. Gianmario, R. Gaia, M. Rossana, D. Maria, L. John and S. Pier, "Real time monitoring of brain tissue oxygen using a miniaturized biotelemetric device implanted in freely moving rats," *Analytical chemistry*, vol. 81, pp. 2235-2241, 2009.
- [8.44] S. Pier, R. Gaia, B. Gianfranco, M. Antonio, P. Giulia, L. John and D. Robert, "Design and construction of low cost single-supply embedded telemetry system for amperometric biosensor applications," *Sensors and Actuators B*, vol. 122, pp. 118-126, 2007.
- [8.45] B. Sljukic, "An overview of the electrochemical reduction of oxygen at carbon based modified electrodes," *Journal of the Iranian chemical society*, vol. 2, pp. 1-25, 2005.
- [8.46] H. Baumgartl, "Oxygen supply of the blood free perfused guinea pig brain in normo and hypotemia measured by the local distribution of oxygen pressure," *Pflugers arch*, vol. 414, 1989.
- [8.47] R. Murr, S. Berger, K. Peter and A. Baethmann, "A novel, remote-controlled suspension device for brain tissue pO₂ measurements with multiwire surface electrodes," *Pflugers archive*, vol. 426, pp. 348-350, 1994.

CHAPTER 9

Final conclusions and further perspectives

The **original elements** of this PhD thesis consist of both the manufacturing and design conditions of the composite microelectrodes based on graphite modified with natural or synthetic zeolite within epoxy matrix and their multiple applications in life and health quality control. The new composite electrode synthesized in this study allowed an easy detection way, fast response, high sensitivity, appropriate for real sample, small volume, avoiding chemical reagents adding for the simultaneous / selective assessment of analytes. These microelectrodes gave the possibility of in-vivo detection application. Thus, **innovation degree** is given by the easy method of synthesis of new composite microelectrodes with improved electrocatalytic properties for the selective/simultaneous detection of dopamine, ascorbic acid and in-vivo detection of extracellular brain oxygen.

Degree of originality and complexity consisted of:

- Elaboration and manufacturing of natural/synthetic zeolite-modified/unmodified graphite-based composite microelectrodes with useful properties for the *in-vitro* electrochemical detection of selective and simultaneous detection of dopamine and ascorbic acid;
- Elaboration and manufacturing of natural/synthetic zeolite-modified/unmodified graphite-based composite macroelectrodes to compare their utility for *in-vitro* electrochemical detection of selective and simultaneous detection of dopamine and ascorbic acid;
- The evaluation of the electrode materials behaviour in phosphate-buffer saline at pH 7 and in the presence of the target analyte, to establish the relationship between obtained electrode material and reaction type;
- Individual detection experiments performance, which provides specific informations, i.e., voltammetric/amperometric detection type, detection potential value, concentration ranges, electrode sensitivity, stability, reproducibility and lifetime, detection limits, calibration, to elaborate the detection protocol;
- Exploitation of the specific features of the pulsed voltammetric techniques, e.g., differential-pulsed voltammetry and square-wave voltammetry to improve the electroanalytical performance for the selective detection of the dopamine in the presence of ascorbic acid;
- Elaboration of specific simultaneous detection protocol of the dopamine and the ascorbic acid;
- Elaboration of selective detection protocol of dopamine in the presence of ascorbic acid with Nafion coated graphite-composite microelectrodes;
- *In-vitro* enhanced sensitive detection of dopamine at carbon nanotubes-film coated graphite composite microelectrodes;
- *In-vivo* amperometric monitoring of dissolved brain oxygen at optimized zeolite-modified graphite-composite microelectrodes;

Several graphite-epoxy composite microelectrodes, i.e., μ -GEC, μ -ZN-GEC and μ -ZS-GEC in comparison with the same composition of macroelectrodes, i.e., M-GEC, M-ZN-GEC and M-ZS-GEC were successfully prepared.

Graphite-epoxy (M-GEC), natural zeolite-graphite-epoxy (M-NZ-GEC), synthetic zeolite-graphite-epoxy (M-SZ-GEC) composite macroelectrodes were obtained as main electrochemical materials. The design of the macrosensors presented disk shaped geometry of 0.196 cm^2 .

The bare graphite-epoxy composite was considered as blank material and zeolite-graphite-epoxy composite electrode materials were constructed for highlighting the superiority of the zeolite presence in the composite matrix in further applications.

Cyclic voltammetry technique was used to determine electroactive surfaces of constructed materials. Electroactive surface area for M-GEC, equal to 0.165 cm^2 , was the highest from all sensors, value which decreased from M-GEC to M-ZS-GEC (0.135 cm^2) and M-NZ-GEC (0.127 cm^2), but in all cases, the electroactive surface areas were smaller than the calculated geometric area of 0.196 cm^2 .

Graphite-epoxy (μ -GEC), natural zeolite-graphite-epoxy (μ -ZN-GEC), synthetic zeolite-graphite-epoxy (μ -ZS-GEC) composite microelectrodes were obtained as main electrochemical materials. The design of the microsensors presented a disk shaped geometry of $2.5 \cdot 10^{-4} \text{ cm}^2$ and a final length of 5 cm. For further investigations Nafion coated microelectrodes (Nafion- μ -GEC, Nafion- μ -ZN-GEC, Nafion- μ -ZS-GEC) and carbon nanotubes film coated microsensors (CNT-film- μ -ZS-GEC) were constructed.

The bare graphite-epoxy composite as blank material and zeolite-graphite-epoxy composite electrode materials were constructed in steps involving several optimization procedures: finding the best epoxy resin polymerization conditions, a proper mixing method of the three-epoxy component with graphite particles following the optimization of graphite-epoxy weight ratio and optimization of graphite-zeolite-epoxy weight ratio, all optimization procedures having a major importance over the sensitivity and reversibility performance of the final sensor.

The classical ferri/ferrocyanide system with cyclic voltammetry technique was used to determine electroactive surfaces of constructed materials. Electroactive surface area for μ -GEC, equal to $1.03 \cdot 10^{-3}$, was the highest from all sensors, value which decreased from μ -GEC to μ -ZN-GEC ($5.7 \cdot 10^{-4} \text{ cm}^2$) and μ -ZS-GEC ($3.8 \cdot 10^{-4} \text{ cm}^2$), but in all cases, the electroactive surface areas were higher than the calculated geometric area of $2.5 \cdot 10^{-4} \text{ cm}^2$, results comparable with values equal with $5.88 \cdot 10^{-4} \text{ cm}^2$ for CNT film- μ -ZS-GEC.

All sensors presented a large number of conducting microzones and the majority of their surface is electroactive. Also, a diffusion-controlled process was found based on the linear relationship of I vs. $v^{1/2}$ in the scan rate ranged from 25 to 454 mV s^{-1} .

A more detailed investigation was done for Graphite-epoxy (μ -GEC), natural zeolite-graphite-epoxy (μ -NZ-GEC), synthetic zeolite-graphite-epoxy (μ -SZ-GEC) composite microelectrodes in terms of macroelectrode/microelectrode array behaviour. All voltammograms at slow scan rates presented a sigmoidal response consistent to a microelectrode behavior. At fast scan rates a more peak shaped response was obvious, especially at μ -SZ-GEC sensor, characteristic for solid macroelectrode behavior and substantial hysteresis appeared at all three composites. Also, a diffusion field overlap for all composites microelectrode assemblies was noticed, aspect characteristic to a macroelectrode behavior and slopes when plotting $\log i$ vs. $\log v$ lower than 0.5 was associated to a mixed linear and spherical diffusion, fact that arises at microelectrodes, depending on experimental time scale.

Taking into consideration that the main goal of these composite material is to detect selectively/simultaneously dopamine (DA) and ascorbic acid (AA), the sorption capacity of both natural and synthetic zeolite towards dopamine and ascorbic acid was investigated. Synthetic zeolite exhibited a good sorption capacity towards DA, which makes it very suitable to be used as a permselective membrane to improve the selective detection of DA in the presence of AA. This property is due to the possibility of DA preconcentration onto synthetic zeolite incorporated onto a carbon based composite electrode improving local concentration and excluding AA presence at the electrode surface.

The voltammetric techniques, *i.e.*, cyclic voltammetry, differential-pulsed voltammetry and square-wave voltammetry, tested for the simultaneous detection of AA and DA on composite macroelectrodes allowed the detection of both analytes with better sensitivity for DA detection using synthetic zeolite-modified graphite-epoxy composite macroelectrode. Also, at this electrode the peak separation value of minimum 200 mV was reached using square-wave voltammetry under the optimized conditions of 0.0025 V step potential, 0.1 V modulation amplitude and 50 Hz frequency. Under the above-presented experimental conditions, the catalytic effect towards dopamine detection was proved for synthetic zeolite-modified graphite-epoxy composite microelectrode, allowing increasing the sensitivity and selectivity for this analyte detection, besides a possible electrostatic attraction between dopamine cation and the negative surface of the synthetic zeolite and electrostatic repulsion with ascorbic acid anion.

Also, synthetic zeolite-modified graphite-epoxy composite macroelectrode gave the best electroanalytical parameters for dopamine detection using chronoamperometry, the most useful technique for the practical applications.

Electrochemical behaviour of AA was investigated by CV at all carbon composite microsensors, namely bare graphite-epoxy composite (μ -GEC) as blank material in comparison with sensors containing natural zeolite (μ -ZN-GEC) and synthetic zeolite (μ -SZ-GEC), as well as CNT-film- μ -ZS-GEC microelectrode offering an image of their sensitivity towards ascorbic acid. CNT-film- μ -ZS-GEC presented the highest sensitivity equal to 2145 nA $\mu\text{M}^{-1}\text{cm}^{-2}$ and the less positive oxidation potential of 0.220 V, while μ -SZ-GEC microsensor presented the lowest sensitivity and the most positive oxidation potential value, equal to 0.521 V.

The catalytic effect of the carbon nanotubes was obvious as well as for the natural zeolite material, which had improved sensitivity values and improved oxidation potential values compared to bare μ -GEC microsensor.

For further applications regarding the selective detection of dopamine in the presence of ascorbic acid, a slightly decreased sensitivity towards AA is desired, fact that was encountered at μ -SZ-GEC microsensor (sensitivity equal to 554.11 nA $\mu\text{M}^{-1}\text{cm}^{-2}$ and $E=0.521$ V). Moreover, to avoid AA interference for DA detection in the practical application, a permselective Nafion membrane can be also investigated.

The direct detection of DA on simple μ -GEC, μ -ZN-GEC and μ -ZS-GEC with CV technique revealed that μ -ZS-GEC microsensor presented good sensitivity (2027 nA $\mu\text{M}^{-1}\text{cm}^{-2}$), improved oxidation potential ($E=0.161$ V) with a peak separation of $\Delta E=0.069$ V and the best LOD value (7.03 μM) compared with μ -GEC and μ -ZN-GEC microsensors.

When compared the bare graphite-synthetic zeolite-epoxy composite microsensor with the one covered with CNT film, the analytical parameters show improved results in terms of sensitivity (12321 nA $\mu\text{M}^{-1}\text{cm}^{-2}$) but not also when compared the oxidation potential of dopamine, which for CNT-film- μ -ZS-GEC was attained at $E=0.216$ V.

The microelectrodes consisted of the same composition as macroelectrodes allowed achieving better sensitivities for DA detection. The sensitivity of $2044 \text{ nA } \mu\text{M}^{-1}\text{cm}^{-2}$ was achieved with synthetic zeolite-modified graphite-epoxy composite microelectrodes versus $0.58 \text{ nA } \mu\text{M}^{-1}\text{cm}^{-2}$ the same composition macroelectrode.

This results obtained for the case of direct dopamine detection can open new approaches for its analytical quantification. In this direction, the above mentioned microsensors were covered with a layer of Nafion.

Although Nf is used widely in electroanalysis, in this particular conditions, bare μ -ZS-GEC is highlighted as being the best material for DA detection. Worth mentioning, when microsensors are covered with Nafion, an indirect detection can be considered, due to the appearance of the well defined peaks in the reduction scan, fact which is also available for CNT-film- μ -ZS-GEC microsensor. The advantage of Nafion polymer modified microsensors to be selective over the most important interference molecule will be exploited for further *in vivo* measurements. The potential to use these microsensors, especially μ -ZS-GEC microsensor which presented the highest repulsion percentage for ascorbic acid (94.95%) calculated from the CV technique, requires although further investigations. It must be highlighted the comparative results of dopamine individual and simultaneous detection on μ -ZS-GEC, which showed that the presence of ascorbic acid increased only with 0.8 % the voltammetric signal corresponding to dopamine detection, which means that ascorbic acid did not interfere the dopamine detection.

The constant potential amperometry (CPA), the most practical technique employed for the direct detection of dopamine, revealed the best results obtained for bare μ -ZS-GEC (in comparison with μ -GEC and μ -ZN-GEC) but comparable with CNT-film- μ -ZS-GEC microsensor, especially at the oxidation potential of 0.150 V. When Nafion membrane was attached, the amperometry result are considerable better in terms of sensitivity and limits of detection, taking into consideration that the oxidation potential was at +0.430 V but not above CNT-film- μ -ZS-GEC microsensor at an oxidation potential of +0.250 V.

No significant interference signals were noticed on exposing composite microsensors covered with Nf film, to the electroactive molecules present in the striatal extracellular fluid even at pharmacologically relevant concentrations (the response of AA was tested for a concentration of 500 μM , DOPAC for 10 μM , UA for 2.97 μM , and for DA for 1 μM) by CPA technique, at a potential value of 0.430 V, chosen to assure the potential value at which all components should be oxidized , and as consequence, the maximum potential to interfere DA detection.

The utility of graphite-epoxy composite microsensors for *in vivo* monitoring of dissolved brain O_2 using Constant Potential Amperometry (CPA) technique, O_2 being the most important oxidative substrate for biochemical reactions and for the production of brain energy was investigated. The concentrations of extra-cellular brain oxygen was stimulated by the injection of 1-methyl-4-phenyl-1,2,3,6-tetrahydropyridine (MPTP), which is known to induce oxidative neuronal. Using *in vitro* or *in vivo* calibrations, it was possible that the concentration of dissolved O_2 , after MPTP administration, to be estimated. The in-vivo procedure using a new zeolite-graphite-epoxy composite microsensor was successfully applied in the detection of extracellular brain oxygen and the molecular oxygen concentration based on pre/post calibrations.

Certain in-vivo or in-vitro clinical applications will imposed the requirements for the electroanalytical performance, which will select the carbon-based microsensors design in the direct relation to the membrane/film presence or not.

Future perspectives

- Optimization of membrane covering to minimize the effect of interfering species and to assure very nice electroanalytical performance for the target analyte
- Development and adaptation of graphite-based composite microelectrodes for other applications: environmental, food, pharmaceuticals
- Design and development ordered graphite-microelectrode array to improve the electroanalytical performance for clinical applications
- Modifying the electrode composition to achieve the high sensitivity and selectivity for specific analyte detection;
- Selection and optimization of the electrochemical technique in relation with the electrochemical behavior of the electrode material to enhance the electroanalytical performance for the analysis method;
- Design and development ordered nanoelectrode arrays made of CNTs /CNFs to improve the electroanalytical performance for clinical applications? Do CNTs/CNFs exhibit toxicity towards biological species?